MICROFLUIDIC TECHNIQUES FOR DNA MELTING ANALYSIS AND DIGITAL POLYMERASE CHAIN REACTION

by

Scott Owen Sundberg

A dissertation submitted to the faculty of
The University of Utah
in partial fulfillment of the requirements for the degree of

Doctor of Philosophy

Department of Bioengineering

The University of Utah

December 2010

The University of Utah Graduate School

STATEMENT OF DISSERTATION APPROVAL

The dissertation of **Scott Owen Sundberg**

has been approved by the following supervisory committee members:

Bruce K. Gale	, Chair	**November 8, 2010** Date Approved
Carl T. Wittwer	, Member	**November 8, 2010** Date Approved
Vladimir Hlady	, Member	**November 8, 2010** Date Approved
David W. Grainger	, Member	**November 8, 2010** Date Approved
Robert A. Palais	, Member	**November 8, 2010** Date Approved

and by **Richard D. Rabbitt**, Chair of the Department of **Bioengineering**

and by Charles A. Wight, Dean of The Graduate School.

ABSTRACT

Microfluidic methods were applied to nucleic acid mutation identification and quantification. DNA melting analysis interrogation volumes were reduced 4 orders of magnitude (down to 1 nL volumes) from commercial instrumentation, allowing less reagent consumption while yielding adequate signal for genotyping and scanning of polymerase chain reaction (PCR) products. A microfluidic instrument was developed for digital PCR applications, using a spinning plastic disk patterned by xurography. The platform offers faster thermocycling times (30 cycles in ~12 min), simplified fluid partitioning, and a less expensive disposable when compared to currently available digital PCR platforms. PCR within the disk was validated by quantifying plasmid DNA sample using "on/off" fluorescence interrogation across 1000 wells (30 nL/well) at varying template concentration. A 94% PCR efficiency and product amplification specificity were determined by aggregate real-time PCR and melting analysis. The technique of quasi-digital PCR was also applied within this platform, wherein a single mutation copy was preferentially amplified from a large background of wild-type DNA, to detect and quantify low levels of rare mutations. This method demonstrated a sensitivity of 0.01% (detecting a mutant to wild-type DNA ratio of 43:450000), by mixing known concentrations of an oncogene mutation with thousands of wild-type template copies. Statistic analysis tools were constructed in order to interpret digital PCR data, with results comparing well to DNA absorption measurements.

TABLE OF CONTENTS

ACKNOWLEDGEMENTS

I thank Drs. Bruce Gale and Carl Wittwer for their constant guidance, patience, and support and allowing me the freedom to explore new directions and ideas. I also thank their respective lab groups for their assistance and friendship; I would name each of you but fear forgetting someone. I thank Dr. Robert Palais for aiding me with statistic analysis tools and thank Drs. Vladimir Hlady, David Grainger and Jerome Ferrance (an external reviewer from the University of Virginia) for so generously lending their time in offering suggestions to improve this work. I am grateful for the funding support I have received these past years from the Utah State Center of Excellence program, the National Science Foundations' Integrative Graduate Education and Research Traineeship Program (NSF IGERT), the University of Utah Research Foundation, and the Utah Science Technology and Research initiative (USTAR) in conjunction with the American Recovery and Reinvestment Act (ARRA).

I am so appreciative of my lovely wife who has supported me (in poverty) unceasingly these past several years and am grateful for my children who constantly teach me lessons of humility and love. I am indebted to my parents who taught me the skills necessary for graduate school and thank my siblings, grandparents, in-laws, and friends for their encouragement. I also acknowledge the hand of God in this work and in my life.

CHAPTER 1

INTRODUCTION

The completion of the Human Genome Project in 2003 represents one of the largest single investigational projects ever completed and is a giant step to further understanding disease. This new knowledge should lead to large advancements in medicine and biotechnology, providing a more individualized approach to linking personal genetic profile to disease, if appropriate diagnostic and analysis tools can be created. Applications of molecular diagnostics include: identifying individuals with increased risk of developing certain disorders, screening populations for specific diseases, diagnosis, prognosis, personalized medicine, therapy response monitoring, forensics, identity testing, histocompatibility, veterinary testing, and environmental monitoring. Infectious disease testing (i.e., HIV, hepatitis C, hepatitis B, chlamydia, and gonorrhea) was the first molecular diagnostics segment explored and remains the largest market for molecular diagnostics. However, the emerging segments of oncologic, genetic, and pharmacogenomic testing are quickly gaining popularity and are the focus of this work.

Microfluidics is still an emerging field but is gaining momentum and is starting to find its niche within molecular diagnostics. There is great appeal for sample-in, answer-out tests, point-of-care testing for quick results, and more multiplexing, which may be made possible using microfluidics. Microfluidics has potential, yet unrealized, advantages as follows: low fluid volume consumption (i.e., less waste, lower reagent

consumption, less sample needed), faster analysis (i.e., short diffusion distances, fast heating, small heat capacities), improved process control due to high surface-to-volume ratios, compact systems with combined functionality, precise volumetric control, potential for massive parallelization, enhancement of analytical performance, reduced fluid handling needs, and a low power consumption. Some disadvantages of microfluidics which have held back the technology to some degree include uniquely dominant physical and chemical effects (i.e., capillary forces, surface roughness, chemical interactions, and adsorption), lower signal-to-noise ratios, laminar flow which makes reagent mixing difficult, difficulty interfacing electronics and fluid interfaces with the macro-world, no direct sample-to-answer capabilities, and the fact that it is still a 'novel' technology that has not been fully validated.

This dissertation presents advancements of two related techniques within molecular diagnostics, the polymerase chain reaction (PCR) and DNA melting analysis, by applying microfluidics. A number of widely diverging topics and techniques are brought together in this dissertation. To aid the reader, terms related to these various topics and techniques are defined and their significance stated along with a brief literature review for each topic. The topics include variations on PCR and tools required for PCR analysis and mutation detection, circulating tumor cell biology, the importance of various genetic targets tested within this dissertation, and a microfluidic manufacturing technique.

Polymerase Chain Reaction

The polymerase chain reaction (PCR), discovered in 1984 by Kary Mullis and winner of a Nobel Prize, has become a gold standard in molecular biology (Mullis et al.

1986) and is the primary technique used in this dissertation. This technique allows a specific DNA segment to be amplified, creating millions of copies of a particular DNA sequence. PCR typically relies on a thermocycling process that denatures the DNA at a "high" temperature, and "cooler" temperatures allow enzymatic replication of the DNA sequence of interest. Primers, short oligonucleotide sequences (~20-25 base pairs), are designed complementary to the DNA and enable replication selectivity by framing the sequence to be replicated, facilitating polymerase binding. Variations from the basic PCR chemistry and fluorescent-based analysis methods have been conceived, with a few of these variations discussed hereafter. A wide variety of PCR uses have been developed including: sequencing (Wong et al. 1987; Ansorge 2009), gene expression analysis (Witsell et al. 1990; Thellin et al. 2009), diagnosis of hereditary diseases (Ballabio et al. 1990; Lindeman et al. 1991), forensic science (Kasai et al. 1990; Morling 2009), detection of infectious disease (Vaira et al. 1990; Watzinger et al. 2006), and phylogenetics (Bhattacharya et al. 1993).

Fluorescent DNA Dyes and Probes for PCR Product Analysis

Detection of amplified DNA, both during and after PCR, is of critical importance in PCR analyses and in this work. Several fluorescent-based PCR product identification methods are available, with some of these methods being discussed within this section.

Double-stranded DNA (dsDNA) fluorescent dyes are the most economical format for detecting, quantifying and determining PCR product genotypes. These dyes are saturating or intercalating dyes that bind to double-stranded DNA. Once bound, they fluoresce at a much higher intensity than in the unbound state when only single-stranded DNA is present. The disadvantage of dyes is that they will bind to any double-stranded

DNA in the reaction, including primer-dimers and other non-specific reaction products as well as certain hydrophobic proteins, thus requiring more optimization.

Various probe methods have been implemented to increase product detection specificity. Probes fall into two general categories: labeled probes and unlabeled probes. TaqMan® (Heid et al. 1996), molecular beacons (Piatek et al. 1998), Scorpions™ (Whitcombe et al. 1999), and hybridization probes (Lay and Wittwer 1997; Livak et al. 1995) are all labeled probe techniques. TaqMan® probes are oligonucleotides with a fluorescent reporter dye attached to the 5' end and a quencher moiety coupled to the 3' end. When unhybridized the proximity of the fluorophore and quencher molecules prevent fluorescent signal. During PCR, when the polymerase replicates a template on which a TaqMan® probe is bound, the 5' nuclease activity of the polymerase cleaves the probe to allow the fluorophore to fluoresce. Molecular beacons are similar to TaqMan® probes except they are designed to remain intact during amplification and must rebind to the target each cycle for signal measurement. Molecular beacons form a stem-loop structure when free in solution, bringing the fluorophore and quencher together to quench fluorescence. Scorpion™ probes use a single oligonucleotide that maintains a stem-loop configuration in the unhybridized state. The fluorophore is attached to the 5' end and is quenched by a moiety coupled to the 3' end. The 3' portion of the stem also contains a sequence that is complementary to the extension product of the primer. After extension of the Scorpion™ primer, the specific probe sequence is able to bind to its complement within the extended amplicon thus opening up the hairpin loop. This prevents the fluorescence from being quenched and a signal is observed. Hybridization probes consist of two oligonucleotides that are each fluorescently labeled. One oligonucleotide has a

donor probe labeled at the 3' end, absorbing excitation light. The other oligonucleotide has an acceptor probe on the 5' end, adjacent to the donor probe, absorbing resonance energy emitted from the donor probe through the process of fluorescence resonance energy transfer (FRET). Therefore, fluorescence from the acceptor probe will only occur when both the donor and acceptor probes have annealed to the PCR product. One downside to labeled probes is that they are expensive to synthesize and thus drive up PCR cost.

Luna Probes® (Zhou et al. 2004; Erali et al. 2008), and snapback primers (Zhou et al. 2008) are unlabeled probe techniques that are much less expensive than labeled probes and take advantage of double-stranded dyes combined with melting analysis to provide specificity. Asymmetric PCR is typically performed to improve the signal-to-noise ratio of the unlabeled probe. A Luna Probe® consists of a 3'-blocked oligonulceotide sequence designed to overlay the mutation site of interest. The melting temperature (Tm) of the unlabeled probe is lower than the PCR amplicon and its melting curve is used to genotype the mutation site by either Tm or melting curve shape. A snapback primer includes a 5' tail complementary to its extension product with the tail "snapping back" to overlay the mutation site with a lower Tm than the PCR amplicon. The snapback hairpin melting curve defines the genotype by either Tm or melting curve shape.

Asymmetric PCR

Asymmetric PCR allows one strand of the DNA double helix to be preferentially amplified more than the other by using unequal concentrations of forward and reverse primers during PCR and is a useful technique used for mutation identification in Chapters

4 and 6 of this dissertation. This method generally uses more temperature cycles than symmetric PCR (Montgomery et al. 2007) because amplification becomes linear after the limiting primer is exhausted. LATE-PCR has been introduced to improve this efficiency by changing primer design based on primer-target hybridization (Sanchez et al. 2004). Asymmetric PCR takes advantage of the excess strand amplified and increases visibility of the probe-amplicon duplex melting transition by limiting the fluorescent signal of the amplicon while increasing the fluorescent signal of the probe.

Quantitative Real-Time PCR (qPCR)

PCR instruments today commonly provide real-time fluorescent signal acquisition. Fluorescent signal, from either dsDNA dye or labeled probes, is measured after each PCR cycle, with the fluorescent intensity increasing proportional to the number of PCR amplicons created. Measuring the process in real-time provides an analog method of quantifying the amount of starting DNA template (Higuchi et al. 1992; Higuchi et al. 1993; Wittwer et al. 1997). This method is used in Chapter 5 of this dissertation to validate digital PCR results and PCR efficiency within our spinning disk platform. A threshold is set at a level that reflects a statistically significant increase over the calculated baseline signal, distinguishing baseline fluorescent signal from amplification signal. The cycle at which the PCR reaches the threshold value is the quantification cycle (Cq) (Bustin et al. 2009). The Cq value will shift depending on the number of starting DNA templates. Positive and negative controls and/or calibration curves are used. This method of quantification relies on consistent PCR efficiencies, fluorescent signal fidelity with increased copy number, and nucleic acid quality between samples for accurate results.

Digital PCR

The term "digital PCR" was first coined in 1999 by Vogelstein (Vogelstein and Kinzler 1999). Limiting dilution was used to detect a minor fraction of altered DNA by diluting to the point of having only one DNA template in a given reaction volume. The PCR was then run with molecular beacon probes in solution. Once amplified, the reaction volumes were fluorescently analyzed; wild-type and mutated DNA were then quantified by relying on binary positive/negative calls. Recently, the concept of digital PCR has been miniaturized using microfluidics to limit the amount of DNA template rather than dilutions. One of the first microfluidic applications presented was multigene analysis of environmental bacteria using multiplex digital PCR (Ottesen et al. 2006). Quantitative population analysis of transcription factor expression was also initially shown (Warren et al. 2006). Each of these microfluidic applications uses Fluidigm's Digital Array chip. Fluid is distributed into parallel dead-end channels using pneumatic pressure. A comb valve is then actuated, deflecting a membrane down to section off thousands of isolated nanoliter-sized reaction chambers. This chip is then thermocycled and analyzed using a microarray scanner. One group has even investigated digital PCR down to picoliter-sized reaction volumes using a microdroplet-based system (Beer et al. 2007; Beer et al. 2008; Kiss et al. 2008). This method is capable of creating thousands to millions of droplets for digital PCR analysis. The statistical data acquired are superior to current approaches but the instrumentation and chemistry are complex and expensive.

This dissertation presents a novel microfluidic digital PCR platform using a spinning disk to passively partition a sample into individual reactions to improve upon these existing methods. Applications of digital PCR include identification of rare

mutations within an excess of normal DNA (Yung et al. 2009), assessing allelic imbalance (Fan and Quake 2007; Fan et al. 2009), copy number variation (Qin et al. 2008), viral load (McMahon et al. 2008), non-invasive prenatal testing (Lun et al. 2008), haplotyping (Menzel et al. 2009) and aiding in next-generation sequencing (White III et al. 2009; Pohl and Shih 2004).

ARMS PCR

Amplification refractory mutation system (ARMS) PCR (Newton et al. 1989) is an allele-specific amplification process that allows single nucleotide polymorphism (SNP) detection at a specific locus. This technique implements a primer with a terminal 3'-nucleotide that is allele-specific. Therefore, one can design this primer to either match the 'mutant' template or match the 'normal' template and be refractory to the mismatch, thus delaying the mismatch's PCR.

ACB-PCR

Allele-specific competitive blocker-polymerase chain reaction (ACB-PCR) was first introduced in 1995 (Orou et al. 1995), providing a "double-kill" method to preferentially amplify either mutant or normal template, thus improving ARMS PCR. A probe is designed to match the template to be suppressed during PCR. Thus, the mismatched ARMS primer is not only refractory to the template but also has to compete with the probe to anneal to the template. ACB-PCR greatly delays PCR of the mismatch but also delays the Cq of the matched template. Zhou and Wittwer, at the University of Utah, have adapted this method and used the probe as an indicator as well as a blocker, using asymmetric PCR combined with DNA melting analysis to semi-quantify the

number of mutant DNA copies present within a pool of normal DNA. This method is capable of reaching sensitivity limits of one mutation copy in as many as 100000 wild type copies (10 ppm).

Quasi-Digital PCR

This approach combines digital PCR with ACB-PCR to provide ultra-sensitive detection and quantification of rare nucleic acid mutations and is the method used in Chapter 6 of this dissertation. It is termed quasi-digital because each well is loaded with multiple copies of wild-type DNA but contains at most one copy of mutation template. Parallel ACB-PCR reactions are performed followed by fluorescence detection to determine how many reactions contain a mutation copy, counting the mutations digitally, for improved quantification over real-time PCR methods. Parallel ACB-PCR reactions can theoretically improve the sensitivity of the method by orders of magnitude (Wang et al. 2010).

Multiplex PCR

Multiplex PCR was first introduced in 1988 for use in identifying exon deletions simultaneously (Chamberlain et al. 1988). This technique is powerful because it allows multiple DNA sites, physically separated by large distances, to be investigated simultaneously. Multiple unique sets of primers are designed to amplify the specific DNA sites desired, which requires careful primer design so as to reduce any nonspecific amplification during PCR (Elnifro et al. 2000). Fluorescently-labeled multicolor probes can be used to distinguish each site. Alternatively, a saturating dye can interrogate multiple mutations by observing their melting temperature and melting shapes (Bernard

et al. 1998; Erali et al. 2006). This concept is suggested for future work based on our digital PCR platform.

DNA Melting Analysis

DNA melting analysis was introduced in 1997 as a method to analyze PCR product (Ririe et al. 1997), and represents the genotyping and scanning methods used throughout this dissertation. Typically, a double-stranded intercalating fluorescent dye is included in the PCR (Wittwer et al. 2003). Following amplification, the temperature of the double-stranded DNA product is raised slowly while fluorescence is continuously monitored. When the double helix denatures or 'melts' the fluorescence rapidly decreases. The melting temperature or Tm of the product is defined as the temperature at which half of the DNA product has denatured. When using this method, homozygous changes cause the absolute Tm to shift (Liew et al. 2004) while heterozygous changes alter melting curve shape (Reed et al. 2004; Hermann et al. 2006). DNA melting analysis provides a rapid solution that reduces complexity and contamination risk as compared to other DNA analysis methods (Zhou et al. 2004).

Analysis of the PCR product melting transition often provides adequate genotyping results. However, probe techniques combined with asymmetric PCR can provide even greater specificity (Zhou et al. 2005). Chapters 2 and 3 show that DNA melting analysis is capable of being miniaturized down to nanoliter interrogation volumes (Sundberg et al. 2007).

Circulating Tumor Cells

The discovery of circulating tumor cells (CTCs) in peripheral blood was first made in 1869 by T.R. Ashworth (Ashworth 1869). This discovery provided the ground work for the 'seed and soil' theory of metastasis, presented in 1889 by Stephen Paget (Paget 1889), which still stands today (Fidler 2003). This theory hypothesizes that tumor cells (the 'seed') can migrate to and implant themselves in other organs that contain the proper microenvironment for proliferation (the 'soil').

Detecting and quantifying CTCs has the potential of providing a non-invasive technique for 1) diagnosing cancer earlier, 2) deciding the most appropriate therapy, 3) monitoring therapy response, and 4) determining drug resistance. The challenge with this method arises from the low concentration of CTCs, which can be as low as 1 cell in 1 ml of blood (Nagrath et al. 2007), or one tumor cell per 10^5 - 10^7 peripheral blood mononuclear cells (Ross et al. 1993), making it difficult to detect and quantify these cancer cells with currently available techniques. Some enrichment techniques have been developed to address the challenge of low CTC concentrations, such as filtration (Vona et al. 2000), density gradient (Müller et al. 2005), flow cytometry (Cruz et al. 2005) and immunomagnetic enrichment (Allard et al. 2004). However, these techniques have been shown to suffer from low specificity, low sensitivity, a loss of CTCs, or false negatives and positives (Alunni-Fabbroni and Sandri 2010). In order to overcome these issues this research proposes the use of quasi-digital PCR to quantify the mutation DNA from CTCs.

Genetic Targets Considered and their Significance

BRAF

V-raf murine sarcoma viral oncogene homolog B1 is a protein encoded by the *BRAF* gene and is involved in sending signals in cells, affecting cell division, differentiation, and secretion. This gene can be mutated in many cancers, which can cause an increase in growth and the spread of cancer cells. *BRAF* mutations have been identified in 66% of malignant melanomas (Davies et al. 2002) and at a lower frequency in a wide range of human cancers including colorectal cancers, liver cancers, lung cancers, breast cancers, papillary thyroid carcinoma, etc. (Namba et al. 2003). The *BRAF* T1796A mutation accounts for approximately 92% of *BRAF* mutations in melanoma (Davies et al. 2002).

DNA Toolbox

A "DNA toolbox" was reported in 1999 to aid in characterization of mutation scanning methods (Highsmith Jr. et al. 1999). The toolbox consists of highly characterized plasmid constructs that contain inserts of 800-1000 bp with GC contents of 40, 50, or 60%. At a central position of the insert are the four possible nucleotide bases. This tool allows one to determine the effects of GC content, nucleotide substitution, PCR fragment length, and location of sequence variation within an amplified fragment.

Warfarin

Warfarin is a commonly used coumadin anticoagulant with wide inter-individual dosage variation. Variants in the *VKORC1* and *CYP2C9* genes and patients' age and height account for 50-60% of the dosage variation (Sconce et al. 2005; Wadelius et al.

2007). Warfarin interferes with vitamin K recycling in the liver and the *VKORC1* gene is what regulates the main protein in the vitamin K epoxide reductase complex. Warfarin is metabolized by cytochrome P450 2C9 (*CYP2C9*), with *CYP2C9* *2 and *3 alleles requiring lower warfarin doses and causing greater risk of bleeding (Sanderson et al. 2005).

CFTR

Mutations within the *CFTR* gene have been found to cause cystic fibrosis, a disease that causes the body to produce thick, sticky mucus which causes difficulty breathing and insufficient enzyme production in the pancreas. This disease is one of the most common autosomal recessive genetic disorders among the Caucasian population, affecting approximately 1 in 3,300 with a carrier rate of 1 in 29 (Heaney et al. 2006). A 3-bp deletion (delta F508 deletion) within this gene is the most common mutation (Riordan et al. 1989).

ATM

Ataxia-telangiectasia is an autosomal recessive disorder which may include cerebellar degeneration, immunodeficiency, chromosomal instability, radiosensitivity and a predisposition for cancer (Platzer et al. 1997). This disorder occurs in about 1 in 40,000 to 1 in 100,000 people worldwide and the gene responsible is *ATM* (Palau and Espinós 2006).

HFE

Hemochromatosis is an autosomal recessive disorder of iron metabolism causing the body to accumulate iron and affects between 1 in 200 to 1 in 400 individuals (Feder et

al. 1996). This excess iron can lead to failure of a variety of organs and can also cause cirrhosis, hepatomas, diabetes, cardiomyopathy and arthritis (Andrews 1999). The major gene correlated with hemochromatosis is *HFE*.

Xurography Rapid Prototyping

Cutting plotters are frequently used in the graphic design industry, typically patterning designs out of adhesive-backed materials for signs or other artwork. Many cutting plotters provide good mechanical resolution, with some offering a step size as low as 5 μm. The first use of this technology for microfluidic fabrication came in early 2005, in which Treise et al. used a cutting plotter to pattern channels in a vinyl film and then sandwiched the patterned layer between two sheets of Plexiglas, with inlet and outlet holes (Treise et al. 2005). Later that same year, Bartholomeusz et al. extensively evaluated this microfabrication process, using multiple materials and techniques (Bartholomeusz et al. 2005). This group coined the cutting plotter method xurography, using the Greek root words *xuron* and *graphe*, which mean razor and writing, respectively. This prototyping method can provide a very short turnaround time; microdevices can be designed, fabricated, and tested within the same day. The process of xurography is used throughout this dissertation.

The feature sizes that xurography can provide depend on several factors. The minimum step size of stepper motors within the cutting plotter, blade sharpness, blade angle, material properties of the substrate, cutting speed, cutting force, and cutting mode all help determine the smallest features possible (Gale et al. 2008). Xurography has been used in shadow masks (Kim et al. 2006), electroplated microchannels (Bartholomeusz et al. 2005), micromolding (Kim and Gale 2005), laminated microfluidic structures

(Sundberg et al. 2010), and double-layer adhesive materials (Greer et al. 2007; Sundberg et al. 2007; Crews et al. 2009).

CO_2 laser micromachining provides a similar manufacturing method to xurography in that both provide a material removal process (Klank et al. 2002). In fact, CO_2 lasers have been shown to effectively pattern double-sided tape (Luo et al. 2007), just as with the work discussed in Chapters 2 and 3 of this dissertation for patterning tape by xurography. The primary disadvantage of using a CO_2 laser is that the upfront equipment cost is an order of magnitude higher than for that of a cutting plotter. Another disadvantage is that the material to be ablated or machined must match well with the wavelength of the laser, otherwise the substrate may char, melt or not machine at all. It can be complex to optimize parameters of a laser system, as one must consider pulses per inch, pulse frequency, power, focal distance, number of passes, and the beam velocity (Liu and Gong 2009). With a cutting plotter the primary parameters are blade speed and force, although other parameters can also affect the quality of the cut to a lesser degree. However, due to the various controllable parameters of a laser system much thicker substrates can be machined and depth of cut can be controlled to ablate features into the substrate, rather than solely relying on the substrate thickness for depth (Snakenborg et al. 2004). Smaller feature sizes can be obtained by focusing the beam spot size and more intricate and precise cutting is available due to the fact that a blade does not have to be dragged through the material. The cutting speed of a pattern can be increased as well, so long as the parameters are such that several passes are not required.

Dissertation Overview

The overarching theme of this dissertation is applying microfluidic techniques to DNA mutation analysis in order to reduce the cost of tests and, in the final chapters, to also improve low-level mutation quantification using a thousand simultaneous reactions and a quasi-digital quantification method. Chapter 2 looks at signal-to-noise ratio reduction as the technique of DNA melting analysis is miniaturized in microfluidics using three different mutation sites to provide data. This chapter is published in its entirety in the peer-reviewed journal *Biomedical Microdevices* (Sundberg et al. 2007). Chapter 3 compares two microfluidic chip fabrication techniques, traditional glass etching and xurography rapid prototyping, using the application of DNA melting analysis as the data for comparison. This chapter is published in its entirety in the peer-reviewed *Journal of Micromechanics and Microengineering* (Greer et al. 2007). Chapter 4 is a pharmacogenomic application of microfluidic DNA melting analysis using three genes involved with warfarin drug dosing. The chapter is published as an extended abstract within the American Institute of Chemical Engineers (AIChE) Annual Meeting conference proceedings (Sundberg et al. 2007). Chapter 5 presents a novel disk design and instrument for microfluidic digital PCR. This chapter is published in the peer-reviewed journal *Analytical Chemistry* and includes a Supplementary Information section (Sundberg et al. 2010). Chapter 6 applies the work presented in Chapter 5 to improve the limits of detection for cancer mutation screening. This chapter will be submitted to the peer-reviewed journal *Analytical Biochemistry*. Chapter 7 provides statistical analysis of the digital PCR disk, providing Poisson distributions and confidence intervals. Lastly,

Chapter 8 provides a conclusion to our microfluidic DNA mutation analysis, presenting contributions developed from this work as well as a future work section.

References

Allard WJ, Matera J, Miller MC, Repollet M, Connelly MC, Rao C, Tibbe AGJ, Uhr JW, Terstappen LWMM. 2004. Tumor cells circulate in the peripheral blood of all major carcinomas but not in healthy subjects or patients with nonmalignant diseases. Clinical Cancer Research. 10:6897-6904.

Alunni-Fabbroni M, Sandri MT. 2010. Circulating tumour cells in clinical practice: methods of detection and possible characterization. Methods. 50:289-297.

Andrews NC. 1999. Disorders of iron metabolism. N Engl J Med. 341:1986-1995.

Ansorge WJ. 2009. Next-generation DNA sequencing techniques. N Biotechnol. 25(4):195-203.

Ashworth TR. 1869. A case of cancer in which cells similar to those in the tumors were seen in the blood after death. Aust Med J. 14:146-149.

Ballabio A, Gibbs RA, Caskey CT. 1990. PCR test for cystic fibrosis deletion. Nature. 343(6255):220.

Bartholomeusz DA, Bouttè RW, Andrade JD. 2005. Xurography: rapid prototyping of microstructures using a cutting plotter. JMEMS. 14(6):1364-1374.

Beer NR, Hindson BJ, Wheeler EK, Hall SB, Kennedy IM, Colston BW. 2007. On-chip, real-time, single-copy polymerase chain reaction in picoliter droplets. Analytical Chemistry. 79(22):8471-8475.

Beer NR, Wheeler EK, Lee-Houghton L, Watkins N, Nasarabadi S, Herbert N, Leung P, Arnold DW, Bailey CG, Colston BW. 2008. On-chip single-copy real-time reverse-transcription PCR in isolated picoliter droplets. Analytical Chemistry. 80(6):1854-1858.

Bernard PS, Ajioka RS, Kushner JP, Wittwer CT. 1998. Homogeneous multiplex genotyping of hemochromatosis mutations with fluorescent hybridization probes. American Journal of Pathology. 153(4):1055-1061.

Bhattacharya D, Stickel SK, Sogin ML. 1993. Isolation and molecular phylogenetic analysis of actin-coding regions from Emiliania huxleyi, a Prymnesiophyte alga, by reverse transcriptase and PCR methods. Mol Biol Evol. 10(3):689-703.

Bustin SA, Benes V, Garson JA, Hellemans J, Huggett J, Kubista M, Mueller R, Nolan T, Pfaffl MW, Shipley GL, Vandesompele J, Wittwer CT. 2009. The MIQE Guidelines: Minimum Information for Publication of Quantitative Real-Time PCR Experiments. Clinical Chemistry. 55(4):611-622.

Chamberlain JS, Gibbs RA, Ranier JE, Nguyen PN, Caskey CT. 1988. Deletion screening of the Duchenne muscular dystrophy locus via multiplex DNA amplification. Nucleic Acids Res. 16:11141-11156.

Crews N, Wittwer CT, Montgomery J, Pryor R, Gale B. 2009. Spatial DNA melting analysis for genotyping and variant screening. Analytical Chemistry. 81:2053-2058.

Cruz I, Ciudad J, Cruz JJ, Ramos M, Gomez-Alonso A, Adansa JC, Rodriguez C, Orfao A. 2005. Evaluation of multiparameter flow cytometry for the detection of breast cancer tumor cells in blood samples. American Journal of Clinical Pathology. 123:66-74.

Davies H, Bignell GR, Cox C, Stephens P, Edkins S, Clegg S, Teague J, Woffendin H, Garnett MJ, Bottomley W, Davis N, Dicks E, Ewing R, Floyd Y, Hall S, Hawes R, Hughes J, Kosmidou V, Menzies A, Mould C, Parker A, Stevens C, Watt S, Hooper S, Wilson R, Jayatilake H, Gusterson BA, Cooper C, Shipley J, Hargrave D, Pritchard-Jones K, Maitland N, Chenevix-Trench G, Riggins GJ, Bigner DD, Palmieri G, Cossu A, Flanagan A, Nicholson A, Ho JW, Leung SY, Yuen ST, Weber BL, Seigler HF, Darrow TL, Paterson H, Marais R, Marshall CJ, Wooster R, Stratton MR, Futreal PA. 2002. Mutations of the BRAF gene in human cancer. Nature. 417:949-954.

Elnifro EM, Ashshi AM, Cooper RJ, Klapper PE. 2000. Multiplex PCR: optimization and application in diagnostic virology. Clinical Microbiology Reviews. 13(4):559-570.

Erali M, Pounder JI, Woods GL, Petti CA, Wittwer CT. 2006. Multiplex single-color PCR with amplicon melting analysis for identification of Aspergillus species. Clin Chem. 52(7):1443-1445.

Erali M, Palais R, Wittwer C. 2008. SNP genotyping by unlabeled probe melting analysis. Methods Mol Biol. 429:199-206.

Fan HC, Quake SR. 2007. Detection of aneuploidy with digital polymerase chain reaction. Analytical Chemistry. 79:7576-7579.

Fan HC, Blumenfeld YJ, El-Sayed YY, Chueh J, Quake SR. 2009. Microfluidic digital PCR enables rapid prenatal diagnosis of fetal aneuploidy. Am J Obstet Gynecol. 200:543.e1543.e7.

Feder JN, Gnirke A, Thomas W, Tsuchihashi Z, Ruddy DA, Basava A, Dormishian F, Domingo Jr. R, Ellis MC, Fullan A, Hinton LM, Jones NL, Kimmel BE, Kronmal GS, Lauer P, Lee VK, Loeb DB, Mapa FA, McClelland E, Meyer NC, Mintier GA, Moeller N, Moore T, Morikang E, Prass CE, Quintana L, Starnes SM, Schatzman RC, Brunke KJ,

Drayna DT, Risch NJ, Bacon BR, Wolff RK. 1996. A novel MHC class I-like gene is mutated in patients with hereditary haemochromatosis. Nat Genet. 13(4):399-408.

Fidler IJ. 2003. The pathogenesis of cancer metastasis: the 'seed and soil' hypothesis revisited. Nature Reviews Cancer. 3:453-458.

Gale BK, Eddings MA, Sundberg SO, Hatch A, Kim J, Ho T. 2008. Fabrication and packaging: Low-cost MEMS technologies. In: Gianchandani Y, Tabata O, and Zappe H, editors. Comprehensive Microsystems, 1st edition, vol. 1. Amsterdam, Netherlands: Elsevier.

Greer J, Sundberg SO, Wittwer CT, Gale BK. 2007. Comparison of glass etching to xurography prototyping of microfluidic channels for DNA melting analysis. J Micromech Microeng. 17:2407-2413.

Heaney DL, Flume P, Hamilton L, Lyon E, Wolff DJ. 2006. Detection of an apparent homozygous 3120G>A Cystic Fibrosis mutation on a routine carrier screen. J Mol Diagn. 8(1):137-140.

Heid CA, Stevens J, Livak KJ, Williams PM. 1996. Real time quantitative PCR. Genome Research. 6(10):986-994.

Herrmann MG, Durtschi JD, Bromley LK, Wittwer CT, Voelkerding KV. 2006. Amplicon DNA melting analysis for mutation scanning and genotyping: cross-platform comparison of instrument and dyes. Clin Chem. 52(3):494-503.

Highsmith Jr. WE, Jin Q, Nataraj AJ, O'Connor JM, Burland VD, Baubonis WR, Curtis FP, Kusukawa N, Garner MM. 1999. Use of a DNA toolbox for the characterization of mutation scanning methods. I: Construction of the toolbox and evaluation of heteroduplex analysis. Electrophoresis. 20:1186-1194.

Higuchi R, Dollinger G, Walsh PS, Griffith R. 1992. Simultaneous amplification and detection of specific DNA sequences. Biotechnology. 10:413-417.

Higuchi R, Fockler C, Dollinger G, Watson R. 1993. Kinetic PCR analysis: real-time monitoring of DNA amplification reactions. Biotechnology. 11:1026-1030.

Kasai K, Nakamura Y, White R. 1990. Amplification of a variable number of tandem repeats (VNTR) locus (pMCT118) by the polymerase chain reaction (PCR) and its application to forensic science. J Forensic Sci. 35(5):1196-1200.

Kim J, Gale BK. 2006. Microfluidic DNA extraction using a patterned aluminum oxide membrane. Proceedings of SPIE: Microfluidics, BioMEMS, and Medical Microsystems IV, San Jose, CA, January 23-28.

Kiss MM, Ortoleva-Donnelly L, Beer NR, Warner J, Bailey CG, Colston BW, Rothberg JM, Link DR, Leamon JH. 2008. High-throughput quantitative polymerase chain reaction in picoliter droplets. Analytical Chemistry. 80:8975-8981.

Klank H, Kutter JP, Geschke O. 2002. CO2-laser micromachining and back-end processing for rapid production of PMMA-based microfluidic systems. Lab Chip. 2:242-246.

Lay MJ, Wittwer CT. 1997. Real-time fluorescence genotyping of factor V Leiden during rapid-cycle PCR. Clinical Chemistry. 43(12):2262-2267.

Liew M, Pryor R, Palais R, Meadows C, Erali M, Lyon E, Wittwer C. 2004. Genotyping of single-nucleotide polymorphisms by high-resolution melting of small amplicons. Clin Chem. 50(7):1156-1164.

Lindeman R, Wallace R, Volpato F, Hu SP, Trent RJ. 1991. Utility of the polymerase chain reaction (PCR) for prenatal diagnosis of genetic disease. Pathology. 23(2):158-163.

Liu H-B, Gong H-Q. 2009. Templateless prototyping of polydimethylsiloxane microfluidic structures using a pulsed CO2 laser. Journal of Micromechanics and Microengineering. 19:037002 (8pp).

Livak KJ, Flood SJA, Marmaro J, Giusti W, Deetz K. 1995. Oligonucleotides with fluorescent dyes at opposite ends provide a quenched probe system useful for detecting PCR product and nucleic acid hybridization. PCR Methods Appl. 4:357-362.

Lun FMF, Chiu RWK, Chan KCA, Leung TY, Lau TK, Lo YMD. 2008. Microfluidics digital PCR reveals a higher than expected fraction of fetal DNA in maternal plasma. Clinical Chemistry. 54:1664-1672.

Luo LW, Teo CY, Ong WL, Tang KC, Cheow LF, Yobas L. 2007. Rapid prototyping of microfluidic systems using a laser-patterned tape. Journal of Micromechanics and Microengineering. 17:N107-N111.

McMahon MA, Siliciano JD, Lai J, Liu JO, Stivers JT, Siliciano RF, Kohli RM. 2008. The antiherpetic drug Acyclovir inhibits HIV replication and selects the V751 reverse transcriptase multidrug resistance mutation. Journal of Biological Chemistry. 283(46):31289-31293.

Menzel S, Qin J, Vasavda N, Thein SL, Ramakrishnan R. 2009. Rapid single-molecule haplotyping in patients with sickle cell disease. European Human Genetics Conference, Vienna, Austria, May 23-26, P11.094.

Montgomery J, Wittwer CT, Palais R, Zhou L. 2007. Simultaneous mutation scanning and genotyping by high-resolution DNA melting analysis. Nature Protocols. 2(1):59-66.

Morling N. 2009. PCR in forensic genetics. Biochem Soc Trans. 37:438-440.

Müller V, Stahmann N, Riethdorf S, Rau T, Zabel T, Goetz A, Jänicke F, Pantel K. 2005. Circulating tumor cells in breast cancer: correlation to bone marrow micrometastases, heterogeneous response to systemic therapy and low proliferative activity. Clinical Cancer Research. 11:3678-3685.

Mullis K, Faloona F, Scharf S, Saiki R, Horn G, Erlich H. 1986. Specific enzymatic amplification of DNA in vitro: the polymerase chain reaction. Cold Spring Harb Symp Quant Biol. 51:263-273.

Nagrath S, Sequist LV, Maheswaran S, Bell DW, Irimia D, Ulkus L, Smith MR, Kwak EL, Digumarthy S, Muzikansky A, Ryan P, Balis UJ, Tompkins RG, Haber DA, Toner M. 2007. Isolation of rare circulating tumour cells in cancer patients by microchip technology. Nature. 450:1235-1241.

Namba H, Nakashima M, Hayashi T, Hayashida N, Maeda S, Rogounovitch TI, Ohtsuru A, Saenko VA, Kanematsu T, Yamashita S. 2003. Clinical implication of hot spot BRAF mutation, V599E, in papillary thyroid cancers. J Clin Endocrinol Metab. 88(9):4393-4397.

Newton CR, Graham A, Heptinstall LE, Powell SJ, Summers C, Kalsheker N, Smith JC, Markham AF. 1989. Analysis of any point mutation in DNA. The amplification refractory mutation system (ARMS). Nucleic Acids Research. 17(7):2503-2515.

Orou A, Fechner G, Utermann G, Menzel HJ. 1995. Allele-specific competitive blocker PCR: a one-step method with applicability to pool screening. Hum Mutat. 6:163-169.

Ottesen EA, Hong JW, Quake SR, Leadbetter JR. 2006. Microfluidic digital PCR enables multigene analysis of individual environmental bacteria. Science. 314:1464-1467.

Paget S. 1889. The distribution of secondary growths in cancer of the breast. Lancet. 571-573.

Palau F, Espinós C. 2006. Autosomal recessive cerebellar ataxias. Orphanet J Rare Dis. 1:47-65.

Piatek AS, Tyagi S, Pol AC, Telenti A, Miller LP, Kramer FR, Alland D. 1998. Molecular beacon sequence analysis for detecting drug resistance in Mycobacterium tuberculosis. Nature Biotechnology. 16(4):359-363.

Platzer M, Rotman G, Bauer D, Uziel T, Savitsky K, Bar-Shira A, Gilad S, Shiloh Y, Rosenthal A. 1997. Ataxia-telangiectasia locus: sequence analysis of 184 kb of human genomic DNA containing the entire ATM gene. Genome Res. 7(6):592-605.

Pohl G, Shih IeM. 2004. Principle and applications of digital PCR. Expert Review of Molecular Diagnostics. 4(1):41-47.

Qin J, Jones RC, Ramakrishnan R. 2008. Studying copy number variations using a nanofluidic platform. Nucleic Acids Research. 36:e116.

Reed GH, Wittwer CT. 2004. Sensitivity and specificity of single-nucleotide polymorphism scanning by high-resolution melting analysis. Clin Chem. 50(10):1748-1754.

Riordan JR, Rommens JM, Kerem B, Alon N, Rozmahel R, Grzelczak Z, Zielenski J, Lok S, Plavsic N, Chou JL, Drumm ML, Iannuzzi MC, Collins FS, Tsui LC. 1989. Identification of the cystic fibrosis gene: cloning and characterization of complementary DNA. Science. 245(4922):1066-73.

Ririe KM, Rasmussen RP, Wittwer CT. 1997. Product differentiation by analysis of DNA melting curves during the polymerase chain reaction. Anal Biochem. 245:154-160.

Ross AA, Cooper BW, Lazarus HM, Mackay W, Moss TJ, Ciobanu N, Tallman MS, Kennedy MJ, Davidson NE, Sweet D, Winter C, Akard L, Jansen J, Copelan E, Meagher RC, Herzing RH, Klumpp TR, Kahn DG, Warner NE. 1993. Detection and viability of tumor cells in peripheral blood stem cell collections from breast cancer patients using immunocytochemical and clonogenic assay techniques. Blood. 82:2605-2610.

Sanchez JA, Pierce KE, Rice JE, Wangh LJ. 2004. Linear-After-The-Exponential (LATE)-PCR: An advanced method of asymmetric PCR and its uses in quantitative real-time analysis. Proc Natl Acad Sci USA. 101(7):1933-1938.

Sanderson S, Emery J, Higgins J. 2005. CYP2C9 gene variants, drug dose, and bleeding risk in warfarin-treated patients: a HuGEnet systematic review and meta-analysis. Genet Med. 7:97–104.

Sconce EA, Khan TI, Wynne HA, Avery P, Monkhouse L, King BP, Wood P, Kesteven P, Daly AK, Kamali F. 2005. The impact of CYP2C9 and VKORC1 genetic polymorphism and patient characteristics upon warfarin dose requirements: proposal for a new dosing regimen. Blood. 106:2329–2333.

Snakenborg D, Klank H, Kutter JP. 2004. Microstructure fabrication with a CO2 laser system. Journal of Micromechanics and Microengineering. 14:182-189.

Sundberg SO, Wittwer CT, Greer J, Pryor RJ, Elenitoba-Johnson O, Gale BK. 2007. Solution-phase DNA mutation scanning and SNP genotyping by nanoliter melting analysis. Biomed Microdevices. 9:159-166.

Sundberg SO, Greer J, Wittwer CT, Gale BK. 2007. Miniaturization of warfarin metabolism genotyping using DNA melting analysis, asymmetric PCR and unlabeled

oligonucleotide probes. American Institute of Chemical Engineers (AIChE) Annual Meeting, Salt Lake City, UT, November 4-9.

Sundberg SO, Wittwer CT, Gao C, Gale BK. 2010. Spinning disk platform for microfluidic digital polymerase chain reaction. Analytical Chemistry. 82(4):1546-1550.

Thellin O, ElMoualij B, Heinen E, Zorzi W. 2009. A decade of improvements in quantification of gene expression and internal standard selection. Biotechnol Adv. 27(4):232-233.

Treise I, Fortner N, Shapiro B, Hightower A. 2005. Efficient energy based modeling and experimental validation of liquid filling in planar micro-fluidic components and networks. Lab Chip. 5:285-297.

Vaira D, Francois-Gerard C, Sondag-Thull D, Rentier B. 1990. Diagnosis by PCR of HIV-1 infection in seronegative individuals at risk. AIDS Res Hum Retroviruses. 6(2):173-174.

Vogelstein B, Kinzler KW. 1999. Digital PCR. Proc Natl Acad Sci USA. 96:9236-9241.

Vona G, Sabile A, Louha M, Sitruk V, Romana S, Schütze K, Capron F, Franco D, Pazzagli M, Vekemans M, Lacour B, Bréchot C, Paterlini-Bréchot P. 2000. Isolation by size of epithelial tumor cells. American Journal of Pathology. 156:57-63.

Wadelius M, Chen LY, Eriksson N, Bumpstead S, Ghori J, Wadelius C, Bentley D, McGinnis R, Deloukas P. 2007. Association of warfarin dose with genes involved in its action and metabolism. Hum Genet. 121:23-34.

Wang J, Ramakrishnan R, Tang Z, Fan W, Kluge A, Dowlati A, Jones RC, Ma PC. 2010. Quantifying EGFR alterations in the lung cancer genome with nanofluidic digital PCR arrays. Clin Chem. 56:623-632.

Warren L, Bryder D, Weissman IL, Quake SR. 2006. Transcription factor profiling in individual hematopoietic progenitors by digital RT-PCR. Proc Natl Acad Sci USA. 103(47):17807-17812.

Watzinger F, Ebner K, Lion T. 2006. Detection and monitoring of virus infections by real-time PCR. Mol Aspects Med. 27:254-298.

Whitcombe D, Theaker J, Guy SP, Brown T, Little S. 1999. Detection of PCR products using self-probing amplicons and fluorescence. Nature Biotechnology. 17(8):804-807.

White III RA, Blainey PC, Fan HC, Quake SR. 2009. Digital PCR provides sensitive and absolute calibration for high throughput sequencing. BMC Genomics. 10:116.

Witsell AL, Schook LB. 1990. Clonal analysis of gene expression by PCR. Biotechniques. 9(3):318-322.

Wittwer CT, Herrmann MG, Moss AA, Rasmussen RP. 1997. Continuous fluorescence monitoring of rapid cycle DNA amplification. Biotechniques. 22:130-138.

Wittwer CT, Reed GH, Gundry CN, Vandersteen JG, Pryor RJ. 2003. High-resolution genotyping by amplicon melting analysis using LCGreen. Clin Chem. 49(6): 853-860.

Wong C, Dowling CE, Saiki RK, Higuchi RG, Erlich HA, Kazazian HH Jr. 1987. Characterization of beta-thalassaemia mutations using direct genomic sequencing of amplified single copy DNA. Nature. 330(6146):384-386.

Yung TKF, Chan KCA, Mok TSK, Tong J, To K-F, Lo YMD. 2009. Single-molecule detection of epidermal growth factor receptor mutations in plasma by microfluidics digital PCR in non-small cell lung cancer patients. Clinical Cancer Research. 15:2076-2084.

Zhou L, Myers AN, Vandersteen JG, Wang L, Wittwer CT. 2004. Closed-tube genotyping with unlabeled oligonucleotide probes and a saturating DNA dye. Clin Chem. 50(8):1328-1335.

Zhou L, Wang L, Palais R, Pryor R, Wittwer CT. 2005. High-resolution DNA melting analysis for simultaneous mutation scanning and genotyping in solution. Clin Chem. 51(10):1770-1777.

Zhou L, Errigo RJ, Lu H, Poritz MA, Seipp MT, Wittwer CT. 2008. Snapback primer genotyping with saturating DNA dye and melting analysis. Clinical Chemistry. 54:1648-1656.

CHAPTER 2

SOLUTION-PHASE DNA MUTATION SCANNING AND SNP GENOTYPING BY NANOLITER MELTING ANALYSIS

This chapter has been reprinted with permission from Springer. The manuscript is published in Biomedical Microdevices, DOI 10.1007/s10544-006-9017-3. Authors are Scott O. Sundberg, Carl T. Wittwer, Jenny Greer, Robert J. Pryor, Oluwole Elenitoba-Johnson, and Bruce K. Gale.

Biomed Microdevices (2007) 9:159–166
DOI 10.1007/s10544-006-9017-3

Solution-phase DNA mutation scanning and SNP genotyping by nanoliter melting analysis

Scott O. Sundberg · Carl T. Wittwer · Jenny Greer · Robert J. Pryor · Oluwole Elenitoba-Johnson · Bruce K. Gale

Published online: 13 December 2006

Abstract Solution-phase, DNA melting analysis for heterozygote scanning and single nucleotide polymorphism (SNP) genotyping was performed in 10 nl volumes on a custom microchip. Human genomic DNA was PCR amplified in the presence of the saturating fluorescent dye, LCGreen® Plus, and placed within microfluidic channels that were created between two glass slides. The microchip was heated at 0.1°C/s with a Peltier device and viewed with an inverted fluorescence microscope modified for photomulitiplier tube detection. The melting data was normalized and the negative first derivative plotted against temperature. Mutation scanning for heterozygotes was easily performed by comparing the shape of the melting curve to homozygous standards. Genotyping of homozygotes by melting temperature (T_m) required absolute temperature comparisons. Mutation scanning of *ATM* exon 17 and *CFTR* exon 10 identified single base change heterozygotes in 84 and 201 base-pair (bp) products, respectively. All genotypes at *HFE* C282Y were distinguished by simple melting analysis of a 40-bp fragment. Sequential analysis of the same sample on the gold-standard, commercial high-resolution melting instrument HR-1™, followed by melting in a 10 nl reaction chamber, produced similar results. DNA melting analysis requires only minutes after PCR and is a simple method for genotyping and scanning that can be reduced to nanoliter volumes. Microscale systems for performing DNA melting reduce the reagents/DNA template required with a promise for high throughput analysis in a closed chamber without risk of contamination.

Keywords DNA melting · Mutation scanning · SNP genotyping · Xurography

S. O. Sundberg (✉)
Department of Bioengineering, University of Utah,
SLC, UT 84112, USA
e-mail: scott.sundberg@m.cc.utah.edu

C. T. Wittwer · R. J. Pryor · O. Elenitoba-Johnson
Department of Pathology, University of Utah,
SLC, UT 84112, USA

J. Greer · B. K. Gale
Department of Mechanical Engineering, University of Utah,
SLC, UT 84112, USA

Introduction

Microsystem technology has generated tremendous interest recently for use in clinical diagnostics and forensics (Verpoorte, 2002). One of the most important analytical tools, the polymerase chain reaction (PCR) (Saiki et al., 1985), can amplify a short region of DNA over 10^6-fold in 10–15 min (Wittwer et al., 1990). Several groups have developed microsystems for performing PCR in nanoliter volumes (Gulliksen et al., 2004; Hühmer and Landers, 2000; Ibrahim et al., 1998; Khandurina et al., 2000; Liu et al., 2002; Yoon et al., 2002), including one group with volumes as small as 86 pl (Nagai et al., 2001). Advantages of microscale PCR include lower reagent and target DNA consumption and better heat transfer rates for faster reaction times during thermocycling. After PCR amplification, many analytical techniques are available for detecting sequence variants, including simple size separation on a gel matrix and complex mass spectrometry methods. Some of these methods have been incorporated into microsystems; for example, PCR followed by electrophoretic separation (Waters et al., 1998; Lagally et al., 2001). However, the fabrication of the chip and integration of the detection method may become complicated.

DNA melting analysis as a complement to PCR was introduced in 1997 (Ririe et al., 1997). A dye is included in

the PCR that fluoresces in the presence of double-stranded DNA, but not single-stranded DNA. After amplification, fluorescence is monitored as the double-stranded DNA product is slowly heated. When the double helix melts, fluorescence rapidly decreases. The negative first derivative of fluorescence with respect to temperature shows the melting temperature (T_m) as maxima. Recent advances in melting analysis instrumentation (Herrmann et al., 2006) and saturating DNA dyes (Wittwer et al., 2003) allow detection and genotyping of single nucleotide polymorphisms (SNPs). If the change is heterozygous, DNA heteroduplexes alter the shape of the melting curve, providing a simple method for mutation scanning (Reed and Wittwer, 2004). If the change is homozygous, the absolute temperature of the melting transition shifts (Liew et al., 2004). DNA melting analysis, when compared to existing PCR analytical techniques, is advantageous because it is less complicated, faster (less than 20 min for PCR and analysis), and prevents contamination of the sample and environment due to its closed-tube format (Zhou et al., 2004). The specific dye used determines the capabilities of the method; LCGreen® Plus detects heterozygotes well and does not inhibit PCR (Wittwer et al., 2003).

DNA melting analysis has been previously reported in microscale systems with oligonucleotides attached to the chip surface (Dodge et al., 2004). However, immobilization of oligonucleotides adds additional complexity and cost to the fabrication of the chip. Furthermore, hybridization to immobilized probes takes significantly longer than solution-phase hybridization and is limited by steric factors and mass transport conditions. By monitoring solution-phase melting analysis on a microchip, the complexity of chip fabrication and analysis time are minimized. Using custom instrumentation and microchannel chips, we demonstrate solution-phase mutation scanning and SNP genotyping in 10 nl reaction volumes using three different genomic DNA targets. To the best of our knowledge this is the first time that solution-phase DNA melting analysis has been performed in nanoliter volumes.

Materials and methods

Microchip fabrication

The microchips were manufactured using Xurography (Bartholomeusz et al., 2005). The process uses Adobe Illustrator® (Adobe, San Jose, CA) to generate the geometry of the channel structures. The output files are exported to a knife plotter (Graphtec, Irvine, CA) which cuts the channel and well structures out of a 25 μm thick, double coated tape (9019, 3M, St. Paul, MN) consisting primarily of polyethylene terephthalate (PET), a material used with PCR in previous research (Northrup et al., 1993). Input and output ports, melting analysis wells, and connecting channels were designed as shown in Fig. 1. The channels had a cross section of 175 $\times$ 25μm. The melting analysis wells had a diameter of 715 μm and a total volume of 10 nl. The patterned tape was then sandwiched between two 25 $\times$ 75 mm glass slides. One of the glass slides had 2 mm diameter holes located at the input and output ports of the channel. A NanoPort™ assembly (Upchurch Scientific, Oak Harbor, WA) was then attached to the outlet port on the glass slide with a luer lock attachment. The input port was placed 22.5 mm from the center of the DNA analysis chamber and was used for loading the sample. A syringe was connected to the luer fitting at the outlet port and was used to create a vacuum and draw the sample through the channel into the analysis chamber. Figure 2 shows a photograph of the entire assembly (A), a photograph of the 10 nl well (B), and a cross-section sketch of the assembled microchip (C).

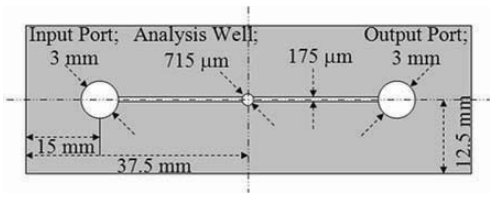

Fig. 1 Dimensioned sketch of the double coated tape cut with the knife plotter. The sketch is not to scale

Fluorescence detection

Figure 3 shows a sketch of the modified inverted microscope used for fluorescent interrogation of the microchip. For excitation, the output of a mercury arc lamp (HBO 50 W, Carl Zeiss, Thornwood, NY) was passed through two neutral density filters (ND-1, Edmund Optics, Barrington, NJ) in series to limit the light intensity, unless otherwise specified. The light passed through an excitation bandpass filter (426–446 nm, Chroma Technology Corp., Rockingham, VT), was reflected at 45° by a dichroic beam splitter (455 nm long-pass, Chroma Technology Corp.), and focused onto the analysis chamber by a 20 $\times$ objective (Ph2 Achrostigmat, NA = 0.45, Carl Zeiss). Emitted light was then collected through the same lens, passed through the dichroic beam splitter and an emission bandpass filter (460–500 nm, Chroma Technology Corp.). Optic filters were designed to match LCGreen® Plus (Herrmann et al., 2006). The collimated light was focused onto the end of a fiber optic cable (400 μm diameter UV/VIS range, CVI Spectral Products, Putnam, CT) with a lens of focal length 12.6 mm and diameter 25.4 mm (AT-SHL-9, CVI Spectral Products). The fiber optic was connected to a photomultiplier tube (PMT) module (714 Photomultiplier Detection System, Photon Technology International, Birmingham, NJ) with

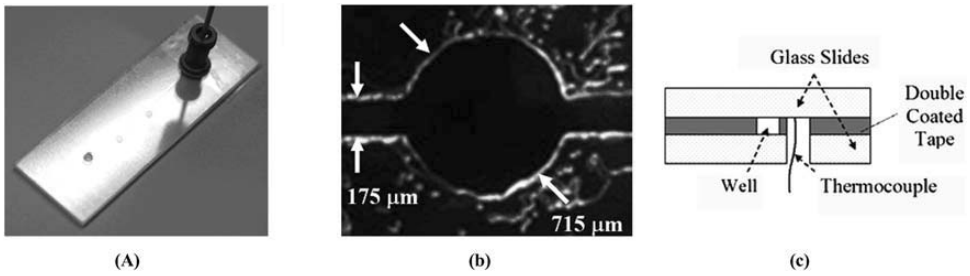

Fig. 2 (A). Photograph of the microchannel assembly with the entire chip being 25 × 75 mm. (B) Photograph of the 10 nl well with a wall height of 25 μm. (C) A cross-section sketch of the microchip at the 10 nl well. The sketch is not to scale

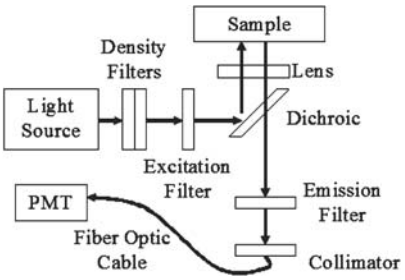

Fig. 3 Sketch of the optics set-up used in the modified inverted microscope

an R1527 PMT (Hamamatsu, Bridgewater, NJ). The analog output of the PMT module was input to a data acquisition (DAQ) card (PCI-MIO-16XE-10, National Instruments, Austin, TX) and analyzed with LabView 7.1 (National Instruments) on a personal computer. Figure 4 shows a diagram (A), and a photograph (B) of the custom system.

Temperature control

A 15 × 15 × 3.2 mm Peltier heater (TZ13153-03, Melcor, Trenton, NJ) contacted the glass slide directly above the interrogation well through a Zinc Oxide/Silicone based heat sink compound (TG-001, Melcor). A 7.5 × 3.5 × 3.5 cm steel block was placed on top of the heater as a heat sink. A J-type thermocouple (TT-J-40-50, Omega, Stamford, CT) was clamped, using a toothless alligator clip and Kapton tape, into a 2 mm diameter hole, drilled approximately 2–3 mm to the side of the analysis well, filled with heat sink compound (Fig. 2(C)). The signal from the thermocouple was amplified and linearized (AD594, Analog Devices, Norwood, MA) and the ouput was connected through a shielded I/O connector block (SCB-68, National Instruments) to the PCI-MIO-16XE-10 DAQ card. The temperature measurement was calibrated using a Fluke thermometer (54 II Thermometer, Fluke, Everett, WA) to within ±0.3°C at 50°C. Heating control was implemented using an analog output from a PCI-6014 DAQ card (National Instruments) connected to a shielded connector block (BNC-2110, National Instruments) that controlled a power supply (Zero-Up, Lamda Instruments, Neptune, NJ) connected to the Peltier device. A 550 mV input to the power supply was increased by 0.83 mV/s, resulting in a heating rate of 0.1°C/s over the temperature range of 65–85°C.

Sample preparation

Rapid cycle PCR was performed in a LightCycler® (Roche Applied Science, Indianapolis, IN) with programmed transition rates of 20°C/s. Each 10 μl mixture consisted of 50 ng of genomic DNA as the template, 0.5 μM of each primer, 200 μM of each deoxynucleotide triphosphate (dNTP), 0.4 U of KlenTaq1 polymerase (AB Peptides, St. Louis, MO), 88 ng of TaqStart antibody (ClonTech, Mountain View, CA), 2 mM $MgCl_2$, and 1 × LCGreen Plus (Idaho Technology, Salt Lake City, UT) in 50 mM Tris (pH 8.3) and 500 ng/μl bovine serum albumin (BSA). Genotyped human genomic DNA was obtained from Coriell Cell Repositories (Camden, NJ) for the *ATM* exon 17 and *HFE* C282Y DNA templates. For *CFTR* exon 10, genomic DNA was isolated and purified using the Puregene™ Genomic DNA Purification Kit (Gentra Systems, Minneapolis, MN) according to its standard protocol for 3 ml whole blood. The DNA concentration was then determined by absorbance at 260 nm (A_{260}), assuming an A_{260} of 1.0 is 50 ng/μl. The purity, according to the A_{260}/A_{280} absorption ratio, for all DNA templates was a minimum of 1.8.

Three different DNA targets were analyzed, two for mutation scanning and one for SNP genotyping. The *ATM* exon 17 PCR product (Genbank Acc.# NM 000051) (Kastan and Lim, 2000) was 84 base-pairs (bp) in length (5′-TGTCCTTTAGGGCAGCTGATATTCGGAGGAAATTG TTAAT**C**/**A**TTAATTGATTCTAGCACGCTAGAACCTAC CAAATCCCTCCACC-3′) with the SNP indicated in bold. It was amplified with primers 5′-TGTCCTTTAGGGCAGCT GAT-3′ and 5′-GGTGGAGGGATTTGGTAGGT-3′ by 30 temperature cycles of 95°C with a 0 s hold, 55°C with a 0 s hold, and 72°C with a 3 s hold.

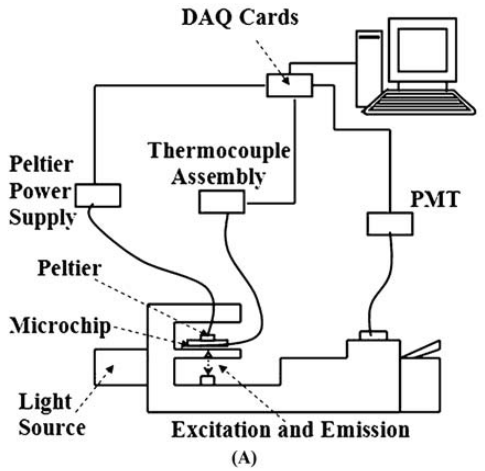

Fig. 4 (A). Diagram of the modified inverted microscope. (B) Photograph of the system with: (1) DAQ Cards; (2) Thermocouple assembly; (3) Photomultiplier assembly; (4) Microchip with thermocouple, Peltier heater, and heat sink; (5) Light source; (6) Excitation and emission filters and objective lens

The *CFTR* exon 10 PCR product (Genbank Acc.# M55115) was 201-bp in length (5′-ACTTCTAATGGTGATTATGGGAGAACTGGAGCCTTCAGAGGGTAAAATTAAGCACAGTGGAAGAATTTCATTCTGTTCTCAGTTTTCCTGGATTATGCCTGGCACCATTAAAGAAAATATCAT**CTT**TGGTGTTTCCTATGATGAATATAGATACAGAAGCGTCATCAAAGCATGCCAACTAGAAGAGGTAAGAAACTATGT-3′) with the 3-bp deletion F508del (Du et al., 2005) in bold. It was amplified with primers 5′-ACTTCTAATGGTGATTATGGG-3′ and 5′-ACATAGTTTCTTACCTCTTC-3′ after a 5 s denaturation at 95°C with 33 temperature cycles of 95°C with a 0 s hold, 54°C with a 0 s hold, and 72°C with a 4 s hold.

The *HFE* C282Y PCR product (Genbank Acc.# Z92910) (Settin et al., 2006) was 40-bp in length (5′-TGGGGAAGAGCAGAGATATACGT**G/A**CCAGGTGGAGCACCCA-3′) with the SNP in bold. It was amplified with primers 5′-TGGGGAAGAGCAGAGATATAC-3′ and 5′-TGGGTGCTCCACCTG-3′ after denaturation for 5 s at 95°C with 29 temperature cycles of 94°C with a 0 s hold, 55°C with a 1 s hold, and 72°C with a 1 s hold. For melting analysis of C282Y, one of the ND = 1.0 filters was replaced with a ND = 0.5 filter.

Microchip preparation

In order to prevent cross-contamination between samples, the microchannels were cleansed with DNA Away™ (Molecular BioProducts, San Diego, CA), flushed with DI water, and then coated with BSA (Al-Soud and Radstrom, 2001), at a concentration of 2.5 mg/ml, before each run. One channel was used for all genotypes of *ATM* exon 17 and one channel was used for *HFE* C282Y targets, allowing optimal temperature reproducibility between genotypes. *CFTR* exon 10 used two chips, one for each of the genotypes tested.

Melting curve acquisition and analysis

After amplification, the LightCycler capillary was transferred to an HR-1™ instrument (Idaho Technology) and heated at 0.1°C/s for a high-resolution reference melting curve. The sample was then spun out of the capillary into a microfuge tube and one μl of sample was injected into the channel inlet port using a micro-pipette. A syringe on the outlet port was used to pull the sample into the channel. The *x* and *y*-axis stage of the inverted fluorescent microscope (Axiovert 100, Carl Zeiss) was used to align the 10 nl well with the optics and the *z*-axis was used for focus. The sample was heated at 0.1°C/s with 20 data points acquired every 1°C. At least three melting curves were obtained for each genotype.

HR-1 and microchip melting data were analyzed using custom software written in LabView as previously described (Gundry et al., 2003; Wittwer et al., 2003). Fluorescence intensity values were normalized between 0 and 100% by defining linear baselines before and after the melting transition of each sample. Negative derivative plots for each curve were calculated using Savitsky-Golay (Press et al., 1992) polynomials of the second-degree at each point with a 33–40 point window for the microchip data. For data from the HR-1, a window of 60–90 points was used. The normalized melting curves reported for *CFTR* exon 10 had the temperature axis of each curve adjusted to superimpose each of the curves over a specified fluorescence interval, as described previously (Wittwer et al., 2003). Temperature axis adjustment allowed shape distinction between the two genotypes

tested. Signal-to-noise ratios (S/N) were calculated, as described previously (Herrmann et al., 2006).

Results and discussion

Solution-phase mutation scanning and SNP genotyping with DNA dyes can be performed within a microchip at a thousand-fold reduction in analysis volume from current systems. Complete genotyping at the C282Y locus was achieved with both homozygotes and the heterozygote easily differentiated. For scanning, a SNP heterozygote was detected within *ATM* exon 17 and a 3-bp deletion within *CFTR* exon 10. Mutation scanning is a process used to scan for mutations within a targeted region of DNA. Heterozygotes were easily identified for the known targets analyzed. Further study of previously unknown mutations would be necessary to establish the sensitivity and specificity of the method. These methods do not require any sample processing, electrophoretic separation, labeled probes, real-time PCR or allele-specific amplification.

Figure 5 shows derivative melting plots of normal and heterozygous DNA for a SNP within an 84-bp fragment of *ATM* exon 17. Panel (A) shows results from a 10 nl sample using the microchip system, in good agreement with panel (B), the HR-1 instrument with a 10 μl sample volume. The HR-1 instrument is the gold standard for high-resolution melting analysis with an absolute temperature standard deviation $< 0.02^{\circ}$C and 200 data points for every 1°C (Herrmann et al., 2006). In both systems, there is a clear distinction between heterozygous and homozygous products, observed as a change in curve shape. This shape change occurs because of the contribution of heteroduplexes to the overall melting curve as previously described (Gundry et al., 2003; Wittwer et al., 2003). Similarly, Fig. 6 shows ten derivative melting plots of both normal and heterozygous DNA for a 3-bp deletion within a 201-bp fragment of *CFTR* exon 10. The 10 nl volume plot (A) again shows good agreement with the 10 μl plot (B) and in both instruments, heterozygotes are clearly identified. The normalized and temperature axis adjusted melting curves showed a distinction by shape of the normal and heterozygous samples within the 10 nl plot (C) and the 10 μl plot (D). It is noted that the temperature variation between chips is large for this target yet the shape of the curves were all distinguishable, thus allowing correct detection of mutations for the 20 samples analyzed.

Figure 7 shows full genotyping at the C282Y locus of *HFE*. Again, the microchip data in (A) is very similar to the HR-1 data in (B). Heterozygous melting curves show the characteristic shape change resulting from heteroduplexes. Wild-type and mutant homozygotes are distinguished by their T_ms, with the mutant allele about 2°C lower than the wild-type allele.

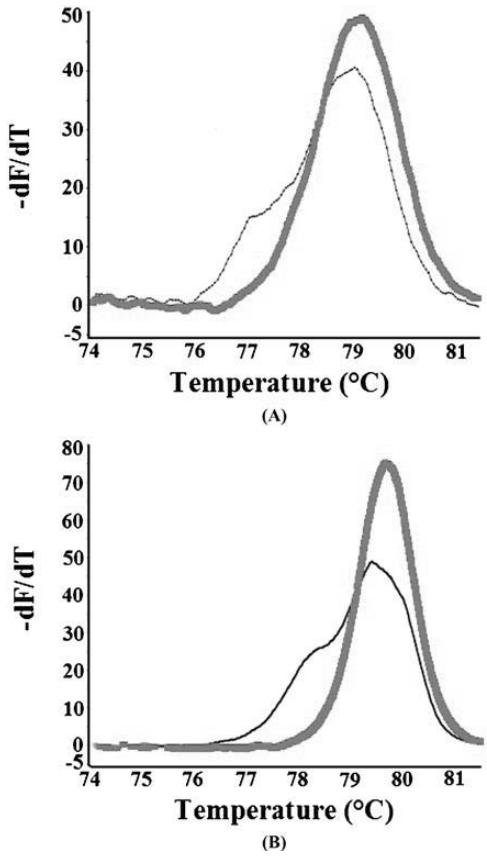

Fig. 5 Negative derivative plots for the microchip (A: 10 nl) and the HR-1 (B: 10 μl) using the *ATM* exon 17 target. Homozygous wild-type template (*red line*); heterozygous mutant template (*black line*)

Table 1 lists the S/N and T_ms for each genotype in both instruments. Even though the reaction volume is decreased by three orders of magnitude, the S/N for the microchip is only 1.5 orders of magnitude less than that of the HR-1. As can be seen from Figs. 5–7, the microchip S/N is adequate for both mutation scanning and genotyping. T_ms were similar on both instruments, although differences between 0.2–1.6°C were observed. These shifts were specific to each microchip studied and are explained by the thermal gradient across the Peltier heater (0.3–0.4°C/mm) and variation in the thermocouple placement relative to the analysis well (0.1–0.4 mm). A larger Peltier device and/or addition of a conducting plate between the heater and the melting chip should distribute heat more evenly. Broader melting transitions of the negative derivative plots were observed on the microchip relative to the HR-1 (Figs. 5–7). This broadening is an artifact of the Savitsky–Golay polynomials, due to the fact that fewer points were fitted for the microchip plots.

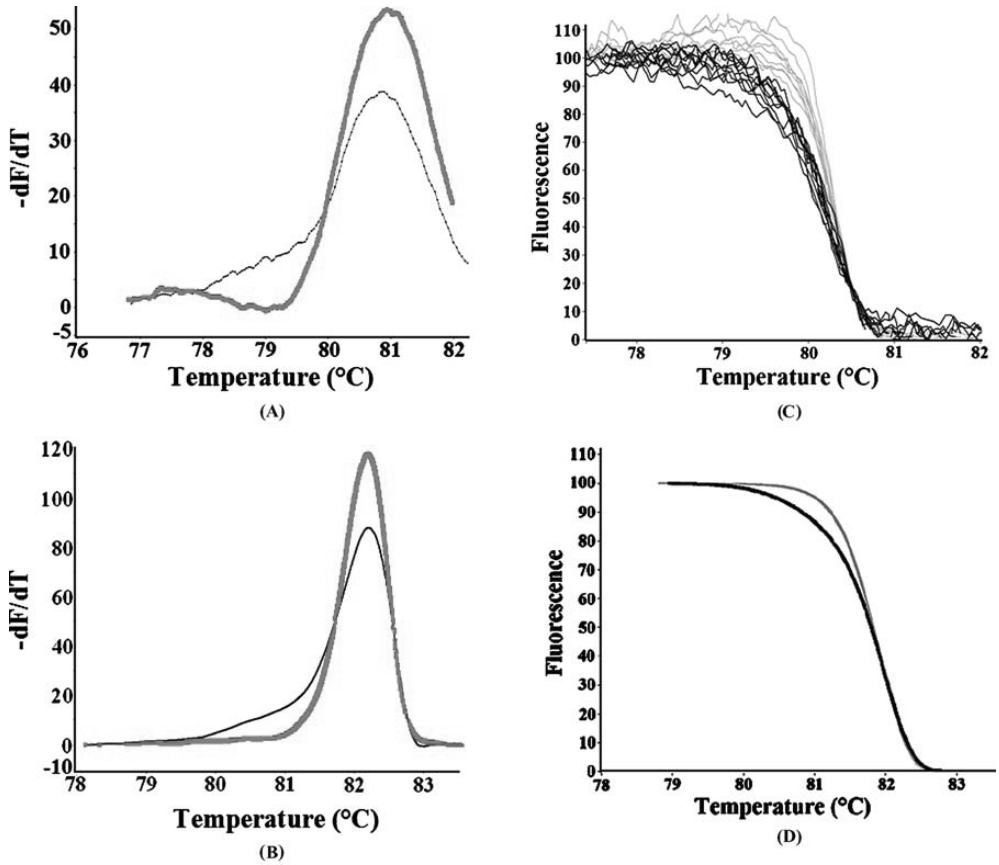

Fig. 6 Negative derivative plots for the microchip (A: 10 nl) and the HR-1 (B: 10 μl) using the *CFTR* exon 10 target. Homozygous wild-type template (*red line*); heterozygous mutant template (*black line*). Normalized and temperature axis shifted melting plots for the microchip (C: 10 nl) and the HR-1 (D: 10 μl) using the *CFTR* exon 10 target. Homozygous wild-type template (*gray lines*); heterozygous mutant template (*black lines*)

Figure 6(C) and (D) indeed show that the slopes of the melting curves between the microchip and HR-1 are very similar.

The Xurography microchip manufacturing process was appealing because it did not require clean room techniques, thus lowering manufacturing costs, and the fabrication was quite rapid (a microchip could be built and DNA tests performed within a working day). One other group has previously reported the use of this manufacturing technique, fabricating a DNA extraction microchip (Kim et al., 2005). Using Xurography, a microchip channel design was cut out of an adhesive-backed plastic and placed within a Petri dish to create a polydimethylsiloxane (PDMS) mold. The method used here is even simpler because no further fabrication processes are required beyond Xurography.

The standard mercury light source in the microscope was far too bright when focused on the sample, causing rapid photobleaching. Neutral density filters were used to reduce the excitation intensity and better match the fluorescence emission to the photomultiplier detector used. Alternative light sources, such as high intensity LEDs to flood illuminate a small area without precise focusing are interesting options. Furthermore, a charge-coupled-device (CCD) camera could image a DNA melting array microchip, thereby creating a higher throughput system. CCDs, although not as sensitive as PMTs, should provide sufficient S/N for nanoliter volume melting of amplified DNA.

Conclusion

Solution-phase DNA melting analysis for mutation scanning and genotyping can be performed in 10 nl reaction chambers within a microchip. The 1000-fold reduction in sample volume from 10 μl in state-of-the art commercial systems to

Table 1 Signal-to-noise (S/N) and melting temperatures (T_ms) of seven genotypes at three loci on the HR-1 (10 μl) and microchip (10 nl) instruments

	S/N		T_m (°C)		
	HR-1	Microchip[a]	HR-1	Microchip[b]	ΔT_m[c]
ATM exon 17					
Homozygous wild-type	2450	69	79.7	78.8 ± 0.7	0.9
Heterozygous mutant	2800	63	79.5	78.1 ± 0.8	1.4
CFTR exon 10					
Homozygous wild-type	5000	168	82.4	80.7 ± 0.5	1.7
Heterozygous mutant	5350	135	82.4	79.9 ± 0.3	2.5
HFE C282Y					
Homozygous wild-type	2680	76	79.6	79.4 ± 0.6	0.2
Heterozygous mutant	2290	60	78.4	77.8 ± 0.7	0.6
Homozygous mutant	2560	111	77.9	77.5 ± 0.5	0.4

[a]Microchip S/N values are averaged over 3 unique melt curves for each genotype of *ATM* exon 17 and *HFE* C282Y. *CFTR* exon 10 represents averaged values over ten unique melt curves for each genotype.

[b]Microchip T_m reports the average value over three melts for *ATM* exon 17 and *HFE* C282Y targets and an average value over ten melts for *CFTR* exon 10 with the standard deviation.

[c]Values represent the difference between the HR-1 T_m and the averaged Microchip T_m.

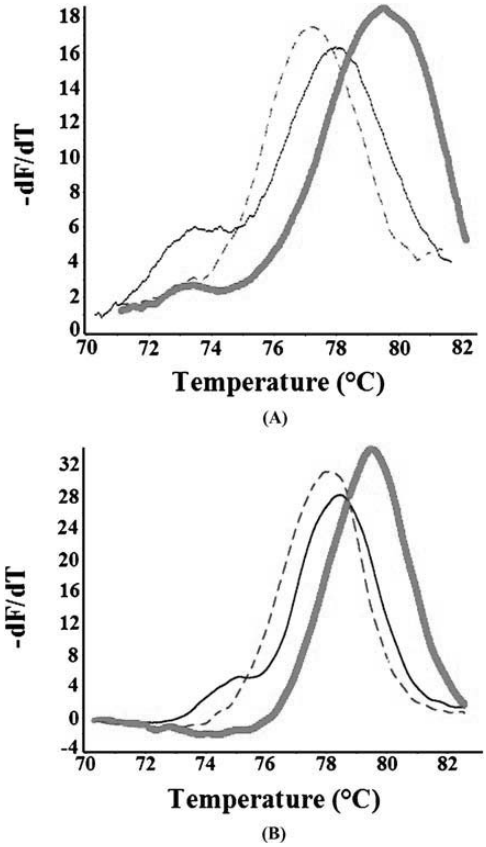

Fig. 7 Negative derivative plots for the microchip (A: 10 nl) and the HR-1 (B: 10 μl) using the *HFE* C282Y target. Homozygous wild-type template (*red line*); heterozygous mutant template (*black line*); homozygous mutant template (*blue dashed line*)

10 nl on the microchip does result in a lower S/N, but is entirely adequate for detecting and genotyping SNPs. Mutation scanning was performed in 84 and 201-bp PCR products, and complete SNP genotyping by melting a 40-bp target. The characteristic features of the melting curves necessary for scanning and genotyping are produced by both the nl microchip and the μl commercial instrument. The next logical step is to integrate PCR with melting analysis on the microchip, potentially in an array format. Such a system would be relatively easy to fabricate and could provide a rapid, inexpensive, high-throughput mutation scanning and genotyping solution that requires no separations, processing, or labeled probes.

Acknowledgments This work was funded by State of Utah Center of Excellence grants for Biomedical Microfluidics and for Homogeneous DNA Melting Analysis, and NSF IGERT grant number DGE-9987616. We thank Luming Zhou and Gudrun Reed for providing samples and PCR protocols for the *ATM* exon 17 and *CFTR* exon 10 targets. We also thank Dr. Wittwer's lab group and Dr. Gale's lab group for valuable advice pertaining to this research.

References

W.A. Al-Soud and P.J. Radstrom, Clin. Microbiol. **39**(2), 485–493 (2001).

D.A. Bartholomeusz, R. Boutté, and J.D. Andrade, J. MEMS **14**, 1364–1374 (2005).

A. Dodge, G. Turchatti, I. Lawrence, N.F. de Rooij, and E. Verpoorte, Anal. Chem. **76**, 1778–1787 (2004).

K. Du, M. Sharma, and G.L. Lukacs, Nat. Struc. Mol. Biol. **12**(1), 17–25 (2005).

A. Gulliksen, L. Solli, F. Karlsen, H. Rogne, E. Hovig, T. Nordstrom, and R. Sirevåg, Anal. Chem. **76**, 9–14 (2004).

C.N. Gundry, J.G. Vandersteen, G.H. Reed, R.J. Pryor, J. Chen, and C.T. Wittwer, Clin. Chem. **49**(3), 396–406 (2003).
M.G. Herrmann, J.D. Durtschi, L.K. Bromley, C.T. Wittwer, and K.V. Voelkerding, Clin. Chem. **52**, 494–503 (2006).
A.F.R. Hühmer and J.P Landers, Anal. Chem. **72**, 5507–5512 (2000).
M.S. Ibrahim, R.S. Lofts, P.B. Jahrling, E.A. Henchal, V.W. Weedn, A. Northrup, and P. Belgrader, Anal. Chem. **70**, 2013–2017 (1998).
M.B. Kastan and D.S. Lim, Nat. Rev. Mol. Cell Biol. **1**, 179–186 (2000).
J. Khandurina, T.E. McKnight, S.C. Jacobson, L.C. Walters, R.S. Foote, and J.M. Ramsey, Anal. Chem. **72**, 2995–3000 (2000).
J. Kim, K.V. Voelkerding, and B.K. Gale, in 3rd Annual International IEEE EMBS Special Topic Conference on Microtechnologies in Medicine and Biology, Kahuku, Oahu, HI, (May 12–15, 2005), pp. 5–7.
E.T. Lagally, C.A. Emrich, and R.A. Mathies, Lab on a Chip **1**, 102–107 (2001).
M. Liew, R. Pryor, R. Palais, C. Meadows, M. Erali, E. Lyon, and C. Wittwer, Clin. Chem. **50**(7), 1156–1164 (2004).
J. Liu, M. Enzelberger, and S. Quake, Electrophoresis **23**, 1531–1536 (2002).
H. Nagai, Y. Murakami, Y. Morita, K. Yokoyama, and E. Tamiya, Anal. Chem. **73**, 1043–1047 (2001).
M.A. Northrup, M.T. Ching, R.M. White, and R.T. Watson, Transducers **93**, 924–927 (1993).
W.H. Press, S.A. Teukolsky, W.T. Vetterling, and B.P. Flannery, Numerical Recipes in C, 2nd ed. (Cambridge University Press, New York 1992), pp. 650–655.
G.H. Reed and C.T. Wittwer, Clin. Chem. **50**(10), 1748–1754 (2004).
K.M. Ririe, R.P. Rasmussen, and C.T. Wittwer, Anal. Biochem. **245**, 154–160 (1997).
R.K. Saiki, S. Scharf, F. Faloona, K.B. Mullis, G.T. Horn, H.A. Erlich, and N. Arnheim, Science **230**, 1350–1354 (1985).
A. Settin, M. El-Bendary, R. Abo-Al-Kassem, and R. El Baz, J Gastrointestin Liver Dis. **15**(2), 131–135 (2006).
E. Verpoorte, Electrophoresis **23**, 677–712 (2002).
L.C. Waters, S.C. Jacobson, N. Kroutchinina, J. Khandurina, R.S. Foote, and J.M. Ramsey, Anal. Chem. **70**, 5172–5176 (1998).
C.T. Wittwer, G.C. Fillmore, and D.J. Garling, Anal. Biochem. **186**(2), 328–331 (1990).
C.T. Wittwer, G.H. Reed, C.N. Gundry, J.G. Vandersteen, and R.J. Pryor, Clin. Chem. **49**(6), 853–860 (2003).
D.S. Yoon, Y. Lee, Y-S. Lee, Y. Lee, H.J. Cho, S.W. Sung, K.W. Oh, J. Cha, and G.J. Lim, Micromech. Microeng. **12**, 813–823 (2002).
L. Zhou, A.N. Myers, J.G. Vandersteen, L. Wang, and C.T. Wittwer, Clin. Chem. **50**(8), 1328–1335 (2004).

Addendum

This chapter makes S/N comparison between a commercial instrument and a custom microchip. The published manuscript states that the microchip reaction volume used is a thousand-fold less than the commercial instrument's reaction volume but that S/N for the microchip is only reduced by 1.5 orders of magnitude. It is clarified that this is a comparison of fluorescently interrogated volumes, not reaction volumes, since the microchip actually requires 1 μL to load. Within the commercial instrument the entire 10 μL is interrogated within a capillary tube so an interrogated volume comparison is accurate.

CHAPTER 3

COMPARISON OF GLASS ETCHING TO XUROGRAPHY PROTOTYPING OF MICROFLUIDIC CHANNELS FOR DNA MELTING ANALYSIS

This chapter has been reprinted with permission from IOP Publishing. The manuscript is published in Journal of Micromechanics and Microengineering, DOI 10.1088/0960-1317/17/12/003. Authors are Jenny Greer, Scott O. Sundberg, Carl T. Wittwer, and Bruce K. Gale.

IOP Publishing Journal of Micromechanics and Microengineering
J. Micromech. Microeng. **17** (2007) 2407–2413 doi:10.1088/0960-1317/17/12/003

Comparison of glass etching to xurography prototyping of microfluidic channels for DNA melting analysis

Jenny Greer[1], Scott O Sundberg[2], Carl T Wittwer[3] and Bruce K Gale[1]

[1] Department of Mechanical Engineering, University of Utah, UT, USA
[2] Department of Bioengineering, University of Utah, UT, USA
[3] Department of Pathology, University of Utah, UT, USA

Received 31 May 2007, in final form 27 September 2007
Published 25 October 2007
Online at stacks.iop.org/JMM/17/2407

Abstract
Two microchannel manufacturing methods—xurography of double-sided tape and glass etching (lithography and wet etching)—were compared using DNA melting analysis. A heterozygous mutation (3 base-pair deletion) was distinguished from wild type (normal) DNA in 10 nL (xurography and glass etching) and 1 nL (xurography) volumes. The results of the 10 nL and 1 nL melting curves were compared to results using commercial high-resolution instrumentation with 10 μL volumes. These 1000-fold and 10 000-fold volume reductions reduced the signal-to-noise ratio (SNR) only 29-fold and 40-fold for xurography (10 nL and 1 nL, respectively,) and 39-fold for 10 nL glass etched microchannels, still providing adequate discrimination for mutation detection. The reduced SNR of the glass etched microchannels compared to the tape microchannels was due to the in-house bonding process which gave poor optical quality on the surface of the microchip. Xurography of double-sided tape reduces the cost by 20 fold and is four times faster to manufacture than glass etching. Microchips created using the rapid prototyping technique of xurography are a reasonable prototyping alternative to channels created using traditional glass etching for DNA mutation detection.

(Some figures in this article are in colour only in the electronic version)

Introduction

Microfluidic technology for use in medical diagnostics, forensics, microbial detection and other bio-analysis has generated enormous interest in recent years (Verpoorte 2002). An important analytical tool is the polymerase chain reaction (PCR) (Sailki *et al* 1985), which can amplify a small region of DNA over 10^6 fold in 10–15 min (Wittwer *et al* 1990). As a complement to PCR, DNA melting analysis was introduced in 1997 as a method of product identification (Ririe *et al* 1997) though DNA melting, or denaturation, was used to analyze the GC content of DNA as early as 1968 (Mandel and Marmur 1968). In DNA melting analysis, a fluorescent dye is present which only fluoresces when the DNA is in double helix form. DNA melting occurs as the DNA sample is heated, causing the double helix to separate into two strands. Mutations are detected by analyzing the melting curve (Wittwer *et al* 2003). Specific mutations manifest themselves as a shift in temperature, a change in shape or a combination of these (Gundry *et al* 2003). Current research is focused on miniaturizing these processes to allow for high throughput at a reduced cost while maintaining sufficient SNR.

The traditional method for creating microfluidic PCR devices is photolithography (Simpson *et al* 1998) with wet etching (Iliescu and Tay 2005) using glass substrates. This method requires a clean room to fabricate the channels, and can be quite costly and time consuming. In recent years, rapid prototyping technology for microfluidic devices has greatly improved. Rapid prototyping is advantageous because designs can be created quickly and at a reduced cost compared to

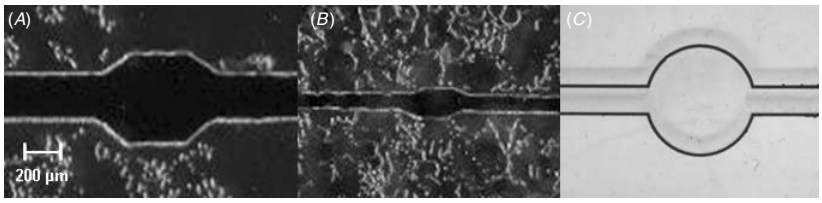

Figure 1. DNA analysis wells: (*A*) 10 nL well in tape with 25 μm depth, (*B*) 1 nL well in tape with 25 μm depth and (*C*) 10 nL well in glass with 22 μm depth.

traditional methods. This allows for more designs to be tested in a given period of time, increasing the effectiveness of the design phase. Some of the rapid prototyping technologies include soft lithography techniques (Xia and Whitesides 1998) with poly(dimethylsiloxane) PDMS (Shin *et al* 2003, Duffy *et al* 1999, Kaigala *et al* 2007), laser micromachining (Yao *et al* 2005, An *et al* 2006), micropowder blasting (Yagyu *et al* 2005) and micromachining (Schabmueller *et al* 2000, Neuzil *et al* 2006) with glass or polymer substrates.

Recently, xurography (Bartholomeusz *et al* 2005) was shown to be an effective method for developing microfluidic channels. Xurography is the process of using a knife plotter to cut various microfluidic designs out of assorted polymer sheets. The unwanted portions of the polymers are removed and the remaining polymer is placed on a substrate for use. Xurography is an attractive alternative to other rapid prototyping techniques due to its fast fabrication time, lack of dependence on clean room facilities, and low equipment and material cost. Using polymers with adhesives on both sides allows for rapid bonding and sealing. Another appealing characteristic of xurography is its dimensional accuracy of 10 μm with feature variability down to 2 μm. In a recent example, the xurography process was used to create a microfluidic channel and analysis well out of a biocompatible tape, which was then used to perform DNA melting analysis (Sundberg *et al* 2007). In the current work, xurography is compared to glass microchip fabrication.

Materials and methods

Microfluidic chip fabrication

Xurography was used to manufacture the tape-bonded microchannels. A knife plotter (Graphtec, Irvine, CA) cut the geometric designs, created using Adobe Illustrator® (Adobe, San Jose, CA), out of 25 μm thick double coated tape (9019, 3M, St Paul, MN). A rhomboidal shape was chosen for the well design to reduce the amount of bubbles in the well compared to a circular shaped well. The rhomboidal well for 10 nL, as seen in figure 1(*A*), expands the channel width of 300 μm to a maximal width of 570 μm for 400 μm over its 800 μm length. The 1 nL rhomboidal well, as seen in figure 1(*B*), expands the channel width of 100 μm to a maximal width of 200 μm for 200 μm over its 400 μm length. Circular wells of 2 mm diameter are placed 25 mm from center on either side of the analysis wells for inlet and outlet ports. The tape is sandwiched between two 25 mm $\times$ 75 mm glass slides (12–550A, Fisher Scientific, NH). One of the glass slides has two 2 mm holes drilled through the glass slide using a Dremel tool with a diamond drill bit. The holes drilled through the glass correspond to the inlet and outlet ports in the tape. To insure a good bond between the glass and tape, the microfluidic chip is clamped with four spring-loaded clips before being placed in a 65 °C oven for 45 min.

Photolithography and wet etching were used to manufacture the glass-bonded microfluidic chips. A 25 mm $\times$ 75 mm soda lime glass microscope slide was pre-cleaned with a piranha etch (3 H_2SO_4: 1 H_2O_2) for 10 min. The etch mask was formed by sputtering (Denton Discovery 18, Denton Vacuum, Moorestown, NJ) a 900 nm layer of chromium onto the glass slide followed by a 2 μm layer of photoresist (1813, Shipley, Marlborough, MA) which was patterned using standard photolithographic procedures. The glass slide was then baked at 120 °C for 60 min and DuPont Kapton tape (5419, 3M) used to mask the uncoated side of the glass slide. Exposed metal was removed by dipping the slide into a chromium etch bath (1 HF: 3HNO_3: 10 H_2O) for 17 min at room temperature. The remaining photoresist and chromium were stripped off by dipping the glass slide into acetone before placing it in a chromium etch bath for 5 min at room temperature. The resulting microfluidic channel was 150 μm in width and 25 μm deep with a circular analysis well of 670 μm diameter, as seen in figure 1(*C*). At each end of the 50 mm channel two circular wells were pattered as guides for the inlet and outlet ports, and were later drilled through using a Dremel tool with a diamond drill bit. The etched glass slide, along with a new glass slide, was put into piranha etch for cleaning. The two glass slides were fused together by baking them at 620 °C for 4 h under 58 Pa of pressure. See figure 2 for a comparison of this technique with xurography as described above.

Loading fluid into the analysis well is the same for the tape- and glass-bonded channels. The sample is loaded into the inlet port and drawn through the channel and well by vacuum pressure created with the use of a syringe at the outlet port. A NanoPort™ assembly (Upchurch Scientific, Oak harbor, WA) is attached to the glass over the outlet port and is connected to the syringe with a luer fitting. Figure 3 shows a picture of microfluidic chip sample loading.

Sample preparation

PCR was performed in a LightCycler® (Roche Applied Science, Indianapolis, IN) having a 20 °C s^{-1} transition rate. The initial denaturation occurred at 95 °C with a 5 s hold time, followed by 33 temperature cycles of 95 °C with no hold time, 54 °C with no hold time and 72 °C with a 4 s hold time.

Each 10 μL mixture of CFTR exon 10 consisted of 200 μM deoxynucleotide triphosphate (dNTP), 0.4 U

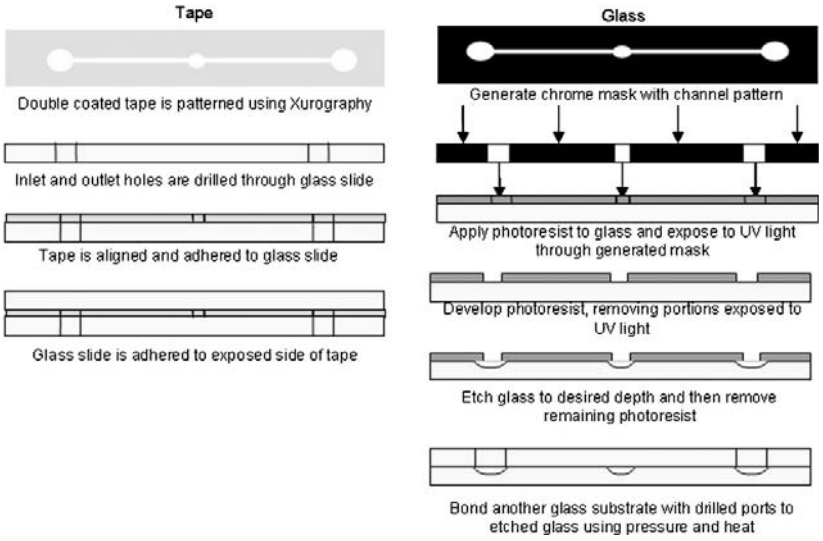

Figure 2. Direct comparison of the process used to create microfluidic DNA melting analysis chips using xurography with double-sided tape and the glass etching method (lithography and wet etching).

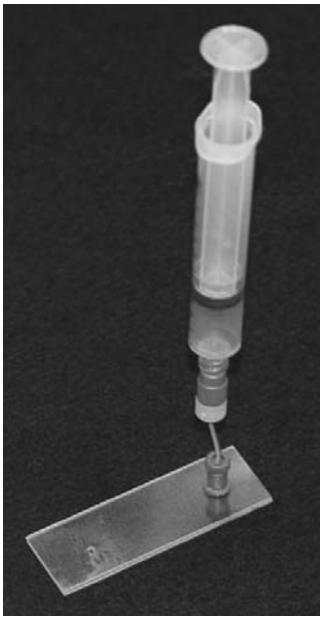

Figure 3. Loading the microfluidic channel, including the chip, the NanoPort™ assembly and the syringe.

KlenTaq1 polymerase (AB Peptides, St Louis, MO), 88 ng TaqStart antibody (ClonTech, Mountain View, CA), 2 mM $MgCl_2$, 1X LCGreen Plus (Idaho Technology, Salt Lake City, UT) fluorescent dye, 0.5 μM of each primer in 50 mM Tris (pH 8.3), 500 ng μL^{-1} bovine serum albumin (BSA) and 50 ng human genomic DNA as the template. The Puregene™ Genomic DNA Purification Kit (Gentra Systems, Minneapolis, MN) was used to isolate and purify the genomic DNA using 3 mL of whole blood. The DNA concentration was then determined by absorbance at 260 nm (A_{260}), assuming that an A_{260} of 1.0 is 50 ng μL^{-1}. The purity, according to the A_{260}/A_{280} absorption ratio, for all DNA templates was a minimum of 1.8.

The CFTR exon 10 PCR product (Genbank Acc.# M55115) was 201 base pairs in length with the 3 base pair deletion F508del (Du *et al* 2005). Primers used to amplify the segment were 5'-ACTTCTAATGGTGATTATGGG-3' and 5'-ACATAGTTTCTTACCTCTTC-3'.

Microchannel preparation

Before the sample is loaded into the tape-bonded microchannels, the channel is coated with 2.5 mg mL^{-1} BSA by filling the channel with 2.5 mg mL^{-1} BSA at room temperature for approximately 30 s. The channel is then placed in a vacuum with a pressure of 12 psi for 1 h to remove excess gas trapped by the adhesive. This process reduces the amount of PCR product (amplicon) that sticks to the channel walls and reduces bubble formation in the channel. Higher concentrations of BSA reduced the SNR, as BSA has some fluorescence, while lower concentrations allowed more amplicon to stick to the channel walls. Different microchips were used for each genotype.

The glass-bonded microchannels were filled with 0.25 mg mL^{-1} BSA at room temperature for approximately 30 s before the sample was loaded into the channel to reduce the amount of amplicon that sticks to the channel walls. This BSA concentration was optimal with glass for maintaining adequate SNR while reducing the amount of amplicon sticking to the channel walls. Between sample runs, the channel was cleaned with DNA Away™ (Molecular BioProducts, San Diego, CA), and flushed three times with DI water before filling with 0.25 mg mL^{-1} BSA.

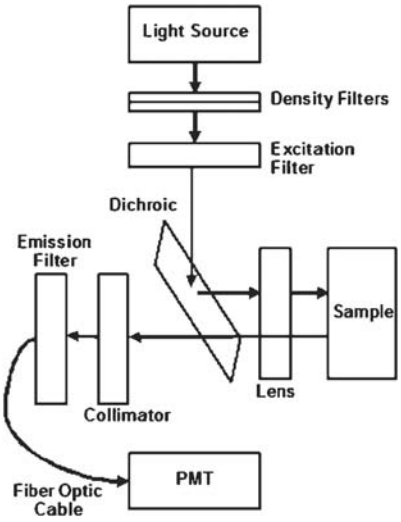

Figure 4. Diagram of the modified inverted microscope optics.

Fluorescence detection

A modified inverted microscope was used for fluorescence detection of the analysis chamber (figure 4). Excitation was achieved by limiting the light intensity of a mercury arc lamp (HBO 50 W, Carl Zeiss, Thornwood, NY) by passing it through a series of neutral density filters (Edmund Optics, Barrington, NJ), whose values are given in table 1 for each microfluidic channel. The excitation light passed through a band pass filter (426–446 nm, Chroma Technology Corp., Rockingham, VT) before being reflected at a 45° incidence angle by a dichroic beam splitter (455 nm long-pass, Chroma Technology Corp.). The light was then focused onto the sample in the analysis chamber by a 20× objective (Ph2 Achrostigmat, NA = 0.45, Carl Zeiss) for the 10 nL analysis chambers or a 32× objective (Ph1 Achrostigmat, NA = 0.40, Carl Zeiss) for the 1 nL analysis chamber. When using this configuration, the excitation volume equals the analysis chamber volume. The emitted light was then collected by the same objective lens, directed back through the dichroic beam splitter and an emission bandpass filter (460–500 nm, Chroma Technology Corp.) A lens with focal length 12.6 mm and diameter 25.4 mm (AT-SHL-9, CVI Spectral Products) then focused the light into the end of a fiber optic cable (400 μm diameter UV/VIS range, CVI Spectral Products, Putnam, CT). A photomultiplier tube (PMT) module (714 Photomultiplier Detection System, Photon Technology International, Birmingham, NJ) with a R1527 PMT (Hamamatsu, Bridgewater, NJ) was connected to the fiber optic cable. A data acquisition (DAQ) card (PCI-MIO-16XE-10, National Instruments, Austin, TX) collected the analog output of the PMT module before being analyzed on a personal computer using LabView 7.1 (National Instruments). Figure 5 shows a diagram (*A*) and a photograph (*B*) of the custom system.

Temperature control

To heat the microfluidic chips uniformly, two 6.4 mm thick aluminum blocks were stacked to create a 13 mm

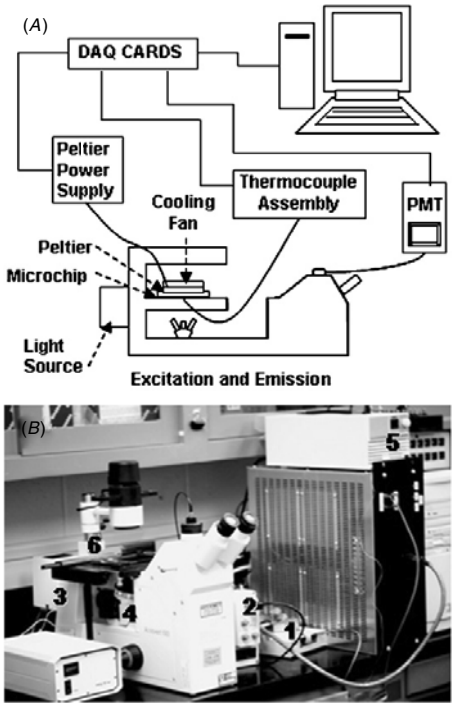

Figure 5. (*A*) Diagram of the modified inverted microscope. (*B*) Photograph of the system with (1) DAQ cards, (2) a photomultiplier assembly, (3) a light source, (4) excitation and emission filters and objective lens, (5) a thermocouple assembly and (6) a microfluidic chip with a thermocouple, a Peltier heater and a heat sink.

Table 1. Neutral density filter values.

	Normal	Mutation
10 nL tape	0.6	0.6
10 nL glass	0.9	1.5
1 nL tape	0.6	0.4

conduction plate. This plate was attached to a 20 × 40 × 3.2 mm Peltier heater (HT4-6-21×43, Melcor, Trenton, NJ) using a zinc oxide/silicone (TG-001, Melcor) heat compound. The aluminum block was placed directly on the glass microchannels over the interrogation well. A metal fin measuring 53 × 53 × 25 mm attached to a small fan (50 × 50 × 10 mm, Commitment to Keep, Inc., Addison, TX) acted as a heat sink and was placed on top of the heater. The Peltier was connected to a power supply (Zero-Up, Lambda Instruments, Neptune, NJ) that was controlled through a shielded connector block (BNC-2110, National Instruments) by an analog output from a PCI-6014 DAQ card (National Instruments). A heating rate of 0.1 °C s^{-1} over a range of 70–88 °C was achieved by increasing a 4.7 V power supply input by 6.4 mV s^{-1}. A J-type thermocouple (TT-J-40-50, Omega, Stamford, CT) was placed in a 2 mm diameter hole, drilled 1–2 mm way from the interrogation well, filled with heat compound. Kapton tape secured the thermocouple to the glass slide. Photographic tape (235, 3M) was placed over the Kapton tape to eliminate

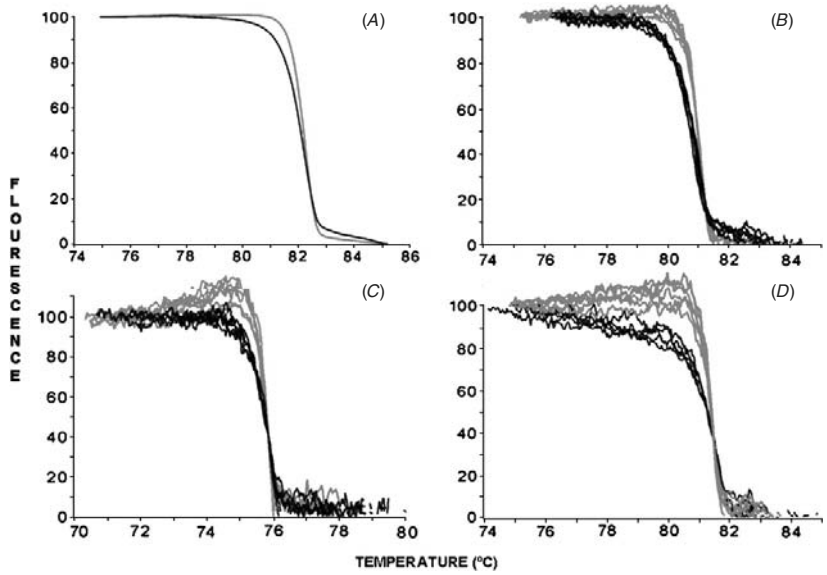

Figure 6. Melting curves for normal DNA (red) and heterozygous DNA (black) found using: (*A*) commercial HR-1^{TM}, (*B*) 10 nL tape, (*C*) 10 nL glass and (*D*) 1 nL tape.

excess fluorescence. The thermocouple signal was amplified and linearized (AD594, Analog Devices, Norwood, MA) before being sent to a PCI-MIO-16XE-10 DAQ card through a shielded I/O connector block (SCB-68, National Instruments). Calibration of the temperature to within ± 0.3 °C at 50 °C was accomplished with a Fluke thermometer (54 II Thermometer, Fluke, Everett, WA).

Melting curve acquisition and analysis

A high resolution reference melting curve was obtained after amplification by transferring the LightCycler® capillary to a HR-1^{TM} instrument (Idaho Technology) that was heated at 0.1 °C s^{-1}. The sample was then spun into a microfuge tube. Using a micropipette, 2 μL of sample was inserted into the inlet port of the microchannel. The sample was then drawn through the channel using vacuum pressure created by a syringe on the outlet port. Plugs designed to fit snugly over the inlet and outlet ports, made of Parafilm (PM-996, Pechiney Plastic Packaging, Menasha, WI), were placed over the ports and held firmly with Kapton tape. The analysis chamber was aligned with the optics using the *x*- and *y*-axis stage of the inverted microscope, while focus was achieved using the *z*-axis. Two data points were acquired every second as the sample was heated at a rate of 0.1 °C s^{-1}.

Custom LabView (Gundry *et al* 2003, Wittwer *et al* 2003) software analyzed the data from the HR-1^{TM} and the microfluidic chip. The fluorescence intensity data was normalized by defining a linear baseline before and after the melting transition of each sample. Then, the curves were superimposed by adjusting the temperature axis in order to compare the melting curve shapes. Signal-to-noise ratios (SNR) were calculated for each sample as described previously (Herrmann *et al* 2006).

Results and discussion

Mutation detection using DNA melting in the 10 nL tape bonded microchannels was comparable to the traditional glass-bonded 10 nL microchannels in terms of the SNR, temperature variation and shape distinction of melting curves. 10 nL is about a 1000 fold reduction from current commercial systems for DNA melting analysis. Figure 6 shows the melting curves for PCR products amplified from normal DNA (red) and heterozygous DNA (black). Heterozygous sequence variants are identified by the altered shape in the melting curve, which is a result of heteroduplexes (Gundry *et al* 2003*, Wittwer et al* 2003), or mismatched pairs in DNA duplexes. Panel (*A*) shows melting curves from the commercial HR-1^{TM} instrument using a 10 μL sample. The HR-1^{TM} instrument, the current 'gold standard' for high-resolution melting analysis, records 200 data points for every 1 °C and has a standard deviation of less than 0.02 °C (Herrmann *et al* 2006). Panels (*B*) and (*C*) show melting curves for a 10 nL sample using the tape-bonded channels and the glass-bonded channels, respectively. The results of six melting curves for each fabrication method are in agreement with the standard HR-1^{TM} instrument, and are comparable. Panel (D) shows the melting curves for 1 nL samples using xurography to create tape-bonded channels.

Table 2 lists the SNR and the melting curve temperature (T_m) for each of the melting analysis chambers. The SNR of the 10 nL melting curves for both the glass-bonded and tape-bonded microchannels is 1.5 orders of magnitude smaller than the commercial HR-1^{TM} system, while the volume was reduced by 3 orders of magnitude. The SNR of the 10 nL tape bonded microchannels was comparable to that of the glass-bonded microchannels. The SNR for the 1 nL tape bonded microchannel is approximately 30% less than that of the 10 nL tape bonded channels. The T_m standard deviations were between 0.1–0.8 °C.

Table 2. SNRs and average T_ms for the melting curves.

	HR-1		10 nL Tape		10 nL Glass		1 nL Tape	
	Normal	Mutation	Normal	Mutation	Normal	Mutation	Normal	Mutation
SNR[a]	5470	5040	188	174	131	136	126	135
SD[b]			±15	±10	±12	±6	±17	±18
T_m (°C)[c]	82.2	82.2	82.4	81.1	78.3	77.0	81.5	81.4
SD[b]			±0.1	±0.3	±0.3	±0.8	±0.1	±0.5

[a] SNRs are an average of six melting curves.
[b] SD (standard deviation for six melting curves).
[c] T_ms are an average of six melting curves for each genotype before temperature shifting.

The difference between the SNR from the tape and glass-bonded microchannels, with tape being slightly higher, suggests that the capabilities of the two techniques are similar and xurography can be used in place of glass etching. The lower SNR than that seen in the HR-1™ are likely caused by more than just the reduction in volume. For the glass- and tape-bonded microchannels, the signal is reduced if light is scattered from small imperfections along the edges of the analysis chambers. These imperfections can be created during manufacturing. For photolithography, residual stresses in the chrome layer may create an uneven etch, while small vibrations in the cutting blade used in xurography may create an uneven cut. For the glass-bonded microchannels, some loss in SNR can be explained by the poor optical quality of the glass chips. Metal blocks are used as weights to provide pressure for bonding the glass slides together during the sealing process. Although the metal blocks are reasonably smooth, small imperfections may be transferred onto the surface of the glass channels. These small imperfections on the glass surface may disrupt the optical path, thus reducing the amount of light and decreasing the SNR. The decreased SNR caused by the metal blocks could be overcome with better, more expensive and time-consuming techniques and equipment, such as a mask bonder/aligner (Grosse *et al* 2001) or anodic bonding (Berthold *et al* 2000). In the tape-bonded channels, the SNR could be increased by using a different type of adhesive or other bonding material. The double-sided tape used for this process also has some background fluorescence which decreases the SNR. The temperature variations are accounted for by thermocouple placement relative to the analysis well (1–2 mm variation). However, these temperature variations do not matter for heterozygous variant detection as shape is used to distinguish these variants from normal DNA (Sundberg *et al* 2007).

Despite these imperfections, the SNRs for the tape and glass-bonded channels are adequate for mutation scanning and detection, as seen in figure 6. Tape-bonded microchannels are an effective alternative to the traditional glass-bonded microchannels. One of the major advantages of the tape-bonded microchannels is the cost. The traditional glass microfluidic chips have a material and equipment cost of $400.00 for six microchips, while the tape-bonded microchannels cost less than $2.00 for six microchips. A second advantage of the tape-bonded microchips is the time in which the microchannels can be made. To make six tape-bonded microchannels, it takes approximately 2 h to fabricate and assemble, with an additional 45 min of bake time for bonding purposes. In contrast, the glass-bonded microchannels take approximately 8 h to fabricate, with an additional 4.5 h of bake time to bond the channels. Including the price of labor with the total manufacturing costs, the price would be over $750 for six glass microchips, while the tape channels are $41 for six, assuming the labor is $20 dollars an hour. To have glass-bonded microchannels fabricated professionally, it is approximately $6000 for six chips. Figure 7 summarizes the time and cost of each method.

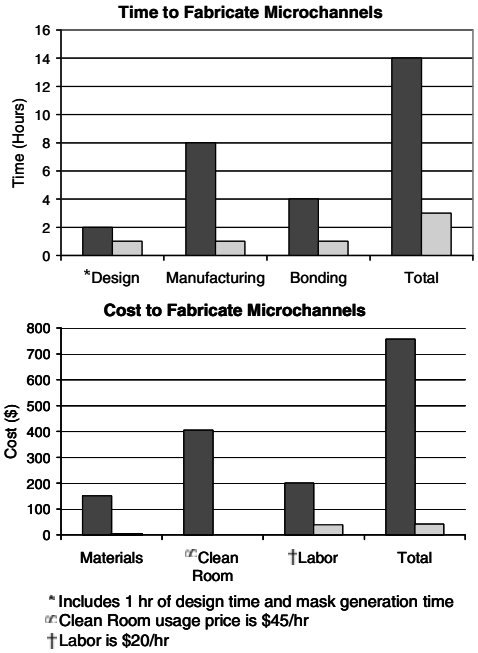

Figure 7. Time and cost comparison of glass (dark blue) and tape (light blue) microchannel fabrication for melting analysis.

Another advantage of tape-bonded microchannels as a prototyping tool is the ability to change designs quickly and inexpensively. One major disadvantage of the glass-bonded microchannels is that each time a new microfluidic design is needed, a new mask must be made. To make a mask for an original design, it costs a minimum of $200 (usually much more) and takes between 1 and 8 h, depending on the complexity of the design. This does not include the time required to generate the design using a CAD program. In contrast, the tape-bonded microchannels are not hampered by the necessity of having to generate a costly mask. To

create a new design in the tape-bonded microchannels, a design generated from a CAD program can be cut immediately into the tape which is used to make the microfluidic channel.

One disadvantage of the tape-bonded microchannels is their life span. Although tape-bonded microchannels can be used more than once, the tape microchannels gradually deteriorate with repeated use and bubbles eventually enter the channel. In contrast, the glass-bonded microchannels can be used many times without apparent deterioration, as long as the channels are cleaned between runs. A second shortcoming of tape-bonded microchannels is the surface quality. Roughness along the channel walls is a result of gaps in the adhesives and vibrations in the cutting knife as it cuts the tape. A final disadvantage of the tape-bonded microchannels is that they are prone to produce bubbles at temperatures above 85 °C. Air pockets which are present between the tape and the glass bonding substrate may expand into the chamber at higher temperatures.

Conclusion

Xurography using double-sided tape is an effective and reliable prototyping alternative to traditional glass etched microchannels. DNA melting analysis performed in the 10 nL tape bonded microchannels was comparable to the 10 nL glass bonded microchannels. The 10 nL and 1 nL volume channels had a 1000-fold and 10 000-fold volume reduction from commercial high resolution DNA melting instrumentation, with only a 10-fold SNR reduction, and were adequate for heterozygote mutation detection. Despite having a shorter life span than the traditional glass-bonded microchannels, the tape-bonded microchannels are significantly less expensive and faster to make, making them an effective prototyping tool for DNA melting analysis.

Acknowledgments

This work was funded by the State of Utah Center of Excellence grants for Biomedical Microfluidics and Homogeneous DNA Analysis. The authors wish to thank Niel Crews for fabricating all the glass-bonded microfluidic channels. The authors also thank Dr Carl Wittwer's lab group for providing valuable advice and for providing samples and PCR protocols for CFTR exon 10. Thanks to Dr Bruce Gale's Lab group for providing valuable advice and support.

References

An R, Li Y, Dou Y, Liu D, Yang H and Gong Q 2006 Water-assisted drilling of microfluidic chambers inside silica glass with femtosecond laser pulses *Appl. Phys. A: Mater. Sci. Process.* **83** 27–9

Bartholomeusz D A, Boutte R W and Andrade J D 2005 Xurography: rapid prototyping of microstructures using a cutting plotter *J. Microelectromech. Syst.* **14** 1364–74

Berthold A, Nicola L, Sarro P M and Vellekoop M J 2000 Glass-to-glass anodic bonding with standard IC technology thin films as intermediate layers *Sensors Actuators* A **82** 224–8

Du K, Sharma M, Lukacus G L and Struc N 2005 The ΔF508 cystic fibrosis mutation impairs domain-domain interactions and arrests post-translational folding of CFTR *Nat. Struct. Mol. Biol.* **12** 17–25

Duffy D C, Schueller O J A, Brittain S T and Whitesides G M 1999 Rapid prototyping of microfluidic switches in poly(dimethyl siloxane) and their actuation by electro-osmotic flow *J. Micromech. Microeng.* **9** 211–7

Grosse A, Greweand M and Fouckhardt H 2001 Deep wet etching off used silica glass for hollow capillary optical leaky waveguides in microfluidic devices *J. Micromech. Microeng.* **11** 257–62

Gundry C N, Vandersteen J G, Reed G H, Pryor R J, Chen J and Wittwer C T 2003 Amplicon melting analysis with labeled primers: a closed-tube method for differentiating homozygotes and heterozygotes *Clin. Chem.* **49** 396–406

Herrmann M G, Durtschi J D, Bromley L K, Wittwer C T and Voelkerding K V 2006 Amplicon DNA melting analysis for mutation scanning and genotyping: cross-platform comparison *Clin. Chem.* **52** 494–503

Iliescu C and Tay F E H 2005 Wet etching of glass *Proc. 2005 Int. Semiconductor Conf., CAS 2005* vol 1 pp 35–44

Kaigala G V, Ho S, Penterman R and Backhouse C J 2007 Rapid prototyping of microfluidic devices with a wax printer *Lab Chip* **7** 384–7

Mandel M and Marmur J 1968 Use of ultraviolet absorbance-temperature profile for determining the guanine plus cytosine content of DNA *Methods Enzymol.* **12** 195–206

Neuzil P, Pipper J and Hsieh T M 2006 Disposable real-time microPCR device: lab-on-a-chip at a low cost *Mol. BioSyst.* **2** 292–8

Ririe K M, Rasmussen R P and Wittwer C T 1997 Product differentiation by analysis of DNA melting curves during the polymerase chain reaction *Anal. Biochem.* **245** 154–60

Sailki R K, Scharf S, Faloona F, Mullis K B, Horn G T, Erlich H A and Arnheim N 1985 Enzymatic amplification of beta-globin genomic sequences and restriction site analysis for diagnosis of sicle cell anemia *Science* **230** 1350–4

Schabmueller C G J, Lee M A, Evans A G R, Brunnschweiler A, Ensell G J and Leslie D L 2000 Closed chamber PCR chips for DNA amplification *Eng. Sci. Educ. J.* **9** 259–64

Shin Y S, Cho K L, Sun H, Chung S, Park S, Chung C, Han D and Chang J K 2003 PDMS-based micro PCR chip with parylene coating *J. Micromech. Microeng.* **13** 768–74

Simpson P C, Woolley A T and Mathies R A 1998 Microfabrication technology for the production of capillary array electrophoreseis chips *Biomed. Microfluics* **1** 7–26

Sundberg S O, Wittwer C T, Greer J, Pryor R J, Johnson O E and Gale B K 2007 Solution-phase DNA mutation scanning and SNP genotyping by nanoliter melting analysis *Biol. Med. Microdev.* **2** 159–66

Wittwer C T, Fillmore G C and Garling D J 1990 Minimizing the time required for DNA amplification by efficient heat transfer to small samples *Anal. Biochem.* **186** 328–31

Wittwer C T, Reed G H, Gundry C N, Vandersteen J G and Pryor R J 2003 High-resolution genotyping by amplicon melting analysis using LCGreen *Clin. Chem.* **49** 853–60

Verpoorte E 2002 Microfluidic chips for clinical and forensic analysis *Electrophoresis* **23** 677–712

Xia Y and Whitesides G M 1998 Soft lithography *Angew. Chem. Int. Ed.* **37** 550–75

Yagyu H, Sugano K, Hayashi S and Tabata O 2005 Micropowder blasting with nanoparticles dispersed polymer mask for rapid prototyping of glass chip *J. Micromech. Microeng.* **15** 1236–41

Yao L, Liu B, Chen T, Liu S and Zuo T 2005 Micro flow-through PCR in a PMMA chip fabricated by KrF excimer laser *Biomed. Microdev.* **7** 253–57

CHAPTER 4

MINIATURIZATION OF WARFARIN METABOLISM GENOTYPING BY MELTING ANALYSIS USING ASYMMETRIC PCR AND UNLABELED OLIGONUCLEOTIDE PROBES

 The manuscript is published in the conference proceedings of the 2007 AIChE Annual Meeting held in Salt Lake City, Utah. Annual Meeting of the American Electrophoresis Society: Topical Conference at the 2007 AIChE Annual Meeting, ISBN 978-16042-3827-3. Authors are Scott O. Sundberg, Jenny Greer, Carl T. Wittwer, and Bruce K. Gale.

Miniaturization of Warfarin Metabolism Genotyping by Melting Analysis using Asymmetric PCR and Unlabeled Oligonucleotide Probes

Scott O. Sundberg[1], Jenny Greer[2], Carl T. Wittwer[3] and Bruce K. Gale[2]
1. Bioengineering Dept., 2. Mechanical Engineering Dept. and 3. Pathology Dept.
University of Utah, Salt Lake City, UT

Abstract

Solution-phase, homogeneous DNA melting analysis was performed in 100 nl volumes on a custom microchip/instrument and compared to the gold-standard 10 μl HR-1™ melting instrument for the *VKORC1* C1173T, *CYP2C9*2* and *CYP2C9*3* targets, the genetic targets involved in determining warfarin dosing used in blood thinners. Normal sample was distinguished from heterozygous and homozygous single-nucleotide polymorphisms (SNPs) simultaneously in an array melting platform using an automatic genotype calling melting analysis software.

Introduction

Warfarin is one of the most widely used coumadin anticoagulants but has a wide interindividual dosage variation. Variants in the *VKORC1* and *CYP2C9* genes and certain environmental conditions (i.e. age, bodyweight and drug interactions) account for about 50-60% of the variation in warfarin dosage (Sconce et al. 2005 and Wadelius et al. 2007). Warfarin functions by interfering with vitamin K recycling in the liver. *VKORC1* encodes for the main protein in the vitamin K epoxide reductase complex. Warfarin is metabolized by cytochrome P450 2C9 (*CYP2C9*). Thus, *CYP2C9* *2 and *3 alleles require lower warfarin doses and may have a greater risk of bleeding (Sanderson et al. 2005).

DNA melting analysis as a complement to PCR was introduced in 1997 (Ririe et al. 1997). A dye is included in the PCR that fluoresces in the presence of double-stranded DNA, but not single-stranded DNA. After amplification, fluorescence is monitored as the double-stranded DNA product is slowly heated. When the double helix melts, fluorescence rapidly decreases. The negative first derivative of fluorescence with respect to temperature shows the melting temperature (T_m) as maxima. Recent advances in melting instrumentation (Herrmann et al. 2006) and saturating DNA dyes (Wittwer et al. 2003) allow detection of single nucleotide polymorphisms (SNPs). If the change is heterozygous, DNA heteroduplexes alter the shape of the melting curve (Reed et al. 2004). If the change is homozygous, the absolute temperature of the melting transition shifts (Liew et al. 2004). DNA melting analysis, when compared to existing PCR analytical techniques, is advantageous because it is less complicated, faster (less than 20 minutes for PCR and analysis), and prevents contamination of the sample and environment due to its “closed-tube” format (Zhou et al. 2004). The specific dye used determines the capabilities of the method; LCGreen® Plus detects homozygous and heterozygous sequences well and does not inhibit PCR (Wittwer et al. 2003).

Analysis of the melting transition is often sufficient for genotyping. However, unlabeled probes combined with asymmetric PCR provide even greater specificity over a smaller region, which may be necessary for variant discrimination (Zhou et al. 2005) and is commonly believed to be essential for clinical assays. A recent publication has demonstrated that DNA

melting analysis is capable of being miniaturized, thus providing initial results for a microarray chip platform, reducing reagent costs (Sundberg et al. 2007).

Materials and Methods

Microchip Fabrication

Xurography (Bartholomeusz et al. 2005) was used to create a PDMS soft lithography mold, with analysis wells being 1.125 mm in diameter and 0.1 mm in height, creating a 100 nl volume. PDMS was then molded and cured in an oven. PDMS ports were cored and then bonded to glass slide substrates using corona discharge, Figure 1.

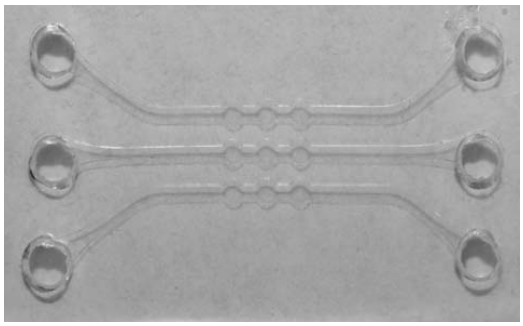

Figure 1. Photograph of the custom microchip showing three channels with three wells per channel. Each well has a diameter of 1.125 mm and a depth of 0.1 mm.

Instrumentation

A Peltier heater (HT4-6-21x43, Melcor, Trenton, NJ) and J-type thermocouple were used for temperature control. Detection used a CCD camera (iXon, Andor Technology, South Windsor, CT) cooled to -80 °C. LEDs (440-460 nm, LXHL-BR02, LUXEON, Philips Lumileds Lighting Company, San Jose, CA) were filtered by an excitation bandpass filter (426-450 nm, Brightline Fluorescent Filters, Semrock, Rochester, New York). Emitted light was collected by a lens (EFS 60mm f/2.8 Macro, Canon, Lake Success, New York) and passed through an emission bandpass filter (467-499 nm, Brightline Fluorescent Filters, Semrock) (Figure 2). All hardware was controlled using LabView 8.0 (NI, Austin, TX).

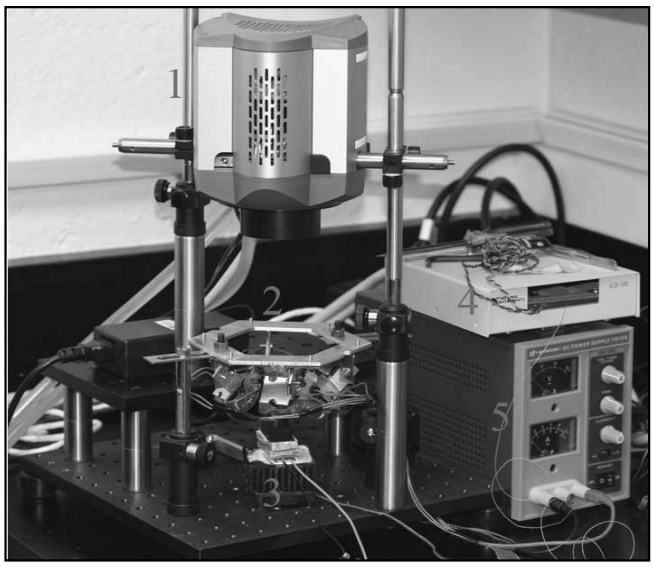

Figure 2. A photograph of the prototype detection instrumentation is shown. (1) CCD camera; (2) LED ring for fluorescence excitation; (3) heating platform using a Peltier heater; (4) thermocouple control; and (5) LED power supply.

Sample Preparation

10X asymmetric PCR with unlabeled oligonucleotide probes was performed on the DNA sample using a LightCycler® and then transferred to an HR-1™ instrument for a high-resolution reference melting curve. 2 μl of the amplified sample was pipetted into the microchip for nanoliter melting analysis. All three genotypes were melted simultaneously and each genotype had three wells for repeat analysis.

Software

The automatic calling software uses an agglomerative, unbiased hierarchical clustering of melting curves (Duda et al. 2001) to make the calls. Given n curves, the two curves that are closest to each other are first determined. The distance between a pair of curves is taken as the mean absolute value of the fluorescence differences between the curves over all temperature acquisitions. The closest two curves are deleted and replaced by their mean, resulting in a new set of n-1 curves. The next nearest pair is then replaced by the weighted mean of that pair. At each step, the weight is the number of original curves that make up each branch being averaged. This process is performed a total of n-1 times until the last pair of curves is merged, producing a dendrogram showing the most likely clusters at each level. The process does not determine the number of clusters (i.e. the number of genotypes) represented by the n curves but does confirm appropriate clustering of samples at each dendrogram level. For these tests three clusters were chosen to represent each of the three genotypes.

Results and Conclusion

Figures 3, 4 and 5 show negative derivative melt plots of normal, heterozygous, and homozygous SNPs within a 190-bp fragment of *VKORC1* C1173T, a 122 bp fragment of

*CYP2C9*2* and 134 bp fragment of *CYP2C9*3*. The 100 nl melts are in good agreement with the 10 μl HR-1 melting curves and each of the genotypes were clearly distinguished in their first melt transition, the unlabeled probe melt region, using an automatic calling software (Idaho Technology) to distinguish the genotypes by setting the cluster number to three. This new platform provides accurate SNP genotyping capability using a hundredth of the volume currently used with gold-standard instrumentation. This technology with further development will lead to a more accurate warfarin dosing within the clinical setting.

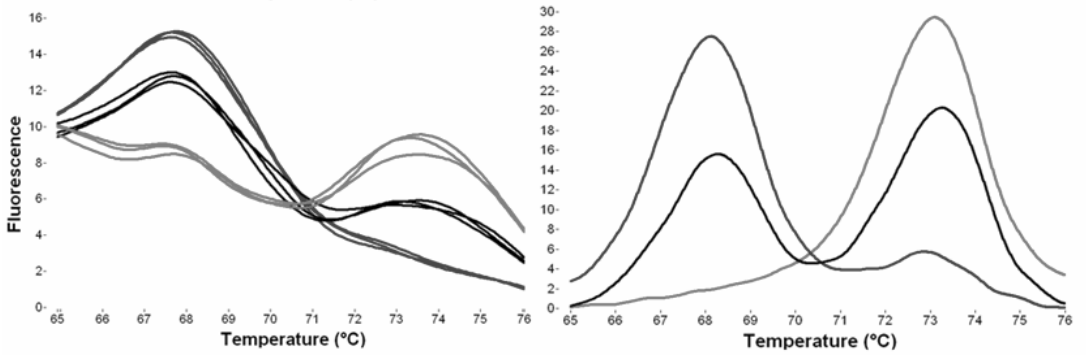

Figure 3. *VKORC1* C1173T negative derivative plots of 100 nl melts (left) and 10 μl melts (right). Normal DNA (red); heterozygous mutation (black); and homozygous mutation (blue).

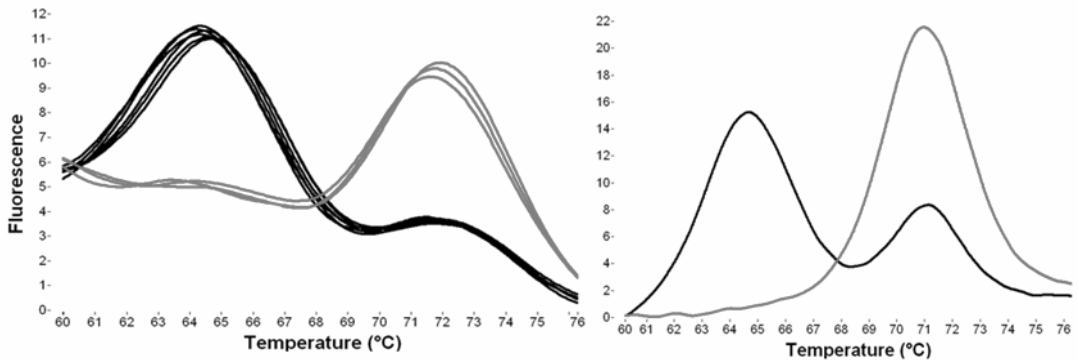

Figure 4. *CYP2C9*2* negative derivative plots of 100 nl melts (left) and 10 μl melts (right). Normal DNA (red) and heterozygous mutation (black).

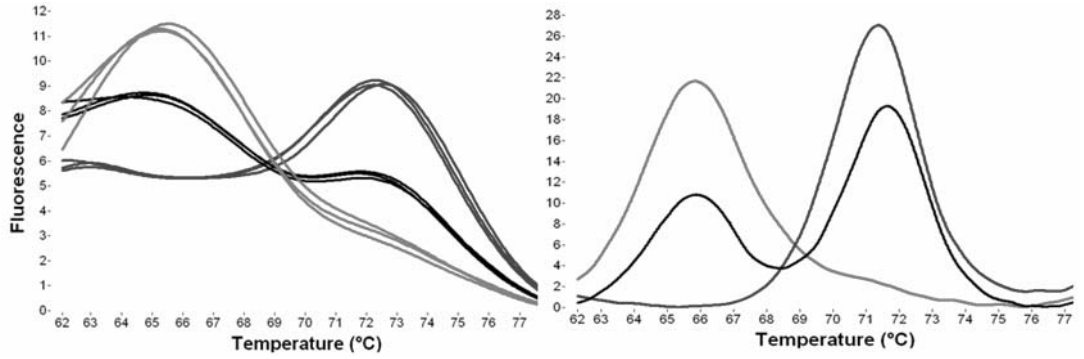

Figure 5. *CYP2C9*3* negative derivative plots of 100 nl melts (left) and 10 μl melts (right). Normal DNA (red); heterozygous mutation (black); and homozygous mutation (blue).

References

Bartholomeusz D, Boutte R and Andrade J. Xurography: rapid prototyping of microstructures using a cutting plotter. *JMEMS* **2005**, *14*:1364-1374.

Duda RO, Hart PE and Stork DG. Pattern classification, 2nd ed. New York: Wiley, 2001:654pp.

Herrmann MG, Durtschi JD, Bromley LK, Wittwer CT and Voelkerding KV. Amplicon DNA melting analysis for mutation scanning and genotyping: cross-platform comparison of instrument and dyes. *Clin Chem* **2006**, *52(3)*:494-503.

Liew M, Pryor R, Palais R, Meadows C, Erali M, Lyon E and Wittwer C. Genotyping of single-nucleotide polymorphisms by high-resolution melting of small amplicons. *Clin Chem* **2004**, *50(7)*:1156-1164.

Reed GH and Wittwer CT. Sensitivity and specificity of single-nucleotide polymorphism scanning by high-resolution melting analysis. *Clin Chem* **2004**, *50(10)*:1748-1754.

Ririe KM, Rasmussen RP and Wittwer CT. Product differentiation by analysis of DNA melting curves during the polymerase chain reaction. *Anal Biochem* **1997**, *245*:154-160.

Sanderson S, Emery J and Higgins J. CYP2C9 gene variants, drug dose, and bleeding risk in warfarin-treated patients: a HuGEnet systematic review and meta-analysis. *Genet Med* **2005**, *7*:97–104.

Sconce EA, Khan TI, Wynne HA, Avery P, Monkhouse L, King BP, Wood P, Kesteven P, Daly AK, and Kamali F. The impact of CYP2C9 and VKORC1 genetic polymorphism and patient characteristics upon warfarin dose requirements: proposal for a new dosing regimen. *Blood* **2005**, *106*:2329–2333.

Sundberg SO, Wittwer CT, Greer J, Pryor RJ, Elenitoba-Johnson O and Gale BK. Solution-phase DNA mutation scanning and SNP genotyping by nanoliter melting analysis**.** *Biomed Microdevices* **2007**, *9*:159-166.

Wadelius M, Chen LY, Eriksson N, Bumpstead S, Ghori J, Wadelius C, Bentley D, McGinnis R and Deloukas P. Association of warfarin dose with genes involved in its action and metabolism. *Hum Genet* **2007**, *121*:23-34.

Wittwer CT, Reed GH, Gundry CN, Vandersteen JG and Pryor RJ. High-resolution genotyping by amplicon melting analysis using LCGreen. *Clin Chem* **2003**, *49(6)*: 853-860.

Zhou L, Myers AN, Vandersteen JG, Wang L and Wittwer CT. Closed-tube genotyping with unlabeled oligonucleotide probes and a saturating DNA dye. *Clin Chem* **2004**, *50(8)*: 1328-1335.

Zhou L, Wang L, Palais R, Pryor R and Wittwer CT. High-resolution DNA melting analysis for simultaneous mutation scanning and genotyping in solution. *Clin Chem* **2005**, *51(10)*:1770-1777.

CHAPTER 5

SPINNING DISK PLATFORM FOR MICROFLUIDIC DIGITAL POLYMERASE CHAIN REACTION

This chapter has been reprinted with permission from the American Chemical Society. The manuscript is published in Analytical Chemistry, DOI 10.1021/ac902398c, and includes a supporting information section. Authors are Scott O. Sundberg, Carl T. Wittwer, Chao Gao, and Bruce K. Gale.

Anal. Chem. **2010,** *82,* 1546–1550

Spinning Disk Platform for Microfluidic Digital Polymerase Chain Reaction

Scott O. Sundberg,* Carl T. Wittwer, Chao Gao, and Bruce K. Gale

University of Utah, Rm 5R441, 1795 E South Campus Dr., Salt Lake City, Utah 84112

An inexpensive plastic disk disposable was designed for digital polymerase chain reaction (PCR) applications with a microfluidic architecture that passively compartmentalizes a sample into 1000 nanoliter-sized wells by centrifugation. Well volumes of 33 nL were attained with a 16% volume coefficient of variation (CV). A rapid air thermocycler with aggregate real-time fluorescence detection was used, achieving PCR cycle times of 33 s and 94% PCR efficiency, with a melting curve to validate product specificity. A CCD camera acquired a fluorescent image of the disk following PCR, and the well intensity frequency distribution and Poisson distribution statistics were used to count the positive wells on the disk to determine the number of template molecules amplified. A 300 bp plasmid DNA product was amplified within the disk and analyzed in 50 min with 58−1000 wells containing plasmid template. Target concentrations measured by the spinning disk platform were 3 times less than that predicted by absorbance measurements. The spinning disk platform reduces disposable cost, instrument complexity, and thermocycling time compared to other current digital PCR platforms.

Digital polymerase chain reaction (PCR) is a highly sensitive DNA and RNA quantification technique that counts each template individually. This technique provides greater precision over quantitative real-time PCR (qPCR) because it is not sensitive to PCR efficiency, transforming exponential, analog signals to linear, digital signals.[1] First published in 1999, limiting dilution was used to detect a minor fraction of altered DNA by diluting to the point of having 0.5 DNA templates per PCR in a microtiter plate format.[2] Molecular beacon probes were analyzed following PCR to quantify the wild type to rare mutation ratio, relying on binary positive/negative calls.

More recently, the concept of digital PCR has been miniaturized to nanoliter volumes using microfluidics to limit the amount of DNA template in a PCR.[3] Miniaturization of PCR volume has benefited digital PCR in three significant ways. First, reagent consumption is reduced 100 to 1000-fold from microtiter plate formats, reducing testing costs dramatically. Second, the number of parallel reactions has increased over 100-fold, thus increasing power, sensitivity, and throughput. Third, testing is simplified by reducing sample dilution steps, using volume as a limiting factor, and eliminating several pipetting steps required with microtiter plates. Miniaturization of digital PCR has been investigated down to 65 pL reaction volumes.[4]

Applications of microfluidic digital PCR include detection of rare mutations within an excess of normal DNA,[5] multigene analysis of bacteria,[6] copy number variation,[7] fetal DNA in maternal plasma,[8] and genetic allelic imbalance.[9,10]

The purpose of this work is to improve upon current microfluidic digital PCR platforms by reducing disposable costs, instrument complexity, and time to result. Our design loads the sample into nanoliter-sized compartments by centrifugation, eliminating the need for valves and pumps and reducing microfluidic loading time. The disk consists of three inexpensive plastic thin film sheets laminated together with an architecture that passively divides a spun sample into a thousand compartments, reducing chip disposable costs. PCR is performed on the rotating disk by rapid thermal cycling in an air chamber, reducing thermocycling time. After PCR, each compartment is interrogated for a positive/negative signal by fluorescence imaging.

In this work, we demonstrate microfluidic digital PCR within a spinning disk platform in less than 35 min (including disk loading, PCR thermocycling, and fluorescent imaging). A single disk provides 1000 nanoliter-sized reactions detected with the dsDNA fluorescent saturating dye LCGreen.[11] No labeled probes are required.

MATERIALS AND METHODS

Disk Design and Manufacturing. The disk design is based on the use of centrifugal force to move fluid along a spiral channel, filling wells along the way. A loading reservoir located near the center of the disk is connected to a spiral channel, 250 μm wide,

* To whom correspondence should be addressed. E-mail: scott.sundberg@m.cc.utah.edu.

(1) Pohl, G.; Shih, Ie. M. *Expert Rev. Mol. Diagn.* **2004**, *4*, 41–47.
(2) Vogelstein, B.; Kinzler, K. W. *Proc. Natl. Acad. Sci. U.S.A.* **1999**, *96*, 9236–9241.
(3) Warren, L.; Bryder, D.; Weissman, I. L.; Quake, S. R. *Proc. Natl. Acad. Sci. U.S.A.* **2006**, *103*, 17807–17812.
(4) Kiss, M. M.; Ortoleva-Donnelly, L.; Beer, N. R.; Warner, J.; Bailey, C. G.; Colston, B. W.; Rothberg, J. M.; Link, D. R.; Leamon, J. H. *Anal. Chem.* **2008**, *80*, 8975–8981.
(5) Yung, T. K. F.; Chan, K. C. A.; Mok, T. S. K.; Tong, J.; To, K.-F.; Lo, Y. M. D. *Clin. Cancer Res.* **2009**, *15*, 2076–2084.
(6) Ottesen, E. A.; Hong, J. W.; Quake, S. R.; Leadbetter, J. R. *Science* **2006**, *314*, 1464–1467.
(7) Qin, J.; Jones, R. C.; Ramakrishnan, R. *Nucleic Acids Res.* **2008**, *36*, e116.
(8) Lun, F. M. F.; Chiu, R. W. K.; Chan, K. C. A.; Leung, T. Y.; Lau, T. K.; Lo, Y. M. D. *Clin. Chem.* **2008**, *54*, 1664–1672.
(9) Fan, H. C.; Quake, S. R. *Anal. Chem.* **2007**, *79*, 7576–7579.
(10) Fan, H. C.; Blumenfeld, Y. J.; El-Sayed, Y. Y.; Chueh, J.; Quake, S. R. *Am. J. Obstet. Gynecol.* **2009**, *200*, 543.e1543.e7.
(11) Wittwer, C. T.; Reed, G. H.; Gundry, C. N.; Vandersteen, J. G.; Pryor, R. J. *Clin. Chem.* **2003**, *49*, 853–860.

10.1021/ac902398c
Published on Web 01/19/2010

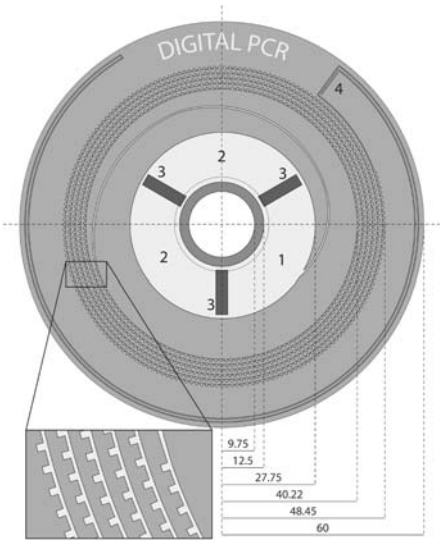

Figure 1. Spinning disk design, with dimensions given in millimeters, shown to scale. The disk consists of a loading reservoir, spiral microchannel with 1000 wells facing radially outward along the channel, and an overflow channel at the edge of the disk. The PCR mixture is pipetted into the loading reservoir at location 1, and mineral oil is pipetted into the loading reservoir at location 2. The Teflon inserts for the loading reservoir are also shown (3). A pin-sized hole is located at the end of the overflow channel (4), and once the disk is loaded, this same location is thermally sealed, creating a closed system for PCR.

that moves toward the outside of the disk. Along the channel are square wells, facing radially outward along the spiral, which are designed as fluid traps. This design is fabricated from thin film plastics to create an inexpensive disposable, requiring only centrifugation for fluid control. The current design consists of 1000 wells each having dimensions of 500 μm × 500 μm × 125 μm. The entire disk is 120 mm in diameter, the size of a CD, and is 375 μm thick. The channel layer disks were manufactured using the process of xurography.[12,13] Figure 1 illustrates the disk design (see Supporting Information for more details).

Sample Preparation. We evaluated the feasibility of digital PCR within the spinning disk using a previously developed DNA "Toolbox".[14] Plasmid from the DNA Toolbox was provided by Lonza (Rockland, ME). The PCR mixture contained plasmid DNA, ranging from 6×10^6 to 6×10^0 copies/μL (determined by absorbance) as the template. Preparation details of the plasmid DNA and PCR mixture can be found in the Supporting Information.

Disk Loading. The sample was loaded by pipetting 40 μL of PCR mix and 250 μL of mineral oil (M5904, Sigma-Aldrich Corporation), dyed with Oil Red O (Matheson Coleman & Bell, Gardena, CA), into the loading reservoir of the disk. Two polycarbonate disks, 750 μm thick with an outer diameter of 75 mm, were then coupled to each side of the disk, using a two-piece collar, to provide more rigidity to the disk during thermocycling. The disk was then spun at 4000 rpm for 5 min to move the fluid from the middle to the outside of the disk, filling each of the wells along the way and leaving the channel filled with the mineral oil, as seen in Figure S1 in the Supporting Information. The end of the spiral channel was then thermally sealed prior to thermocycling to create a closed system. The collar was attached to the servo motor shaft within the thermocycler using a set screw.

Thermocycling. A previously described rapid air thermocycling instrument[15] was modified to spin the disk at controllable speeds, measure disk temperature during thermocycling, and measure the average fluorescence of disk wells, as seen in Figure S2 (see Supporting Information for more details). Forty-five cycles of 45 °C annealing for 0 s, 72 °C extension for 2 s, and 90 °C denaturing for 0 s was achieved in under 25 min while spinning the disk at 2500 rpm (33 s/cycle).

A fluorimeter was mounted to the thermocycler with an excitation spot size of 1 mm in diameter aimed 45 mm from the center of the disk, providing an average real-time fluorescence reading over hundreds of wells due to the disk spinning during fluorescence acquisition (see Supporting Information for details). The fluorimeter optics scheme is shown in Figure S3. The real-time fluorescence data at PCR extension was normalized, multiplying the extension fluorescence value by the difference between the annealing and denaturing fluorescence values at each cycle. The quantification cycle (C_q) for each test was determined by inputting these normalized fluorescence values into LightCycler Software vs 3 (Roche Diagnostics, Indianapolis, IN). The melting temperature (T_m) of the amplified product was also determined by LightCycler software, inputting the temperature and fluorescence data for the last thermocycle between 70 and 90 °C. The T_m is defined as the maxima of the negative first derivative of fluorescence.[16] The fluorescent signal is sufficient to obtain melting curves even within nanoliter volumes.[17]

Disk Imaging and Analysis. The disk was fluorescently imaged following PCR for digital well analysis, with the imaging setup seen in Figure S4 (see Supporting Information for more details). ImageJ[18] software was used to threshold, size exclude, and then create histograms of well intensity for each disk image. The threshold and minimum pixel number was operator defined. Histogram frequency distributions were then used to determine the number of positive and negative wells for each test.

Measuring Well Volume Variation. PCR amplicon with dsDNA fluorescent dye and mineral oil were spun into the disk to determine well volume variation. A fluorescent image of the disk was taken. The number of pixels of each well along with the mean and standard deviation of well fluorescence was obtained using custom LabView software. The pixels were used to calculate the surface area of fluid within each well. This surface area was then multiplied by the depth of the well, which is the thickness of the middle layer of plastic, to determine well volume. A nonfluorescent imaging method was also used to determine well

(12) Bartholomeusz, D. A.; Bouttè, R.; Andrade, J. D. *J. Microelectromech. Syst.* **2005**, *14*, 1364–1374.
(13) Greer, J.; Sundberg, S. O.; Wittwer, C. T.; Gale, B. K. *J. Micromech. Microeng.* **2007**, *17*, 2407–2413.
(14) Highsmith, W., Jr.; Jin, Q.; Nataraj, A.; O'Connor, J.; Burland, V.; Baubonis, W.; Curtis, F.; Kusukawa, N.; Garner, M. *Electrophoresis* **1999**, *20*, 1186–94.
(15) Wittwer, C. T.; Ririe, K. M.; Andrew, R. V.; David, D. A.; Gundry, R. A.; Balis, U. J. *Biotechniques* **1997**, *22*, 176–181.
(16) Ririe, K. M.; Rasmussen, R. P.; Wittwer, C. T. *Anal. Biochem.* **1997**, *245*, 154–160.
(17) Sundberg, S. O.; Wittwer, C. T.; Greer, J.; Pryor, R. J.; Elenitoba-Johnson, O.; Gale, B. K. *Biomed. Microdevices* **2007**, *9*, 159–166.
(18) Rasband, W. S. U.S. National Institutes of Health, Bethesda, Maryland, http://rsb.info.nih.gov/ij/ 1997−2009 (Accessed June 8, 2009).

manufacturing variation. Well dimensions were determined by measuring the edges of 5% of the wells to calculate the surface area, using pixels to determine edge lengths, and then multiplying the surface area by well depth for manufactured well volume variation.

RESULTS AND DISCUSSION

The spinning disk platform performed digital PCR with rapid PCR thermocycling using only a dsDNA fluorescent saturating dye, providing quantification results within 50 min. Thermocycle times (33 s cycles) were much faster than some reported platforms (~120 s cycles[3] and 55 s cycles[4]). The disk disposable was inexpensive and easy to load, requiring less than 5 min. Fluorescent imaging of the disk required an additional 5 min. Image analysis required 15 min for positive well quantification but could be streamlined in future software. Microfluidics allows digital PCR to use much less reagent than microtiter plate systems, and the absence of labeled probes further reduced costs by simply using a dsDNA fluorescent saturating dye.

Well Volume Variation. PCR amplicon with dsDNA dye and mineral oil were spun into the disk to determine well volume variation. The wells had a mean volume of 33 nL with a standard deviation of ±5.2 nL or a 16% volume CV, across all 1000 wells. It was further found that the manufacturing method alone causes a 10% volume CV due to variation in well cutting from the cutting plotter based on cut well dimensions.

Dilution Series. A dilution series was performed using the spinning disk platform to determine PCR efficiency and to identify the concentrations required for optimal digital PCR results. The dilution series ranged from 6×10^6 to 6×10^0 plasmid copies/μL, or about 200 000 to 0.2 plasmid copies/well. An example of the unprocessed real-time data is shown in Figure 2 for the highest plasmid concentration of 6×10^6 plasmid copies/μL. Figure S5 in the Supporting Information shows the real-time PCR curves for each dilution. Table 1 provides the C_qs, T_ms, and number of positive wells for each plasmid concentration run in the spinning disk platform. A PCR efficiency of 94% was calculated, using the 6×10^6 to 6×10^2 C_q data and excluding the last two concentrations because they were in the "digital range", from the equation

$$\text{PCR efficiency} = 10^{-1/\text{slope}} - 1 \quad (1)$$

where the slope is found when the logarithm of template concentration is plotted on the x axis and C_q is plotted on the y axis. The slope was −3.47 with a correlation coefficient, R^2 value, of 0.989 for the dilution series. Figure 3 shows fluorescent images of the disk for the four lowest concentrations in the dilution series. A histogram for the concentration of 6×10^1 plasmid copies/μL is also shown in Figure 3 to illustrate the frequency distributions that were used to determine the number of positive wells within each disk. The PCR product T_ms had a mean temperature of 84.4 °C and a standard deviation of 0.7 °C. The T_m helps validate PCR product specificity.

The digital PCR concentrations, 6×10^1 and 6×10^0 plasmid copies/μL, had 518 and 58 positive wells, respectively. Because the plasmid is homogeneously mixed within the PCR, a Poisson distribution is assumed to statistically determine the number of plasmid copies present for each disk. As the number of positive wells increases, the chance of having more than one copy of DNA in a given positive well also increases. The Poisson distribution follows the equation

$$f(x) = (\lambda^x) \times (e^{-\lambda}) / (x!) \quad (2)$$

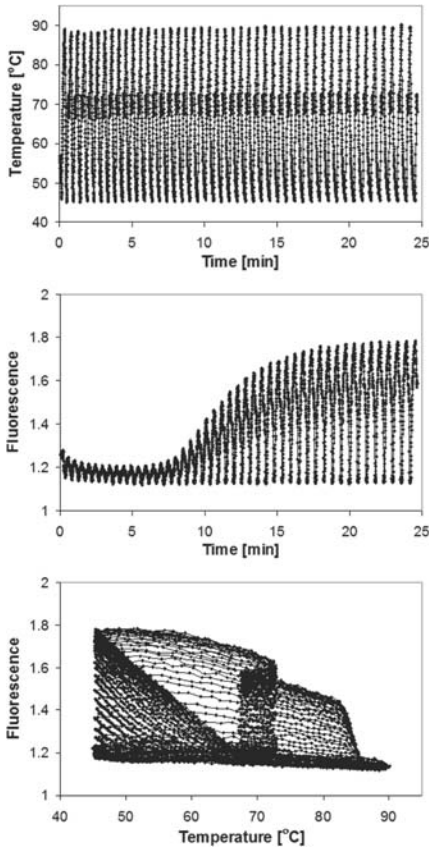

Figure 2. Real-time plots are shown of temperature vs time (top), fluorescence vs time (middle), and fluorescence vs temperature (bottom) at a concentration of 6×10^6 plasmid copies/μL. The top plot illustrates that 45 thermocycles required less than 25 min; the middle plot shows the exponential increase in fluorescence with a C_q of 16, and the bottom plot provides the T_m of the amplified product, seen at 84.6 °C.

Table 1. Quantification Cycle (C_q), Melting Temperature (T_m), and Number of Positive Wells for Template Dilution on the Spinning PCR Disk

conc. [copies/μL]	C_q [cycle no.]	T_m [°C]	positive wells
6×10^6	16	84.6	997
6×10^5	19.57	85.3	992
6×10^4	24.05	84.6	974
6×10^3	27.13	84.5	995
6×10^2	29.57	83.1	939
6×10^1	32.02	84.1	518
6×10^0	32.28	*a*	58

[a] Signal was too low to detect the melting transition at this concentration.

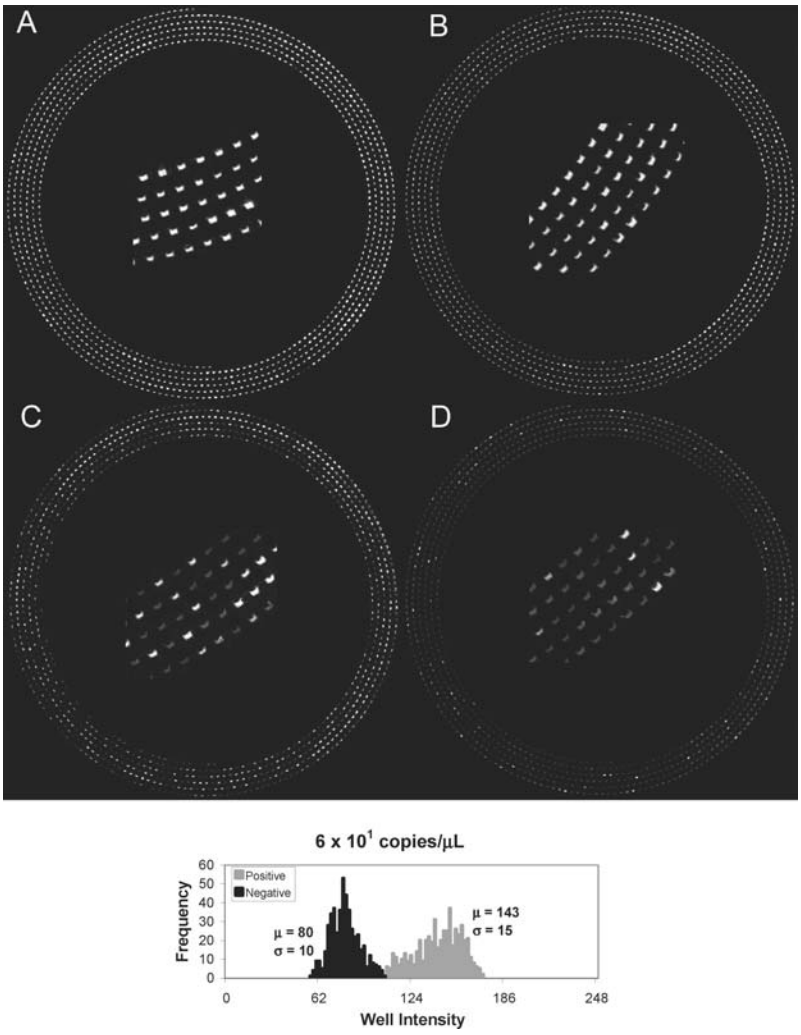

Figure 3. (Top) Fluorescent images are presented for 6×10^3 plasmid copies/μL (A), 6×10^2 plasmid copies/μL (B), 6×10^1 plasmid copies/μL (C), and 6×10^0 plasmid copies/μL (D). A lower right section of each disk image is enlarged. Digital PCR is achieved with dilutions C and D, where image C has 518 and image D has 58 out of 1000 wells fluorescing. (Bottom) An example of the histogram data used to determine the number of positive wells is shown for the 6×10^1 plasmid copies/μL concentration.

where λ is the mean number of template copies and x is the number of templates of interest present for a given well. If 48.2% of the wells are empty, as is the case with the 6×10^1 plasmid copies/μL disk, then the expected number of copies per well is $-\ln 0.482$ or 0.730 (which is the λ value solved when $f(0) = 0.482$ and $x = 0$). Therefore, although 518 positive wells are present, there are ~730 plasmid copies that have actually been amplified. A similar calculation is made for the 6×10^0 plasmid copies/μL disk in which the expected number of copies per well is 0.060; in other words, ~60 plasmid copies were amplified although 58 positive wells were counted.

A discrepancy exists between the absorbance measurements of the plasmid and the digital results found in the two lowest concentrations. At 6×10^1 plasmid copies/μL, there should be 2 copies/well although only 0.730 copies per well was measured, and at 6×10^0 plasmid copies/μL, there should be 0.2 plasmid copies/well although only 0.060 plasmid copies/well was measured. This means that the spinning disk platform differs from absorbance measurements by about a factor of 3. The plasmid purity is unknown and may account for some of the discrepancy. There may also be a portion of the plasmid not cleaved or linearized that delays PCR amplification. Another possibility is that some of the plasmid may adsorb to the plastic as it moves through the loading reservoir and spiral microchannel. The addition of PVP to the PCR mix diminishes these effects greatly but may not entirely resolve the issue. This is apparent in the three lowest concentrations where the first several wells do not fluoresce, possibly caused by plasmid adsorbing to the plastic in the frontrunner fluid and then filling those first wells without template.

Not all wells fluoresced with the positive controls. Some of this stems from the cutting plotter which occasionally creates undesirable ridges next to a well, causing irregular fluid flow and allowing mineral oil to fill the well rather than the PCR mix. The other issue is that the disk manufacturing did not take place in a clean room, and therefore, an occasional dust particle was present in a well, disrupting adequate PCR amplification.

CONCLUSION

Plasmid DNA was efficiently PCR amplified within the spinning disk platform and analyzed in 50 min with 58−1000 wells containing template. Subsequent work will focus on improving the plastic disk manufacturing, eliminating DNA adsorption to the disk, reducing analysis time, designing a rapid air cycler fitted to the disk for faster thermocycling, and investigating new digital PCR applications. A fluorescent scanner for the disk is also envisioned to replace disk imaging following PCR to provide higher "on/off" fluorescence resolution and further reduce instrumentation cost.

ACKNOWLEDGMENT

The authors thank the University of Utah Research Foundation for kindly supporting this work. We also thank Dr. Wittwer's lab group and Dr. Gale's lab group for valuable advice pertaining to this research.

SUPPORTING INFORMATION AVAILABLE

Additional information as noted in text. This material is available free of charge via the Internet at http://pubs.acs.org.

Received for review October 22, 2009. Accepted December 31, 2009.

AC902398C

Supporting Information

Spinning Disk Platform for Microfluidic Digital PCR

Scott O. Sundberg, Carl T. Wittwer, Chao Gao, and Bruce K. Gale*

MATERIALS AND METHODS (SUPPORTING INFORMATION)

Disk Design and Manufacturing

When selecting disk material and manufacturing techniques the following were considered: low auto-fluorescence levels at 425-550 nm excitation, minimal PCR inhibition, capable of withstanding thermocycling temperatures, ease of channel fabrication, low cost, and an easy bonding method. The solution found was to use a cutting plotter to pattern a layer of glycol-modified polyethylene teraphthalate (PETG) and laminate that layer between two separate PETG layers.

The channel layer disks were manufactured using the process of xurography. This process includes designing the microchannel pattern with SolidWorks® (Concord, MA), importing the design into Adobe Illustrator® (Adobe, San Jose, CA) and exporting to a cutting plotter (CE5000-60, Graphtec, Santa Ana, CA). A PETG thin film sheet, 125 μm thick, (Sabic Polymershapes, Fresno, CA) was cut with the spiral channel and 1000 wells. This patterned sheet was then thermally bonded between two other PETG thin film sheets of the same thickness by laminating the plastics together at 130°C using an EL-12 laminator (Ibico, Skokie, IL). Three 500 μm thick Teflon strips (Scientific Commodities Incorporated, Lake Havasu City, AZ) were inserted into the loading reservoir to allow more loading volume and a pin-sized hole was created at the very end of the channel to allow air to escape while loading the fluid.

Sample Preparation

Plasmid from a DNA Toolbox was used as the template. Briefly, a 1000 bp region with an approximate GC content of 40% was identified in M13 and this construct was placed into pUC19 plasmid. Forward primer 5’ GATATTTGAAGTCTTTCGGG 3’ and reverse primer 5’

TAAGAGCAACACTATCATAA 3' were used to amplify a 300 bp product. The concentration of initial plasmid stock was determined by absorbance at 260 nm (A_{260}), assuming an A_{260} of 1.0 is 50 mg/L. A 10X series dilution was performed with the plasmid DNA, ranging from 6×10^9 to 6×10^1 copies/μL. Fifty μL of each dilution was added to 50 μL of PCR buffer containing 20 mM $MgCl_2$, 2.5 μg/μL bovine serum albumin (BSA), and 500 mM Tris (pH 8.3). Plasmid DNA was digested by adding 10 units of the restriction enzyme HindIII (New England BioLabs, Ipswich, MA) to each dilution mixture and incubating for 24 hours at 37°C. The restriction enzyme was then inactivated at 65°C for 1 hour.

The PCR mixture comprised plasmid DNA, ranging from 6×10^6 to 6×10^0 copies/μL, as the template, 0.5 μM of each primer, 200 μM of each deoxynucleotide triphosphate (dNTP), 0.04 U/μL of KlenTaq1 polymerase (AB Peptides, St. Louis, MO), 6.4 ng/μL of Anti-Taq Monoclonal Antibody (eENZYME, Montgomery Village, MD), 2 mM $MgCl_2$, and 1X LCGreen Plus (Idaho Technology, Salt Lake City, UT) in 50 mM Tris (pH 8.3), 500 ng/μL BSA, and 3.75% polyvinylpyrrolidone (PVP) (Av. Mol. Wt. 360,000, Sigma-Aldrich Corporation, St. Louis, MO).

Thermocycling

Figure S2 provides a photograph and scheme of the custom instrument. A 0.04" gauge J-type thermocouple (Omega, Stamford, CT) was used for temperature monitoring. The signal from the thermocouple was amplified and linearized (AD594, Analog Devices, Norwood, MA) and the output was connected through a shielded I/O connector block (SCB-68, National Instruments) to a PCI-MIO-16XE-10 DAQ card. The temperature measurement was calibrated to the inside of the disk using DNA standards of known melting temperatures: complementary synthetic oligonucleotides at 62°C, and PCR products at 79.5°C, and 92°C. The disk was spun using a servo motor (200627, Maxon Precision Motors, Fall River, MA) controlled by a power driver (MID-7652, National Instruments) connected to a PCI-7344 DAQ card.

The fluorimeter consisted of light from a 465 nm blue LED passed through a 475 DF30 bandpass filter and dichroic beam splitter and was then focused with a glass asphere lens onto the disk. Emitted light was collected through this same lens and reflected 90^{o} by the dichroic beam splitter 505DRSP. This light was reflected 90^{o} by a 540DRLP dichroic beam splitter, passed through a 524 DF20 bandpass filter and detected with an OPT301M photodiode (Burr-Brown, Tuscon, AZ) for real-time fluorescence monitoring during PCR. A scheme of the fluorimeter is seen in Figure S3. The output from the fluorimeter was connected to the same I/O connector block as the thermocouple and LabView 7.1 (National Instruments) was used to analyze the temperature and fluorescence data at a frequency of 1 kHz.

Disk Imaging and Analysis

A 455 nm blue LED was positioned 120 mm below the disk with an excitation filter of 438 DF20. The emitted fluorescent light from the disk was collected with a lens (Ultrasonic EF 20mm 1:2.8, Canon, Tokyo, Japan) positioned 260 mm above the disk. This collected light then passed through a 483 DF32 bandpass filter and was imaged with a CCD camera (iXon, Andor Technology, South Windsor, CT), as seen in Figure S4. Andor iXon software vs. 4.0 (Andor Technology) was used to take a 15 second exposure background subtraction image followed by a 15 second exposure. The image threshold was set from 0-5000, saved as a jpg file, and imported into ImageJ for analysis.

FIGURES (SUPPORTING INFORMATION)

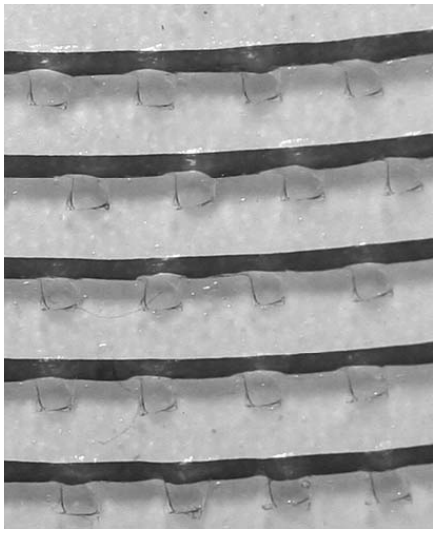

Figure S1. A photograph of a small section of the disk is shown with wells filled with PCR mixture and the channel filled with mineral oil dyed with Oil Red O.

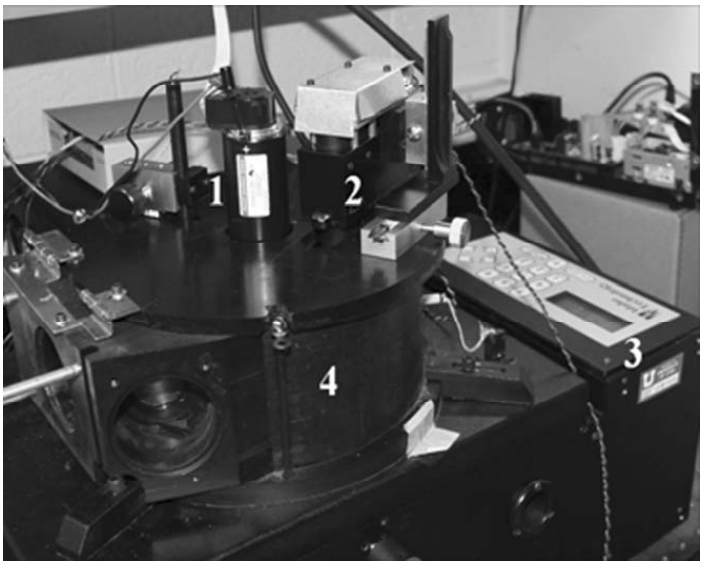

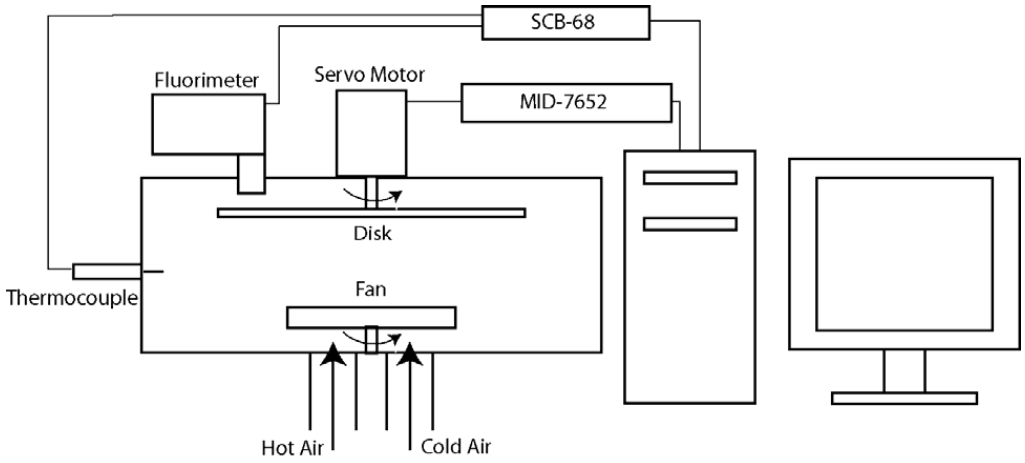

Figure S2. (Top) A photograph of the rapid air thermocycler is shown with: (1) servo motor, (2) fluorimeter, (3) temperature profile input keypad and display, and (4) air chamber for disk thermocycling. (Bottom) A scheme is shown of the spinning disk platform.

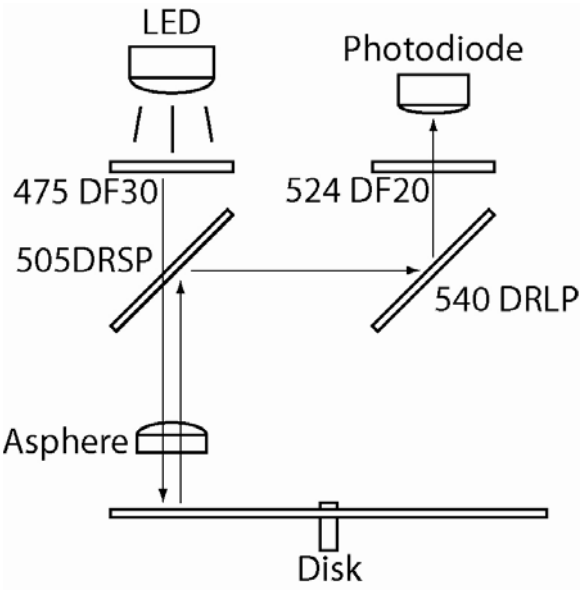

Figure S3. A scheme of the fluorescence manifold used for real-time fluorescence monitoring of the wells during PCR.

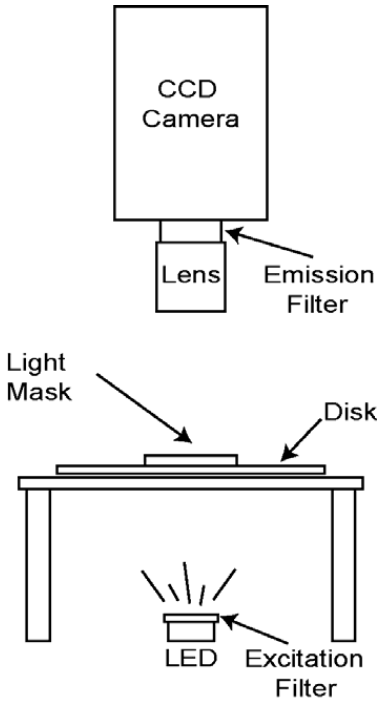

Figure S4. A scheme is shown of the disk imaging set-up.

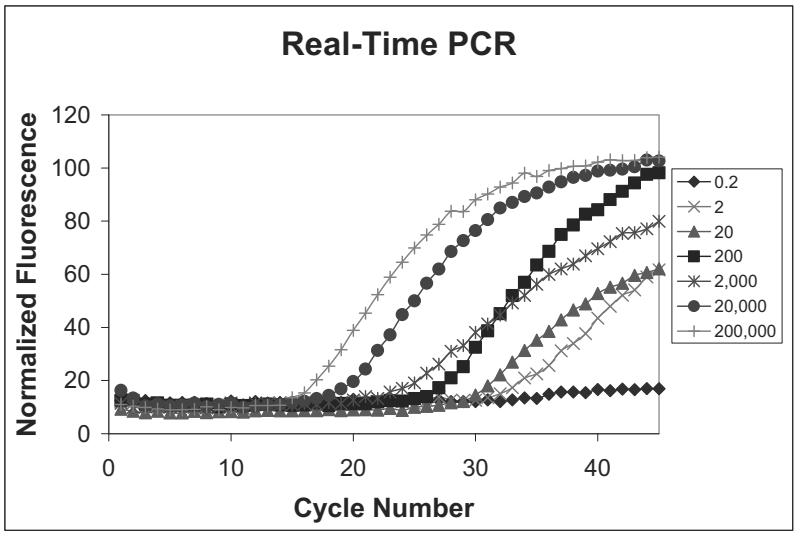

Figure S5. Real-time PCR data is presented for each dilution test within the spinning disk platform, reporting the normalized fluorescence value for each cycle. Concentrations are provided in plasmid copies per well.

CHAPTER 6

QUASI-DIGITAL PCR: ENRICHMENT AND QUANTIFICATION OF RARE EVENT MUTATIONS

Abstract

A previously described spinning disk platform with 1000 unique wells was utilized with a technique we call quasi-digital PCR, in which at most one rare mutation is preferentially amplified in a reaction well that also contains multiple wild-type background templates, for enhanced mutation enrichment and quantification. The allele-specific PCR technique of allele-specific competitive blocker-PCR (ACB-PCR) provided preferential amplification of the mutation. A CCD camera acquired a fluorescent image of each disk following PCR, and the well intensity frequency distribution and Poisson distribution statistics were used to count the positive wells and to determine the number of template molecules amplified on the disk. A 111 bp genomic DNA product was amplified within the disk and analyzed in about one hour, with PCR cycle times of 23 s. Two separate dilution series were compared to validate that this quasi-digital PCR technique did suppress wild-type template amplification. A detection sensitivity of 0.01% was determined by this method, detecting 42 mutation template molecules amongst 450000 wild-type template molecules, and the number of positive reactions compared well with absorbance measurements. The spinning disk platform reduces disposable cost, instrument complexity, and thermocycling time and the ACB-PCR chemistry improve

sensitivity and lowers assay cost over previously described methods. This technique has application in detecting and quantifying rare event mutations including from circulating tumor cells, which is the focus of this work.

Introduction

The discovery of circulating tumor cells (CTCs) in peripheral blood was first made in 1869 by T.R. Ashworth (Ashworth 1869). Detection of these CTCs has the potential to provide a noninvasive, sensitive technique to detect cancer earlier and provide information for proper therapy selection and drug resistance. Thus, there is a significant ongoing effort to be able to detect and quantify CTCs, as well as understand the genetic mutations associated with them. The main challenge in identifying, quantifying, or collecting CTCs is that CTC concentrations can be as low as one cell in one ml of blood (Nagrath et al. 2007), or one tumor cell per 10^5 - 10^7 peripheral blood mononuclear cells (Ross et al. 1993), making it difficult to detect and quantify the cancer cells with current techniques. Enrichment approaches have been applied in order to overcome the difficulties associated with such low concentrations such as filtration (Vona et al. 2000), density gradient (Müller et al. 2005), flow cytometry (Cruz et al. 2005), and immunomagnetic enrichment techniques (Allard et al. 2004). However, these methods can suffer from low specificity, low sensitivity, a loss of CTCs, or false negatives and positives (Alunni-Fabbroni and Sandri 2010). Thus, there remains a need for a rapid, sensitive, specific and repeatable method for detecting and quantifying CTCs.

PCR based techniques have overcome some of these sensitivity and specificity issues. One such technology that has improved sensitivity is the technology BEAMing (beads, emulsion, amplification and magnetics), finding mutated circulating free DNA at

a detection rate as low as 0.18% of all circulating free DNA in plasma of colorectal cancer patients (Diehl et. al 2008; Dressman et. al 2005). Another PCR technique used is the amplification refractory mutation system (ARMS) PCR (Newton et al. 1989), providing allele specific amplification. This technique implements a primer with a terminal 3'-nucleotide that is allele specific. Therefore, one can design this primer to match the mutant template and be refractory to the wild-type, thus delaying the mismatch's PCR. To further improve on the ARMS primer design, allele-specific competitive blocker-polymerase chain reaction (ACB-PCR) has been introduced (Orou et al. 1995), providing a 'double kill' methodology to preferentially amplify the mutant template. A probe is designed to match the template to be suppressed during PCR. Therefore, the mismatched ARMS primer competes with the probe to anneal to the template. This method greatly delays PCR of the mismatch but also delays the Cq of the matched template.

Digital PCR (Vogelstein and Kinzler 1999) uses limiting dilution or volume to detect minor fractions of mutated DNA by having only one DNA template in a given reaction volume. Once amplified, the reaction volumes are fluorescently analyzed; relying on binary positive/negative calls (Ottesen et al. 2006; Warren et al. 2006). A variation on this method has been implemented, which we call quasi-digital PCR, combining the amplification refractory mutation system (ARMS) PCR, a scorpion primer and digital PCR, achieving a detection rate as low as 0.02% (Wang et al. 2010), to selectively amplify the mutation allele. We term this method as quasi-digital because each well is loaded with multiple copies of wild-type DNA but contains at most only one copy of the mutation. Parallel reactions occur simultaneously followed by fluorescence

detection to determine how many reactions contain a mutation copy, counting the mutations digitally, for improved quantification over real-time PCR methods. Furthermore, by running multiple reactions one can theoretically improve on the sensitivity of the method by orders of magnitude, depending on the number of reactions performed.

The focus of this work is to achieve a more rapid, less expensive process for quasi-digital PCR with capabilities for lower limits of detection by implementing ACB-PCR, using an ARMS primer and molecular beacon probe, rapid air thermocycling, and 1000 individual nanoliter-sized reactions using a previously described spinning disk platform (Sundberg et al. 2010). The goal is to detect one tumor cell per 10^5 - 10^7 background cells, to make detection and quantification of tumor cells from a blood sample more straightforward. Towards this goal, this work uses the mutation T1796A *BRAF*, a known mutation site prevalent in malignant melanomas (Yazdi et al. 2003) and papillary thyroid cancer (Xing et al. 2004) and can also be found within other cancers (Davies et al. 2002). The mutation target was mixed with a large background of wild-type DNA to demonstrate the feasibility of counting CTCs using the proposed method.

Methods and Procedures

Disk Design and Manufacturing

The digital PCR disk design utilizes centrifugal force to move fluid from a loading reservoir, located near the center of the disk, along a spiral channel and fill 1000 individual square wells that are facing radially outward from the channel. The spiral channel is 250 μm wide and each well has dimensions of 500 μm x 500 μm x 125 μm, or a 30 nL volume. This design is fabricated from thin film plastics to create an inexpensive

disposable and requires only centrifugation for fluid control. The entire disk is 120 mm in diameter, the size of a CD, and is 375 μm thick (see Figure 6.1). The prototyping method of xurography (Bartholomeusz et. al 2005) was used to pattern the channel layer disks. Briefly described, the microchannel is patterned with SolidWorks® (Concord, MA), imported into Adobe Illustrator® (Adobe, San Jose, CA) and exported to a cutting plotter (CE5000-60, Graphtec, Santa Ana, CA). An FR83-Black polycarbonate thin film sheet, 125 μm thick, (Sabic Polymershapes, Fresno, CA) was patterned with the loading reservoir, spiral channel and 1000 wells. This sheet was then thermally bonded between two other FR83-Clear polycarbonate thin film sheets (Sabic Polymershapes) of the same thickness, laminating the plastic layers together at 175°C for 2 min using a JetPress 14 heat press (Geo Knight, Brockton, MA). Two 500 μm thick Teflon strips (Scientific Commodities Incorporated, Lake Havasu City, AZ) were inserted into the loading reservoir, allowing larger loading volumes, and a pin-sized hole was created at the end of the overflow channel to allow air to escape during fluid loading.

ACB-PCR Design

ACB-PCR utilizes a ‘double kill’ technique to preferentially amplify the mutation allele by utilizing an ARMS primer that matches the mutation allele while refractory to wild-type and a probe designed to match the wild-type to further inhibit primer annealing on the wild-type allele (Figure 6.2). The forward primer 5’ GTGATTTTGGT-CTAGCTACAG**A** 3’ and reverse primer 5’ TCAGTGGAAAAATAGCCTCAATTC 3’ were designed to amplify a 111 bp product from the mutant allele. The competitive blocker probe used was molecular beacon probe 5’ FAM-CGGTCTAGCTAC-AG**T**GAAATCTCGACCG–BHQ 3’ (Biosearch Technologies, Novato, CA). The bolded

nucleotides in the forward primer and molecular beacon probe sequences represent the location of the mutation site for T1796A *BRAF*.

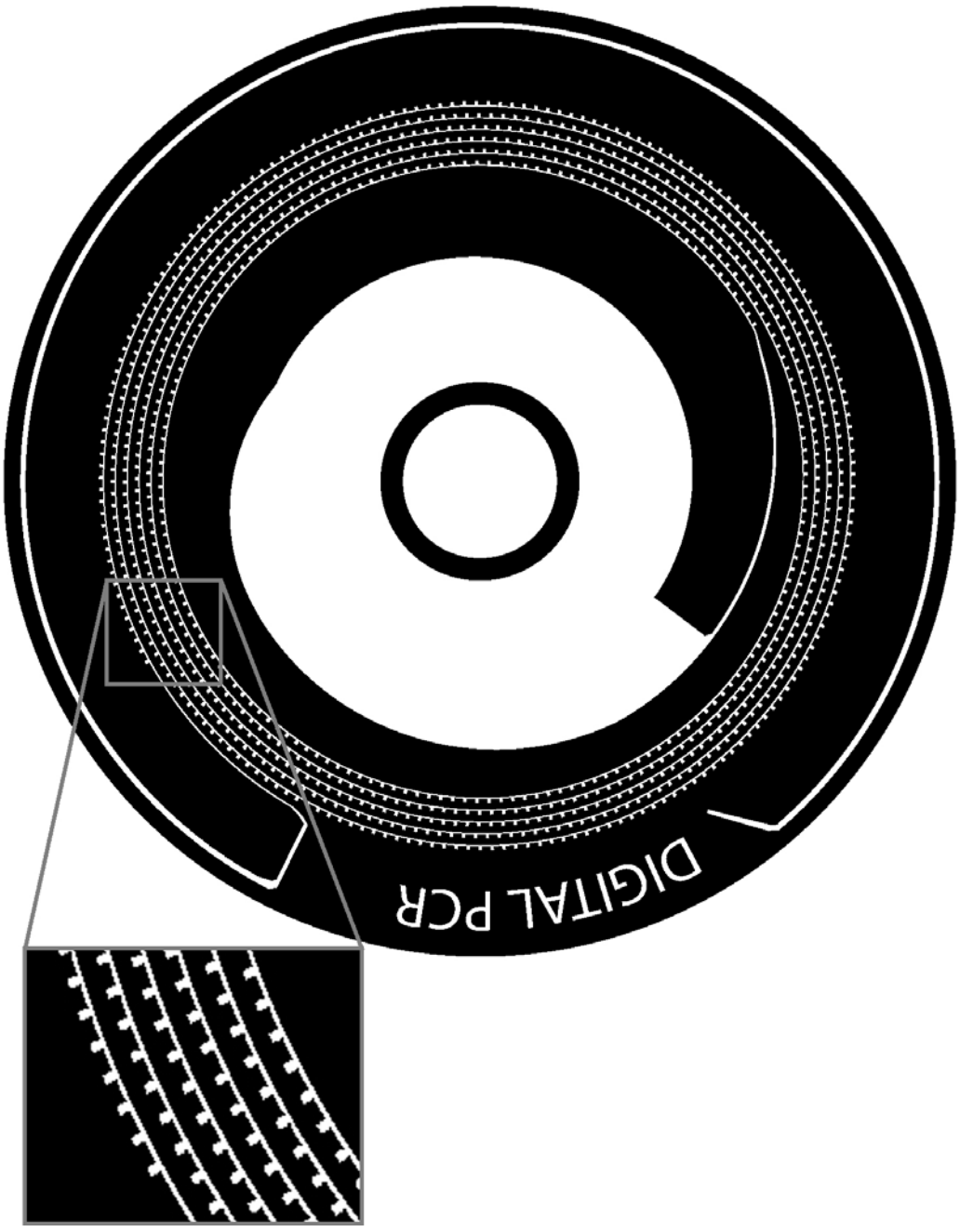

Figure 6.1. Disk design shown to scale. The disk consists of a loading reservoir, spiral microchannel with 1000 wells facing radially outward along the channel, and an overflow channel at the edge of the disk.

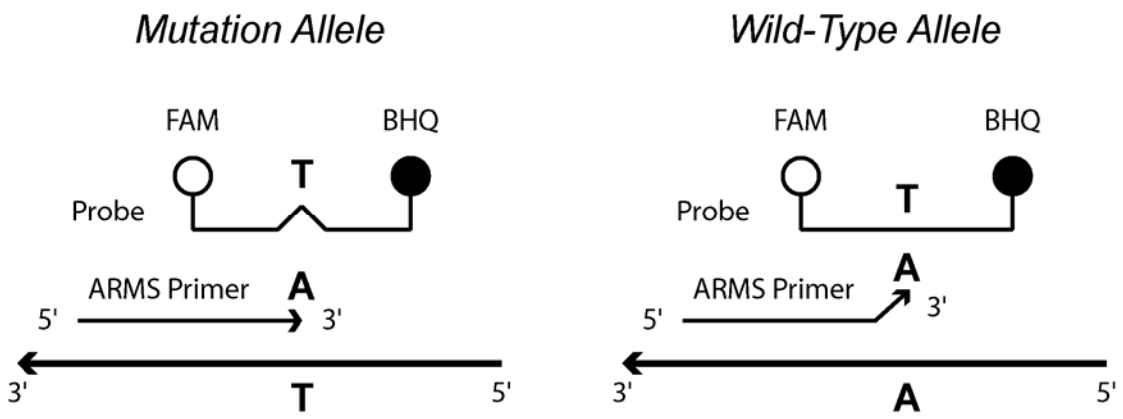

Figure 6.2. An illustration of the ACB-PCR chemistry concept.

PCR Preparation

Wild-type human genomic DNA was extracted from human blood and the *BRAF* homozygous mutation was obtained from the ATCC as purified DNA (HTB-72D, American Type Culture Collection, Manassas, VA). The concentrations of genomic DNA were determined by absorbance at 260 nm (A_{260}), assuming an A_{260} of 1.0 is 50 mg/L.

The PCR mixture comprised *BRAF* mutation DNA, ranging from 0.5 to 0.005 ng/μL, as the template with 1 μM reverse primer, 0.2 μM forward primer, 0.5 μM molecular beacon probe, 200 μM of each deoxynucleotide triphosphate (dNTP), 0.04 U/μL of KlenTaq1 polymerase (AB Peptides, St. Louis, MO), 6.4 ng/μL of Anti-Taq Monoclonal Antibody (eENZYME, Montgomery Village, MD), 2 mM $MgCl_2$, and 1X LCGreen Plus (Idaho Technology, Salt Lake City, UT) in 50 mM Tris (pH 8.3), 500 ng/μL BSA, and 2.5% polyvinylpyrrolidone (PVP) (Av. Mol. Wt. 360,000, Sigma-Aldrich Corporation, St. Louis, MO). Tests involving a mixture of mutation and wild-type DNA also contained 50 ng/μL wild-type DNA.

Forty μL of PCR mix and 100 μL of mineral oil (M5904, Sigma-Aldrich Corporation), dyed with 1 mg/mL Oil Red O (Matheson Coleman & Bell, Gardena, CA),

were pipetted into the disk loading reservoir. Two polycarbonate disks, 750 μm thick with an outer diameter of 75 mm, were then coupled to each side of the disk. The disk was spun for 5 min at 4500 rpm to load each of the wells along the spiral channel path and to fill the channel with mineral oil. The end of the spiral channel was then thermally sealed prior to thermocycling to create a closed system.

Thermocycling

The disk rapid air thermocycling instrument has been described previously (Wittwer et al. 1997; Sundberg et al. 2010). For disks containing only mutation template, 100 cycles of 50°C annealing for 0 s, 72°C extension for 2 s, and 95°C denaturing for 0 s was achieved in about 45 min while spinning the disk at 4500 rpm (27 s/cycle). The annealing temperature was raised for disks that contained mutation template with wild-type background to prevent wild-type amplification, with 100 cycles of 55°C annealing for 0 s, 72°C extension for 2 s, and 95°C denaturing for 0 s in about 38 min (23 s/cycle).

Disk Imaging and Analysis

The disk was fluorescently imaged following PCR for digital well analysis using the set-up shown in Figure 6.3. This consisted of a 470 nm blue LED positioned 70 mm below the disk with an excitation filter of 469 DF35 (FF01-469/35-25, Semrock, Rochester, NY). The excitation light source was mounted on a turntable with the LED located 45 mm from its center. This turntable was rotated by a stepper motor (PK266-01A, Oriental Motor, Torrance, CA) controlled using an MID 7604 motor driver and PCI 7330 card (National Instruments, Austin, TX). The excitation light was rotated one

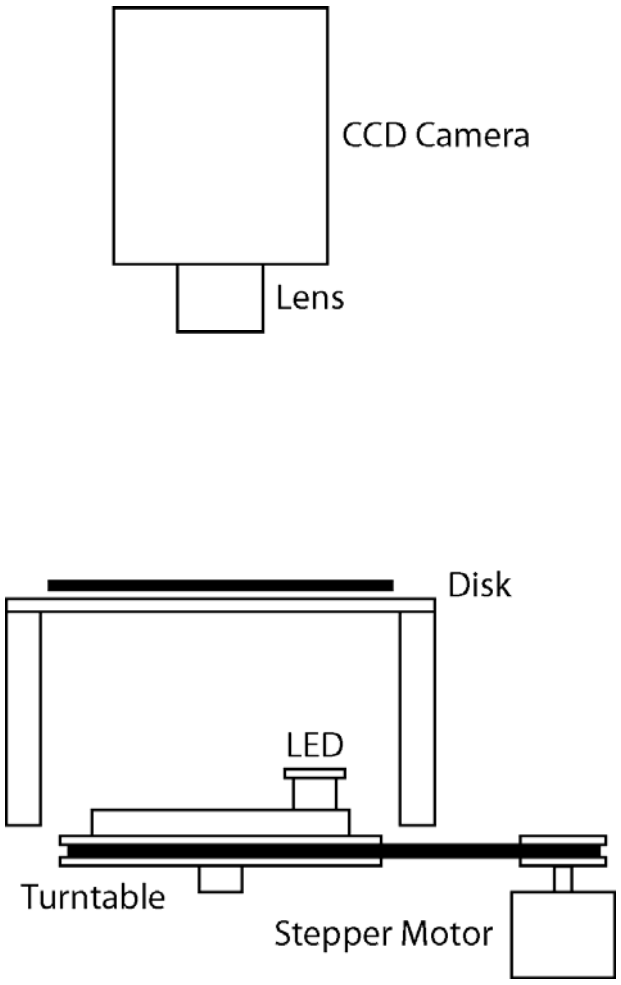

Figure 6.3. A scheme is shown of the disk imaging set-up.

revolution during imaging at a velocity of 10 rpm to achieve more uniform excitation over all of the wells within the disk. The emitted fluorescent light from the disk wells was collected with a lens (Ultrasonic EF 20mm 1:2.8, Canon, Tokyo, Japan) positioned 350 mm above the center of the disk. This collected light then passed through a 525 DF20 bandpass filter (FF01-525/20-25, Semrock) and was imaged with a CCD camera (iXon, Andor Technology, South Windsor, CT) cooled to -20 °C. Andor iXon software vs. 4.0 (Andor Technology) was used to take a 45 s exposure background subtraction image followed by a 45 s exposure. The image threshold was set from 0- 2500, saved as a jpg file, and imported into ImageJ (Rasband 1997) for analysis. This software was then used

to threshold, size exclude, and create histograms of well intensity for each disk image. The threshold and minimum pixel number was operator defined. Histogram frequency distributions were then used to determine the number of positive and negative wells for each test with normal distribution curves fitted to the histogram data using Minitab 15 statistical software (Minitab, State College, PA). The intersection of the two normal distribution fitted curves determined the cut-off point for positive and negative calls.

Results and Discussion

Quasi-digital PCR quantification results with rapid PCR thermocycling were provided in about an hour. Thermocycle times (23 s cycles) were much faster than reported from the recently published ARMS-scorpion PCR technique (>90 s cycles), which also requires a 10 min hot start time. Although our technique required twice as many cycles the total PCR time was still less than half the time required with the ARMS-scorpion assay. Furthermore, by eliminating scorpion primers assay costs have been reduced.

A dilution series was performed with only the *BRAF* mutation DNA in order to demonstrate PCR within the spinning disk, as seen in Figure 6.4. The dilution series ranged from 0.5 to 0.005 ng/μL, or about 4.5 to 0.045 copies/well. A dilution series was then performed with the *BRAF* mutation DNA within a larger wild-type background. The *BRAF* mutation concentration again ranged from 0.5 to 0.005 ng/μL while the wild-type background was held constant at 50 ng/μL or about 450 copies/well, as seen in Figure 6.5. The ACB-PCR chemistry effectively suppressed wild-type amplification, by comparing the two dilution series and obtaining similar positive well results for mutation copy concentration. For example, mutation template with a concentration of 0.45

copies/well had 384 positive wells as compared to mutation template with wild-type background results where an average of 405 positive wells were found with a standard deviation of 18 positive wells across three individual tests. It is seen in Figures 6.4 and 6.5 that well intensity distributions of the different panels drifts. This is due to the user-defined brightness and contrast, and threshold settings of the fluorescent images, which varied during analysis. Table 6.1 provides the number of positive wells within each disk as well as the number of copies amplified for each dilution series. The number of copies amplified was statistically determined from the Poisson distribution, as described previously (Sundberg et al. 2010), but has also taken into consideration the probability of having more than two through ten copies present in a well, not simply the probability of having more than one copy in a well, to provide a more accurate approximation. The number of DNA template copies amplified based on statistical analysis correlates well with the absorption measurements taken from the DNA samples prior to testing.

A detection sensitivity of 0.01% was calculated based on an average of 43 mutation copies among 450000 wild-type copies across three individual tests. This sensitivity is a slight improvement over the previously published quasi-digital PCR work, although the background copy number used in this study was nearly three orders of magnitude greater per well (450 copies/well compared to 6-7 copies/well). The histogram distribution detection scheme with this work currently prevents further detection sensitivity. Disk imaging could be improved for more uniform fluorescence excitation across the entire disk's well array to provide better separation between the positive and negative distributions, allowing for a more sensitive thresholding implementation. If the fluorescence detection was improved for higher "on/off" resolution one could

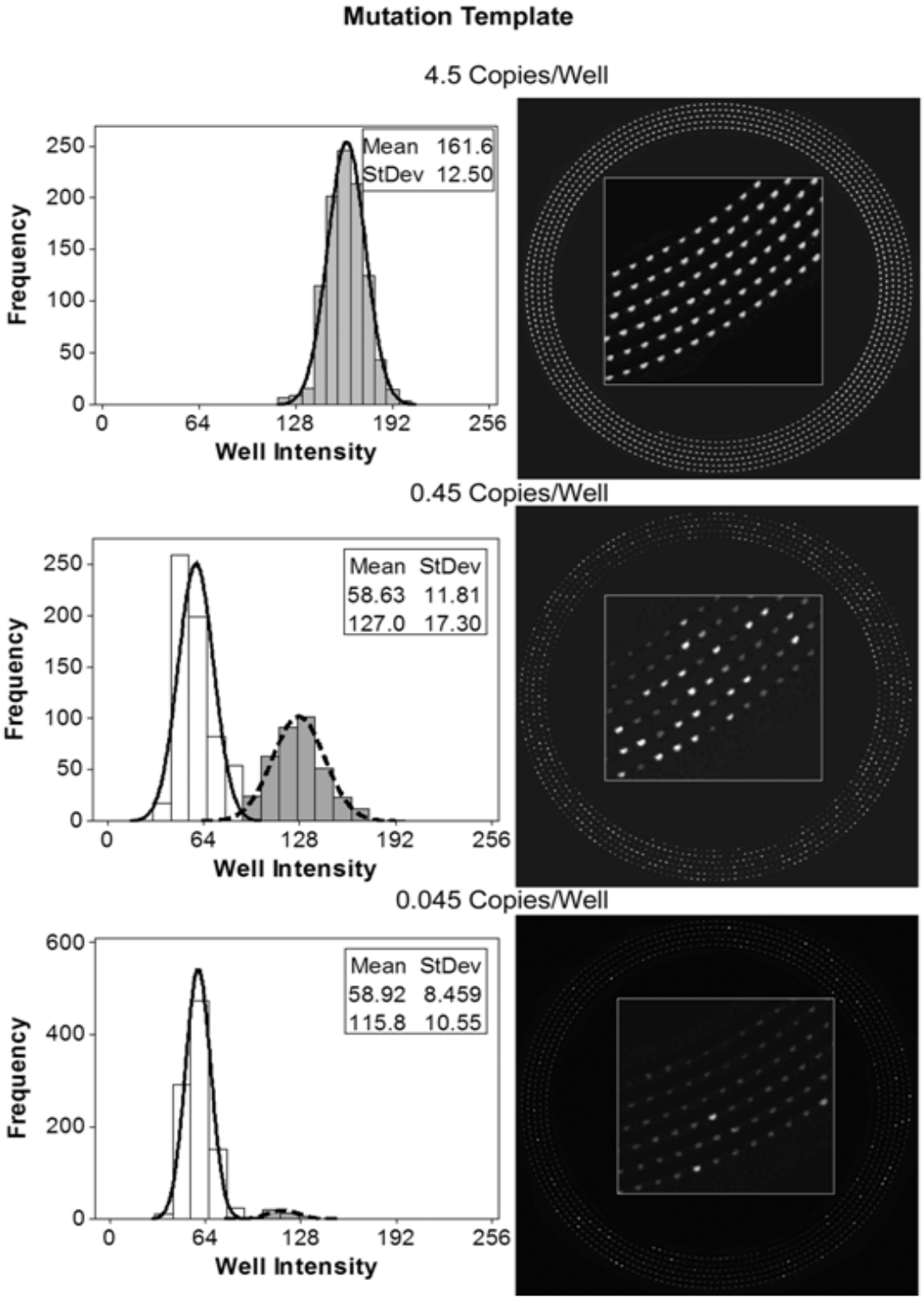

Figure 6.4. Fluorescent images are presented for a dilution series of *BRAF* mutation DNA concentration ranging from about 4.5 – 0.045 copies/well. Histogram data corresponding to each image is also presented; including frequency distribution, normal distribution fit curves, the mean, and standard deviation.

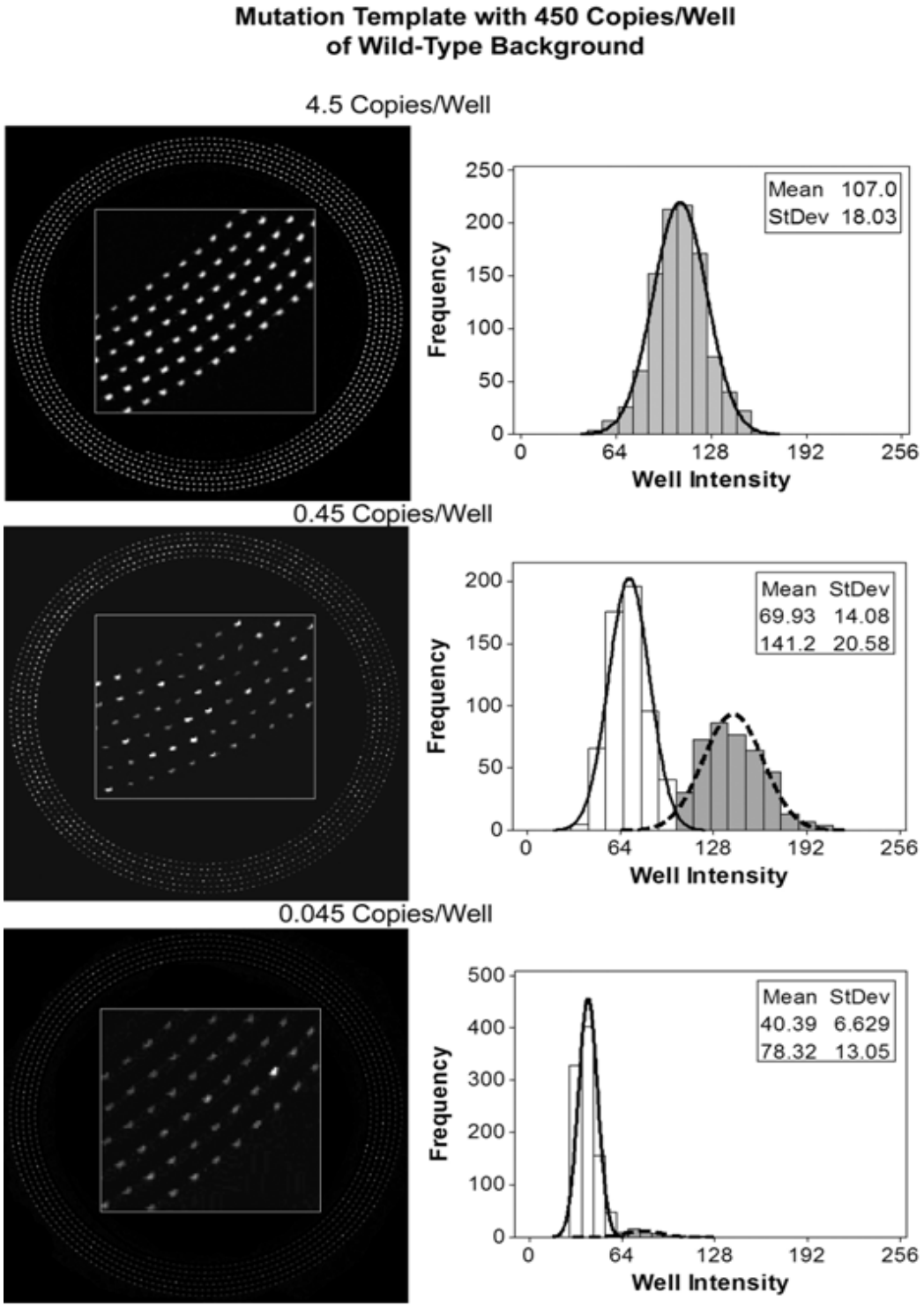

Figure 6.5. Fluorescent images are presented for a dilution series of *BRAF* mutation with wild-type background, mutation DNA concentration ranging from about 4.5 – 0.045 copies/well and 450 copies/well of wild-type DNA. Histogram data corresponding to each image is also presented; including frequency distribution, normal distribution fit curves, the mean, and standard deviation.

Table 6.1. Number of positive wells and number of copies amplified for two template dilution series on the spinning PCR disk. Tests involving background wild-type DNA and within the digital range were run in triplicate. The average and standard deviation are shown in this table for these repeat tests.

DNA Concentration (Copies/Well)	***Mutation Template***		***Mutation Template with 450 Copies/Well of Wild-Type Background***	
	Number of Wells Amplified	Number of Copies Amplified*	Number of Wells Amplified	Number of Copies Amplified*
4.5	992	N/A	996	N/A
0.45	384	423	405 ± 18	452 ± 26
0.045	42	42	43 ± 8	43 ± 8

*Determined using Poisson distribution statistics

theoretically achieve a detection sensitivity of 0.0002%, using the current chemistry and well configuration, by simply diluting the mutation sample to detect 1 copy amongst the same wild-type background.

Not all wells fluoresced with the highest mutation concentrations of the dilution series, with a few wells either failing or being negative in each case. One of the causes for this occurrence is the manufacturing process. The cutting plotter on rare occasion creates a ridge next to a well, causing irregular fluid flow, allowing mineral oil to fill the well rather than the PCR mix. These wells are easily detected within the fluorescent image due to a much lower fluorescent signal than a negative well's fluorescent signal. More consistent and accurate manufacturing methods need to be investigated in order to eliminate this issue. Another cause of obtaining a negative well with the highest concentration is the low probability of having zero mutation copies in a well. The Poisson distribution approximation calculates that with an average concentration of 4.5 copies per well there is approximately a 1% chance that a well would not have any mutation DNA present.

T1796A *BRAF* mutation DNA was successfully amplified and analyzed within the spinning disk with and without 450 wild-type background copies per well in about an

hour. Future work will aim to improve disk manufacturing, thermocycling rates, fluorescence interrogation of the disk's well array, and ease of data analysis. Additional oncogene mutation targets will also be investigated. These improvements should allow us to reach the goal of having adequate sensitivity for detection and quantification of CTCs with a faster, more user-friendly platform.

Acknowledgements

The authors thank the University of Utah Research Foundation and the Utah Science Technology and Research initiative (USTAR) in conjunction with the American Recovery and Reinvestment Act (ARRA) for kindly supporting this work. We also thank Dr. Wittwer's lab group and Dr. Gale's lab group for valuable advice pertaining to this research.

References

Allard WJ, Matera J, Miller MC, Repollet M, Connelly MC, Rao C, Tibbe AGJ, Uhr JW, Terstappen LWMM. 2004. Tumor cells circulate in the peripheral blood of all major carcinomas but not in healthy subjects or patients with nonmalignant diseases. Clinical Cancer Research. 10:6897-6904.

Alunni-Fabbroni M, Sandri MT. 2010. Circulating tumour cells in clinical practice: methods of detection and possible characterization. Methods. 50:289-297.

Ashworth TR. 1869. A case of cancer in which cells similar to those in the tumors were seen in the blood after death. Aust Med J. 14:146-149.

Bartholomeusz DA, Bouttè RW, Andrade JD. 2005. Xurography: rapid prototyping of microstructures using a cutting plotter. JMEMS. 14(6):1364-1374.

Cruz I, Ciudad J, Cruz JJ, Ramos M, Gomez-Alonso A, Adansa JC, Rodriguez C, Orfao A. 2005. Evaluation of multiparameter flow cytometry for the detection of breast cancer tumor cells in blood samples. American Journal of Clinical Pathology. 123:66-74.

Davies H, Bignell GR, Cox C, Stephens P, Edkins S, Clegg S, Teague J, Woffendin H, Garnett MJ, Bottomley W, Davis N, Dicks E, Ewing R, Floyd Y, Hall S, Hawes R,

Hughes J, Kosmidou V, Menzies A, Mould C, Parker A, Stevens C, Watt S, Hooper S, Wilson R, Jayatilake H, Gusterson BA, Cooper C, Shipley J, Hargrave D, Pritchard-Jones K, Maitland N, Chenevix-Trench G, Riggins GJ, Bigner DD, Palmieri G, Cossu A, Flanagan A, Nicholson A, Ho JW, Leung SY, Yuen ST, Weber BL, Seigler HF, Darrow TL, Paterson H, Marais R, Marshall CJ, Wooster R, Stratton MR, Futreal PA. 2002. Mutations of the BRAF gene in human cancer. Nature. 417:949-954.

Diehl F, Schmidt K, Choti MA, Romans K, Goodman S, Li M, Thornton K, Agrawal N, Sokoll L, Szabo SA, Kinzler KW, Vogelstein B, Diaz Jr LA. 2008. Circulating mutant DNA to assess tumor dynamics. Nature Medicine. 14(9):985-990.

Dressman D, Yan H, Traverso G, Kinzler KW, Vogelstein B. 2005. Transforming single DNA molecules into fluorescent magnetic particles for detection and enumeration of genetic variations. Proc Natl Acad Sci USA. 102:16368-16373.

Müller V, Stahmann N, Riethdorf S, Rau T, Zabel T, Goetz A, Jänicke F, Pantel K. 2005. Circulating tumor cells in breast cancer: correlation to bone marrow micrometastases, heterogeneous response to systemic therapy and low proliferative activity. Clinical Cancer Research. 11:3678-3685.

Nagrath S, Sequist LV, Maheswaran S, Bell DW, Irimia D, Ulkus L, Smith MR, Kwak EL, Digumarthy S, Muzikansky A, Ryan P, Balis UJ, Tompkins RG, Haber DA, Toner M. 2007. Isolation of rare circulating tumour cells in cancer patients by microchip technology. Nature. 450:1235-1241.

Newton CR, Graham A, Heptinstall LE, Powell SJ, Summers C, Kalsheker N, Smith JC, Markham AF. 1989. Analysis of any point mutation in DNA. The amplification refractory mutation system (ARMS). Nucleic Acids Research. 17 (7): 2503-2515.

Orou A, Fechner G, Utermann G, Menzel HJ. 1995. Allele-specific competitive blocker PCR: a one-step method with applicability to pool screening. Hum Mutat. 6:163-169.

Rasband WS. U.S. National Institutes of Health, Bethesda, Maryland, USA, http://rsb.info.nih.gov/ij/, 1997-2010.

Ross AA, Cooper BW, Lazarus HM, Mackay W, Moss TJ, Ciobanu N, Tallman MS, Kennedy MJ, Davidson NE, Sweet D, Winter C, Akard L, Jansen J, Copelan E, Meagher RC, Herzing RH, Klumpp TR, Kahn DG, Warner NE. 1993. Detection and viability of tumor cells in peripheral blood stem cell collections from breast cancer patients using immunocytochemical and clonogenic assay techniques. Blood. 82:2605-2610.

Sundberg SO, Wittwer CT, Gao C, Gale BK. 2010. Spinning disk platform for microfluidic digital polymerase chain reaction. Analytical Chemistry. 82(4):1546-1550.

Vogelstein B, Kinzler KW. 1999. Digital PCR. Proc Natl Acad Sci USA. 96:9236-9241.

Vona G, Sabile A, Louha M, Sitruk V, Romana S, Schütze K, Capron F, Franco D, Pazzagli M, Vekemans M, Lacour B, Bréchot C, Paterlini-Bréchot P. 2000. Isolation by size of epithelial tumor cells. American Journal of Pathology. 156:57-63.

Wang J, Ramakrishnan R, Tang Z, Fan W, Kluge A, Dowlati A, Jones RC, Ma PC. 2010. Quantifying EGFR alterations in the lung cancer genome with nanofluidic digital PCR arrays. Clin Chem. 56:623-632.

Wittwer CT, Ririe KM, Andrew RV, David DA, Gundry RA, Balis UJ. 1997. The LightCycler: a microvolume multisample fluorimeter with rapid temperature control. Biotechniques. 22:176-181.

Xing M, Vasko V, Tallini G, Larin A, Wu G, Udelsman R, Ringel MD, Ladenson PW, Sidransky D. 2004. *BRAF* T1796A transversion mutation in various thryroid neoplasms. The Journal of Clinical Endocrinology & Metabolism. 89(3):1365-1368.

Yazdi AS, Palmedo G, Flaig MJ, Puchta U, Reckwerth A, Rütten A, Mentzel T, Hügel H, Hantschke M, Schmid-Wendtner M-H, Kutzner H, Sander CA. 2003. Mutations of the BRAF gene in benign and malignant melanocytic lesions. Journal of Investigative Dermatology. 121:1160-1162.

CHAPTER 7

DIGITAL PCR STATISTICS

In order to validate digital PCR results it is important to have a standard with which to compare results and also to understand the statistical significance of each test. Specific statistics of importance in this work are, 1) the probability that more than one DNA copy is in a well, 2) accurate estimation of the average copy number per positive well, and 3) the statistical confidence one has in a given result. This chapter utilizes the Poisson distribution to address the first two areas and applies the Wilson score interval to the third area. These statistical methods also apply to the quasi-digital PCR approach presented in Chapter 6 with the exception that on/off results represent mutation DNA copies only.

DNA Concentration Standards

To properly validate our digital PCR tests we must have a standard with which to compare our results. Absorption at 260 nm (A_{260}) was used to measure genomic DNA and plasmid DNA concentrations, due to the fact that nucleic acids have an absorption maximum at this UV wavelength. The subsequent paragraphs explain how the absorption measurement is used to determine the number of copies per microliter.

In Chapter 5 the plasmid DNA stock concentration was determined using the following relationships and Equations 7.1-7.4 based on absorption at A_{260}:

- The number of base pairs (bp) within the plasmid DNA is 3686
- 1 A_{260} = 50 μg/ml for a 10 mm path
- 6.02 x 10^23 copies/mol = 6.02 x 10^17 copies/μmol
- The average molecular weight (MW) of a base is 330 μg/μmol (multiply by 2 to account for double stranded DNA, so a base pair is 660 μg/μmol)

$$\frac{copies}{\mu l} = \left(X_{A260}\right)\left(\frac{50\mu g}{ml}\right)\left(\frac{1\mu mol}{Y\mu g}\right)\left(\frac{1ml}{1000\mu l}\right)\left(\frac{6.02\times10^{17}copies}{1\mu mol}\right) \tag{7.1}$$

$$\frac{copies}{\mu l} = \frac{\left(X_{A260}\right)\left(3.01\times10^{16}\right)}{Y_{MW}} \tag{7.2}$$

$$Y = (3686_{bp})(660) = 2.43\times10^{6} \tag{7.3}$$

$$\frac{copies}{\mu l} = (1.24\times10^{10})X_{A260} \tag{7.4}$$

Similar calculations were made for human genomic DNA in Chapter 6 to determine that one copy is approximately 3.3 pg. At the common concentration of 5 ng/μl, as determined by A_{260} absorption, used with PCR within our lab there are approximately 1500 copies/μl. At this concentration there would be 1.5 copies in a 1 nl well. Dilution of DNA is necessary to lower the concentration to allow wells to be 30 nl in size. For example, diluting the initial DNA concentration 100 times (~15 copies/μl) would provide a mean number of 0.45 DNA molecules within a 30 nl well.

Poisson Distribution

The Poisson distribution is used to determine what DNA concentration should be used to limit the probability of having more than one DNA molecule in a given well, or in the case of quasi-digital PCR, the probability of having more than one mutation DNA molecule in a given well, as seen in Equation 7.5, where λ is the mean number of DNA copies per well and *k* is the number of DNA copies of interest per well (i.e., 1, 2, 3, 4, etc. copies that may be present in a given well). Therefore, if 67% of the wells are negative then the expected number of DNA copies per well would be –ln 0.67 or 0.40 (the λ value solved when $P_k(0) = 0.67$ and $k = 0$). The probability that a positive chamber contains more than one DNA template would be $1-0.67-((e^{-0.40})*(0.40^1))/(1!)$ or 6.2%. One must also take into consideration the probability of having more than 2, 3, 4, 5, etc. copies of DNA in a positive well to obtain a more accurate approximation. This can be done by the summing of Poisson distributions. Thus, the probability that a positive well contains more than two DNA templates would be $1-0.67-((e^{-0.40})*(0.40^1))/(1!)-((e^{-0.40})*(0.40^2))/(2!)$ or 0.82%. The probabilities for each case are then summed together and used to determine the total number of DNA templates present. For the case of having 67% of the wells being negative, a probability summation of 7.2% is calculated, which for 1000 wells would represent 357 DNA molecules that have been amplified by PCR. Figure 7.1 provides a graphical representation of Poisson distributions, showing the average number of copies/positive well as a function of the proportion of positive wells. It is seen that as the proportion of positive wells increases the average number of copies/well increases dramatically.

$$P_k(\lambda) = \frac{\lambda^k \cdot e^{-\lambda}}{k!} \tag{7.5}$$

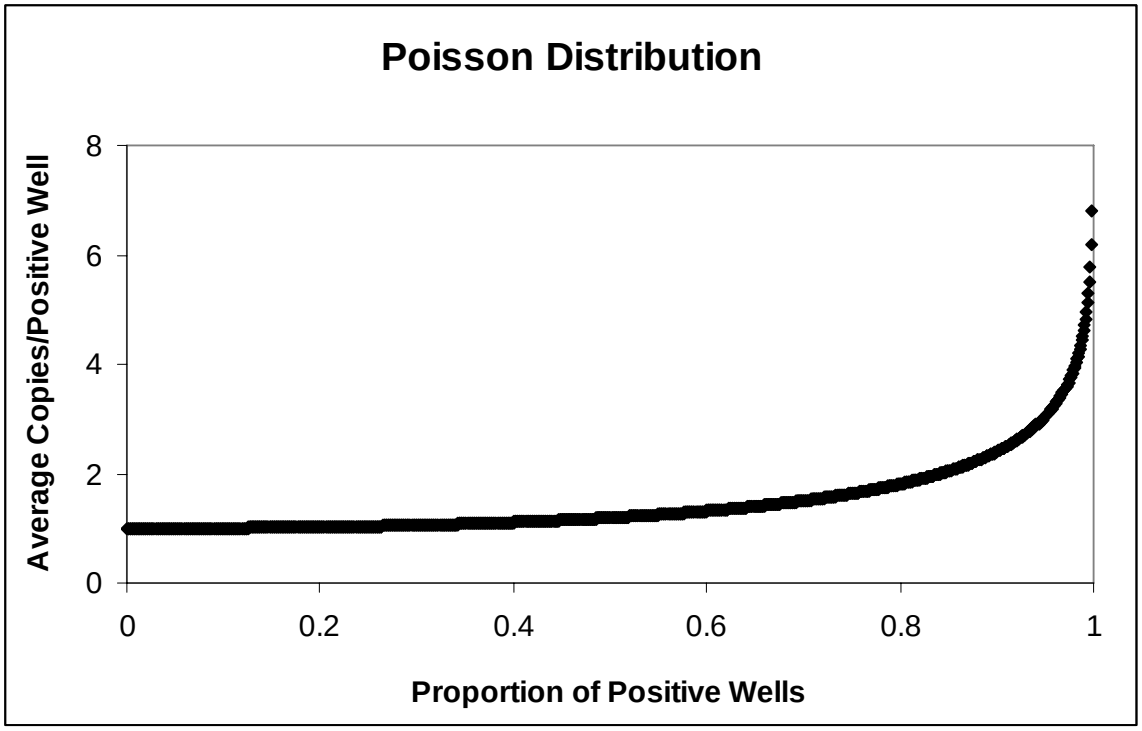

Figure 7.1. Plot shows the average number of copies/positive well as a function of the proportion of positive wells, determined by Poisson distributions. This plot considers the probability of having more than one through more than 10 DNA templates in a given positive well at a set DNA input concentration.

Confidence Intervals

In this section confidence intervals of sample proportions to estimate the population proportion are constructed. The confidence interval calculations assume that the data are binary, the probability of success is the same for each trial, and the trials are statistically independent. The population proportion is symbolized *p* and the point estimate of the population proportion, or sample proportion, is symbolized by *p-hat*. The standard error of a sample proportion is the estimated standard deviation of a sampling distribution. The exact standard error of a sample proportion is given in Equation 7.6, where *p* is the population proportion and *n* is the sample size.

$$se = \sqrt{p(1-p)/n} \tag{7.6}$$

The typical estimated standard error is known as the Wald interval (Wald and Wolfowitz 1939). The number of successes and the number of failures must be at least 5 each and this approximation does not work well when *p* is the near the boundaries, either near 0 or 1. In fact, it has been found that even when *p* is not near the boundaries erratic behavior can occur (Agresti and Coull 1998). Although this method represents a simple solution to solving the confidence interval it is typically inadequate, especially for digital PCR applications where many of the solutions involve *p* near the boundaries.

The Wilson score interval (Wilson 1927) provides more accurate results, especially for smaller sample sizes and proportions close to 0 and 1 (Brown et al. 2001). The Wilson score interval is calculated according to Equation 7.8, where $z_{1-\alpha/2}$ is the 1-$\alpha/2$ percentile of a standard normal distribution. For example, for a 95% confidence interval let $\alpha = 0.05$ and so $z_{1-\alpha/2} = 1.96$. The center of the Wilson score interval (Equation 7.9) is a weighted average, with *p-hat* receiving greater weight as the sample size increases.

$$\frac{\hat{p} + \frac{1}{2n} z_{1-\alpha/2}^2 \pm z_{1-\alpha/2} \sqrt{\frac{\hat{p}(1-\hat{p})}{n} + \frac{z_{1-\alpha/2}^2}{4n^2}}}{1 + \frac{1}{n} z_{1-\alpha/2}^2} \tag{7.8}$$

$$\frac{\hat{p} + \frac{1}{2n} z_{1-\alpha/2}^2}{1 + \frac{1}{n} z_{1-\alpha/2}^2} \tag{7.9}$$

The reader should note that the sample size represents the number of DNA copies present, not the number of wells of the disk. The type of sample and genetic mutation being tested will determine what sample proportion is needed and also determine the confidence level desired for that sample proportion.

Applying the Wilson Score Interval

An example applicable to quasi-digital PCR is presented in Figure 7.2 utilizing the Wilson score method. Three confidence levels of 90%, 95% and 99% are applied to calculate the Wilson score interval for one million DNA copies with mutation population proportions being 0.01% (100 mutation copies), 0.001% (10 mutation copies), 0.0001% (1 mutation copy), and 0.00001% (0.1 mutation copy). It is noted that erratic behavior occurs with this method when approaching one mutant DNA copy. Table 7.1 illustrates in more detail this behavior as the proportion approaches zero for a 95% confidence level with populations of 10^5, 10^6, and 10^7 DNA copies. This error is introduced due to rounding error when applying a two-sided interval at the boundary. In 2001, Brown et al. described a modified Wilson score interval to diminish this error, wherein a one-sided Poisson approximation is applied for the lower or upper bound when approaching very near the boundaries. However, with the very low mutation population proportions of interest with quasi-digital PCR even this method provides only modest improvement. One must be cautious with statistical analysis of results that approach detection of one mutation within a test.

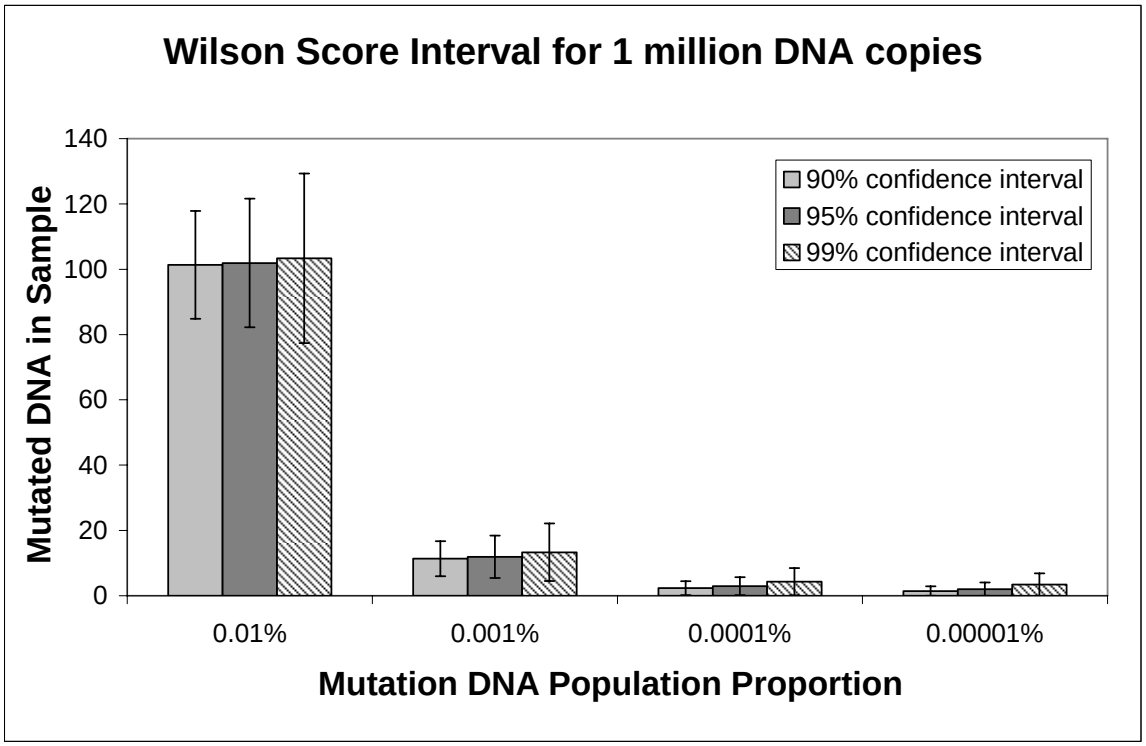

Figure 7.2. Wilson score centers with error bars representing Wilson score intervals are shown for 90%, 95% and 99% confidence levels at varying mutation DNA population proportions.

Table 7.1. Wilson score centers and intervals for a 95% confidence level are shown at varying DNA copy numbers and mutation population proportions.

95% Confidence

No. of DNA Copies	Mutation Pop. Proportion	No. Mutated DNA	Wilson Score Center [No. Mutated DNA]	Wilson Score Interval [No. Mutated DNA]
1.E+05	5%	5000	5001.73	± 135.09
1.E+05	1%	1000	1001.88	± 61.70
1.E+05	0.1%	100	101.92	± 19.68
1.E+05	0.01%	10	11.92	± 6.49
1.E+05	0.001%	1	2.92	± 2.74
1.E+05	0.0001%	0.1	2.02	± 2.02
1.E+05	0.00001%	0.01	1.93	± 1.93
1.E+06	5%	50000	50001.73	± 427.17
1.E+06	1%	10000	10001.88	± 195.03
1.E+06	0.1%	1000	1001.92	± 61.98
1.E+06	0.01%	100	101.92	± 19.69
1.E+06	0.001%	10	11.92	± 6.49
1.E+06	0.0001%	1	2.92	± 2.74
1.E+06	0.00001%	0.1	2.02	± 2.02
1.E+07	5%	500000	500001.73	± 1350.84
1.E+07	1%	100000	100001.88	± 616.70
1.E+07	0.1%	10000	10001.92	± 195.91
1.E+07	0.01%	1000	1001.92	± 62.01
1.E+07	0.001%	100	101.92	± 19.69
1.E+07	0.0001%	10	11.92	± 6.49
1.E+07	0.00001%	1	2.92	± 2.74

Quasi-Digital PCR Statistics Example

By way of example consider a quasi-digital PCR experiment with 1000 wells containing an average concentration of 500 DNA copies/well for a total of 500000 DNA copies. Following PCR 190 wells are found to be positive, due to at least one mutation copy being present in each of these positive wells. Since more than one copy of DNA may be present in a well the Poisson distribution approximation is applied to determine that approximately 194 mutation copies have actually been amplified within the wells of the disk, due to a calculated 2.07% increase of DNA copies. Therefore, the mutation

population proportion is 0.0388%, which yields 196 ± 27 DNA copies at a 95% confidence level using the Wilson score method.

Conclusion

A set of equations for computing DNA concentrations from absorption measurements has been provided. This allows one to use standards to validate digital PCR results. The Poisson distribution approximation shows that as DNA template concentration increases the average number of copies per positive well increases. The Wilson score method provides additional information as to what window, or interval, of DNA copies may be present at a given confidence level.

References

Agresti A, Coull B. 1998. Approximate is better than 'exact' for interval estimation of binomial proportions. The American Statistician. 52: 119-126.

Brown LD, Cai TT, DasGupta A. 2001. Interval estimation for a binomial proportion. Statistical Science. 16(2): 101-133.

Wald A, Wolfowitz J. 1939. Confidence limits for continuous distribution functions. The Annals of Mathematical Statistics. 10:105–118.

Wilson EB. 1927. Probable inference, the law of succession, and statistical inference. Journal of the American Statistical Association. 22:209-212.

CHAPTER 8

CONCLUSION

Several key scientific contributions have been made by the author in the furthering of nucleic acid identification and quantification by miniaturizing and simplifying current molecular diagnostic techniques. These contributions have ultimately resulted in a platform capable of performing digital PCR accurately using relatively simple and rapid methods. A brief summary of the scientific contributions and conclusions drawn are presented hereafter along with suggestions for future work.

Contributions

This dissertation makes contributions and draws conclusions within the following areas:

- **Miniaturization of DNA melting analysis.** DNA melting analysis has been miniaturized to nanoliter-sized interrogation volumes. While the reaction volume was reduced three orders of magnitude the signal-to-noise ratio was only reduced 1.5 orders of magnitude, which still provided sufficient signal for accurate genotyping and scanning. The 20 data points collected per degree Celsius does not qualify this method as high resolution melting analysis but does provide sufficient data points for genotyping and scanning of many targets. This reduction in interrogation volume provides evidence that less reagent consumption and DNA starting template and

more parallelization is possible with melting analysis for a more rapid, inexpensive, high-throughput solution that requires no separations, processing or labeled probes.

- **Xurography rapid prototyping development.** Advancements were made within rapid prototyping to further develop the method of xurography. This provides a rapid, inexpensive technique to quickly design and manufacture microfluidic chips and disks for research purposes. It was found that tape-bonded microchannels do have a shorter life span than the traditional glass-bonded microchannels but are an order of magnitude less expensive and four times faster to make for prototyping purposes. Knife plotter resolution was also found to be sufficient for patterning the digital PCR disks with its array of 1000 wells.
- **New method for fluid partitioning.** Our spinning disk design reduces disposable and instrument costs by requiring minimal fluid control, relying on centrifugation rather than valves, pumps or microdroplet dispensers. The disk consists of three inexpensive plastic thin film sheets laminated together with an architecture that passively divides a spun sample into a thousand compartments.
- **Spinning Disk Platform for Microfluidic Digital PCR.** A novel disk platform was developed that quickly and easily partitions a DNA sample and quantifies the number of DNA templates present in the sample by digital PCR. This method further allows rapid air thermocycling to be used for much quicker PCR turnaround times than is currently available, with cycle times as fast as 23 s/cycle. Following PCR, each compartment is interrogated for a positive/negative signal by fluorescence imaging. Furthermore, aggregate real-time PCR and DNA melting analysis data are provided for amplicon and assay validation. Although the melting

curve Tm standard deviation between runs is larger than preferred for genotyping it still provides product specificity evidence that the region of interest has been amplified rather than nonspecific amplification.

- **Quasi-digital PCR method.** The concept of digital PCR was taken one step further by using a quasi-digital PCR method. This allows one to load each well with large amounts of background wild-type DNA and preferentially amplifying rare event mutation DNA template using the allele-specific chemistry of ACB-PCR. This method reduces cost and improves sensitivity (0.01%) over a previously described quasi-digital PCR method, and offers higher quantification accuracy than most analog quantification methods.
- **Statistic analysis tools for digital PCR.** Statistic tools have been developed to more completely determine digital PCR results based on the Poisson distribution and Wilson score method to calculate confidence intervals.
- **Additive protocol for improved PCR.** It was found that adding 2.5-3.75% polyvinylpyrrolidone (PVP) into the PCR mix greatly improved results within the digital PCR disks. PVP has a high affinity for polycarbonate and PETG and is able to adsorb to the plastic walls of the microchannel, effectively competing with and preventing other PCR mix components from adsorbing to the plastic due to surface chemistry effects.
- **Published works.** Three manuscripts have been published from this work, with a fourth manuscript in process of being submitted. A book chapter involving low-cost manufacturing techniques was also published. These publications are as follows:

1. Sundberg SO, Wittwer CT, Greer J, Pryor RJ, Elenitoba-Johnson O and Gale BK. Solution-phase DNA mutation scanning and SNP genotyping by nanoliter melting analysis. Biomed Microdevices 2007, 9:159-166.
2. Greer J, Sundberg SO, Wittwer CT and Gale BK. Comparison of glass etching to xurography prototyping of microfluidic channels for DNA melting analysis. J. Micromech. Microeng. 2007, 17:2407-2413.
3. Sundberg SO, Wittwer CT, Gao C and Gale BK. Spinning disk platform for microfluidic digital polymerase chain reaction. Analytical Chemistry 2010, 82(4):1546-1550.
4. Sundberg SO, Wittwer CT, Zhou L, Palais B, and Gale BK. Quasi-digital PCR: Enrichment and quantification of rare event mutations. To be submitted to Analytical Biochemistry.
5. Gale BK, Eddings MA, Sundberg SO, Hatch A, Kim J and Ho T. Fabrication and packaging: Low-cost MEMS technologies, in Comprehensive Microsystems, 1st Ed. Gianchandani Y, Tabata O and Zappe H eds. Elsevier Amsterdam, Vol. 1, pp. 341-378, 2008.

A patent has been filed, PCT/US2009/035859, to protect intellectual property involving the spinning disk microfluidic digital PCR platform.

Future Work

Improve Digital PCR Platform Instrumentation

Future instrumentation can be improved to be more user-friendly and reduce analysis and thermocycling times while also lowering instrument cost. A fluorescent scanner is envisioned to replace disk imaging following PCR to provide higher “on/off”

fluorescence resolution and further reduce instrumentation cost by simplifying the optics. The thermocycler can also be better fitted to the disk for faster thermocycling rates. Melting analysis on individual wells may be explored as well. The next prototype version will aid in commercialization of this platform to further digital PCR research.

Improve Spinning Disk and Explore New Configurations

The cutting plotter occasionally creates undesirable ridges next to a well, causing irregular fluid flow and allowing mineral oil to fill the well rather than PCR mix. Improved manufacturing methods need to be investigated for more controlled and consistent well dimensions within the disk. Configurations should also be designed and manufactured to handle multiple samples within a disk, rather than single sample use. Varying volumes and numbers of wells for quasi-digital PCR can also be investigated to determine if different configurations can lower limits of detection than is currently possible.

Investigate Other Digital PCR Applications

Other applications of digital PCR should be investigated aside from rare event oncogene mutation quantification. Multi-color probe assays can be designed for ratio quantification of wild-type to mutation template for gene expression analysis. Viral load quantification assays could be designed for targets such as HIV. Haplotyping for determining if combinations of mutations are in *cis* or *trans* with each other can also be clinically useful. This data could be obtained by multiplex DNA melting analysis with digital PCR reactions. Noninvasive prenatal testing of targets such as trisomy 21 could also be explored.